THESIS
Submitted in fulfilment of the requirements for the degree
MASTER OF SCIENCE
in
PHYSICS
in the Faculty of Science
University of the Witwatersrand, Johannesburg, South Africa

SOLAR CELL SIMULATION USING AB INITIO METHODS

by
Milica Zdravković

Student no. **1615819**
e-mail: 1615819@students.wits.ac.za

Supervisors: Prof. Alexander Quandt, Dr. Robert Warmbier

February 2024

DECLARATION

I declare that this thesis is my original work and is being submitted for the Degree of Master of Science at the University of the Witwatersrand, Johannesburg. It has not been previously submitted for any degree or examination at another university.

Candidate Signature: 

Signed on: 13 May 2024 at: Johannesburg, South Africa

Abstract

Solar cells are a great source of renewable energy, but they are yet to reach their thermodynamic efficiency limits. Common commercial solar cells run at approximately 20% power conversion efficiency, and almost all efficiency loss comes from thermalisation. Ab initio simulations can reduce the need for physical experiments to quantify these losses while also providing insights into the quantum mechanical properties of materials. Note that density functional theory reformulates the expression for the ground-state energy of a many particle system such that it is a functional of the electron density, thereby allowing the electronic energy to be solved for numerically. But the underlying mechanism behind thermalisation is the electron-phonon interaction. Using the theory of Green's functions, the electron-phonon interaction self-energy and charge-carrier lifetimes can be calculated. A method of approximating the charge-carrier lifetimes using the hydrostatic deformation potential interaction, which is only valid for longitudinal acoustic phonons, is presented. Deformation potentials of -10.125eV for Silicon and -18.663eV for Gallium Arsenide, commonly used solar cell materials, are calculated in good agreement with literature. Furthermore, the electron-phonon interaction lifetimes were calculated to be in the order of 2.0×10^{-15}s for Si and 4.0×10^{-16}s for GaAs, which could have indications that the optimal thickness of a GaAs absorption layer is much thinner than for Si. Thus the deformation potential method provides a satisfactory approximation for the electron-phonon quasiparticle lifetimes based on ab initio methods.

Contents

List of Figures

List of Tables

1. Introduction

Solar energy is a promising source of sustainable power, but it is yet to reach its maximum potential. Various factors limit a solar panel's efficiency, often leading to thermalisation. Computer simulations, including ab initio simulations can lead to a deeper understanding of these factors, and can alleviate the need invest a lot of resources into experiments.

1.1. Background

A solar cell (SC) is a device that converts the energy of photons from sunlight into electricity [1]. Solar cell technology is continually advancing and Solar Photovoltaic (PV) power is a great source of renewable energy in an age of climate change and excessive fossil fuel consumption. Currently most solar cells that are used commercially have approximately 15% to 20% conversion efficiency [2].

One may often find seemingly conflicting information about the efficiency and cost of Solar Photovoltaic (PV) cells. It is not that these sources are incorrect, but that over the last few years, solar cell cost per kilowatt-hour has declined so rapidly that information becomes quickly outdated. According to a press release by the International Renewable Energy Agency (IRENA) on 22 June 2021, the cost of Solar PV power dropped from just under 400USD per MWh in 2010 to almost 50USD per MWh in 2020 [3]. Hence Solar PV went from being one of the most expensive energy sources in 2010 to one of the cheapest sources of renewable energy in just 10 years. In some cases, renewable energy sources such as wind and Solar PV are already cheaper than non-renewable coal power, at the utility scale [4].

With continuing research, the cost of solar PV power may continue its exponential decline, but given the current prices, the cost is no longer the issue but rather the efficiency and the reliability of solar PV cells (although an even lower cost is always an advantage). For countries with a relatively high amount of cloudy days and longer nights, the current solar cells are still not cost effective. Here in South Africa, there is the advantage of sunny days for most of the year, putting it in a position to make good use of solar PV power. South Africa averages about 220W/m^2 of solar radiation per 24 hours, over double the average of Europe and more than the 150W/m^2 in parts of the USA [5].

Although the majority of current solar cells in use are made of a simple bulk crystalline Silicon p-n junction, functioning solar cells made in other ways or from other materials are still being researched and developed. We should not assume by default that Si has the highest efficiency and lowest cost. To improve on the efficiency, production cost, and production by-products of Silicon SCs, a so-called "second generation" of SCs began its development. Amorphous Silicon (a-Si), microcrystalline Si and polycrystalline Si will also work as SCs [6]. Apart from the Si containing variants, there are also multicomponent SCs which are made from GaAs, CdTe, $CuInS_2$ (also called a CIS Solar Cell), $(Cu(In,Ga)(Se,S)_2)$ (CIGS) $(Cu_2ZnSn(S,Se)_4)$ (CZTS) and other materials. Although the a-Si:H (hydrogenated

amorphous Silicon), CIGS and CdTe SCs have low efficiency and can be unstable when exposed to environmental conditions outside of a lab, they have relatively low cost as little material is needed to make them. In general, however, multicomponent SCs have a high efficiency but are currently expensive to make and/or have high production toxicity [6]. A lot of second generation SCs have their function deteriorate from environmental factors such as dirt and snow. Interestingly, many of them are thin and flexible and can be used on irregular surfaces, unlike the conventional flat and rigid solar panel [6].

There is yet even a third generation of solar cells. Some of these cells involve conducting polymers, pigments and organic dyes, quantum dots, and hot electron SCs [6]. These currently have low efficiency, and/or a low service life and/or are unstable in real-world environmental conditions, although research on them is progressing rapidly. Organic SCs and SCs that combine organic and inorganic semiconductors fall under third generation as well. These include perovskites and Grätzel cells [6]. Perovskites are also often combined with or layered onto other cells such as Grätzel cells to improve efficiency. SCs with Solar spectrum splitting currently produce highest efficiencies. "Solar spectrum splitting" is done by a multi-junction solar cell - a collection of thin solar cells from different materials, all which are suited for a different radiation range, and these SCs are then serially layered onto each other. They have record efficiencies of 45% to 46%, however they are extremely expensive to manufacture and are reserved mainly for spacecraft rather than commercial and residential use. The thin SCs in the multi-junction cell can be placed in "parallel", where small cells are laid out in a plane [6]. This lowers the production cost, but the efficiency is also considerably lowered. To achieve efficiency of 43%, optics are used to split the solar light spectrum when radiation is incident on the cell, but this increases the cost again to almost as much as the series multi-junction SC [6]. A detailed review of third generation SCs can be found in [7].

Despite the many advancements in SC technology, SCs have not been able to reach even 50% solar-to-electrical power conversion efficiency. There are a wide variety of factors that lead to efficiency loss. These can be broken down into intrinsic and extrinsic losses [8]. Intrinsic losses are linked to the SC material and structure itself, and require the SC to be modified for the losses to be minimised. These losses include the following:

- *Optical loss* occurs due to materials having some amount of reflectance and transmittance, and energy is lost due to any photons that are not absorbed.
- Loss due to incoming light having energy *below the band gap (E_g)* of the SC material, meaning these photons are unable to excite the electrons in the SC and simply contribute to the heating of the SC.
- *Thermalisation loss* is caused from all the photons in the incoming light spectrum with energy higher than E_g. Only energy equal to the band gap is needed to excite the electrons, and any surplus energy contributes to heat in the SC.
- *Emission loss* occurs from radiative recombination of electron-hole pairs in the SC.
- Work needs to be done to transfer energy from the hot Sun and the cold SC, resulting in the *Carnot loss*.

- The difference in the incident angle of light on the SC and the angle of emission of photons from radiative recombination results in *angle mismatch loss*.

The above constitute the intrinsic losses [8]. Aside from these, the extrinsic losses in a SC can also cause significant decrease in efficiency, in particular in single bandgap SCs (as opposed to multi junction SCs or Tandem SCs). These losses are considered more avoidable as they may be caused by the production process or by defects in the SC. Extrinsic losses include the following [8]:

- Structural defects and impurities in the SC can lead to *non-radiative electron-hole recombination*, causing charge carriers to recombine in the SC before reaching the electrical contacts.
- *Series resistance loss* occurs due to resistance in the SC and of the metal contacts, which also leads to thermalisation.
- *Shunt resistance* also leads to heat increase and recombination.

Out of all the losses mentioned, more than half of all power lost is due to the thermalisation loss and the loss due to incident light being below the band gap of the SC material. In other words, more than half of losses are due to the spectral mismatch between the band gap and the incoming photons. Angle mismatch loss also plays a large role [8]. Furthermore, below band gap and angle mismatch loss also contribute to increased thermalisation of the SC, causing a further decrease in efficiency. These are intrinsic losses that will happen to some degree no matter the material used, and so in order to minimise them it may be necessary to augment existing SC types as opposed to replacing the SC material. Some ways to augment SCs are as follows:

- Augumentation features could be used to reduce angle mismatch. When electrons and holes recombine in the solar cell, a photon may be released. This photon can be released at a solid angle of up to 4π steradians, in other other words, in any direction. However, light from the Sun is incident at a solid angle of 6×10^{-5} steradians. This angle mismatch means that there is an increase in entropy (thermal energy that cannot do useful work) which reduces efficiency. A nanophotonic structure could reduce the emission angle and thus reduce the entropy increase [9].
- *Up-conversion* is the process where light of low frequency is converted to light of a higher frequency. For example a material with a low bandgap may be used to, for every two infra-red photons absorbed, emit one photon in the visible spectrum. These photons are then used by the SC, ensuring that photons which previously had energy below the bandgap are not wasted. Materials that can be used include polycyclic aromatic hydrocarbons, as well as ions of Ln^{3+}, Ti^{2+} and other f-block and d-block elements [7]. Thermal up-conversion can also be done through heating low energy photons and re-emitting them [7].

- Down-conversion is the reverse of up-conversion, where for every UV photon absorbed, two visible-spectrum photons may be released. Down-shifting is a similar process, but instead one high energy photon is converted to one lower-energy photon, and the extra energy is lost to thermalisation. This may reduce efficiency losses due to surface recombination [7].
- Plasmonic nanoparticles can also be used to increase SC efficiency. Metal nanoparticles in perovskite SCs can increase photon flux and the generation of electron-hole pairs [10]. A good review of the use of plasmonic nanostructures in photovoltaics can be found in [11].

Due to the many loss processes, even the types of SCs currently in use still have not reached the thermodynamic limits of their efficiencies. It is possible that systematic changes to the engineering of SCs that use nanostructures for better light trapping can lead to current SCs reaching their thermodynamic efficiency limits [9].

One of the many reasons for the rapid decline of the cost of Solar PV power over the years is also the use of computer simulations. Using knowledge of material properties and interactions between light and matter, we can predict the characteristics and performance of a solar cell or a solar cell candidate. This allows us to rapidly 'test' many kinds of potential solar cell materials' configurations before investing into constructing them physically. Although we can take the properties of key materials from experiment, we can also use 'ab-initio' ("from the beginning") methods to accurately predict these properties and how the resulting solar cell system will function, starting from the atomic structure of bulk materials. Ab initio methods can be used to simulate and analyse all of the key aspects of a working solar cell [1]. With the new understanding gained from these simulations, better, more efficient and cost-effective solar power can be developed.

As discussed above, one of the largest factors that cause SC efficiency loss is thermalisation, that is, energy lost to the SC heating up. This thesis aims to gain insights into thermalisation by carrying out calculations to determine how quick an individual electron thermalises (referred to as the electron-phonon interaction lifetime) in various materials. The speed of this process would also affect the diffusion length for a p-n junction (the distance an electron can travel in the p-n junction before losing enough energy to heat that it recombines with a hole instead of being collected at the metal contacts). Hence when we find the lifetime for this process, we may gain insight into the manner in which a material as well as its thickness influence SC efficiency, and going forward, have real numbers we can put to use when predicting the efficiency of a particular SC.

This thesis will present numerical simulation results for bulk Silicon and Gallium Arsenide, where the problem of thermalisation is worked out using first principles quantum mechanical simulation methods - also known as ab initio methods.

1.2. Overview

The aim of this thesis is to study the theory behind ab initio simulations based on density functional theory (DFT), and to propose an approximate electron-phonon interaction lifetime by means of the deformation potential interaction between electrons and longitudinal acoustic phonons. This is done for Silicon and Gallium Arsenide, materials commonly used in solar PV cells.

Section 2 contains some fundamentals of semiconductor and p-n junction SC physics. We define conduction and valence bands, and p-type, n-type and intrinsic semiconductors, the Fermi level and the Fermi function. Next we introduce the p-n junction, the depletion region, and how the J-V characteristics of a p-n junction are governed by the Diode equation. Applying the discussion of p-n junctions to SCs, the light current density of an SC can be simulated by defining the charge-carrier generation rate. We then discuss the equations to model the power loss in an SC due to spectral mismatch, the loss due to photons with energy higher or lower than the band gap of the SC material.

Section 3 is an overview of the theory underlying DFT, DFPT (Density functional perturbation theory) and the electron-phonon interaction Hamiltonian. First we define the electron density, and show how it can be reduced to a sum of single-particle spin orbitals for a many-particle wavefunction that is written as a Slater determinant. We state and prove the two Hohenberg-Kohn theorems, the pillars of DFT. We discuss the Born-Oppenheimer approximation, dividing the many-body problem into a nuclear system and an electronic system, the latter of which forms a potential energy surface (PES) for the nuclear system. We discuss how the phonon frequencies are the eigenvalues of the matrix of interatomic force constants (IFC), the second derivative of the PES. The PES is the ground state energy of the electronic system, and to solve it, the Kohn-Sham equations are introduced. The Fourier transform of the IFC matrix is called the Dynamical matrix, which is used to calculate the phonon frequencies numerically (to that end it also allows for use of the plane-wave basis set). LDA, GGA, and hybrid exchange-correlation functionals are introduced. First order perturbation theory is used to determine the linear response of the electron density, and this approach is known as DFPT. Finally, this section discussed how the electron-phonon interaction Hamiltonian is determined from the external potential that arises in the Kohn-Sham equations.

Section 4 describes how electron-phonon self-energy is derived by means of Green's functions, followed by deriving an expression for the longitudinal-acoustic (LA) phonon matrix element using the concept of a deformation potential. We define the fermionic and bosonic Green's functions for both a system of coupled and non-coupled electrons and phonons. We use the Dyson equation to define the electron-phonon self-energy. The imaginary part of the retarded electron-phonon self-energy yields the electron-phonon interaction lifetime. To find the matrix element corresponding to LA phonons, we derive the deformation potential using fluid dynamics. The electron-acoustic phonon interaction Hamiltonian is then written in terms of the deformation potential, allowing us to find the LA phonon matrix element.

Section 5 presents the results of this thesis, that is the electron-phonon interaction lifetimes for Si and GaAs. Using the DFT software packages Quantum Espresso and GPAW, we determine the phonon dispersion relations and group velocities for both Si and GaAs, as well as their deformation potentials using the Lowest Unoccupied Molecular Orbital (LUMO) energy. The expression for the electron-phonon interaction lifetime is drastically simplified to be expressed in terms of the deformation potential and phonon group velocity. The numerical results are compared to those found in other sources, followed by a discussion of possible inaccuracies in the result.

Finally, Section 6 summarises the results and motivations of this thesis, as well as closing thoughts on ab initio simulations of SCs.

2. Solar Cell Basics

Before we discuss how Solar Cells can be simulated using quantum mechanical methods, which is the main focus of this thesis, the following section aims to first introduce the general concepts governing a typical p-n junction solar cell, and the history of its development. Once we have an overview of the semiconductor and p-n junction physics and SC loss processes, we can motivate for modelling thermalisation using ab initio methods.

2.1. Literature: Solar cells and ab initio methods

The first Silicon solar cell was patented by R. S. Ohl in 1946 [12]. While studying resistance properties of high purity Silicon ingots, it was found that light from a desk lamp affected the current (in one direction) as seen on an oscilloscope. Ohl determined that the photovoltaic properties of Silicon were comparable to those of other photovoltaic materials known at the time. The P-N junction of Ohl's photovoltaic cell had two zones made of Silicon, but of different structure. For the n-zone, powdered Silicon grains were used to form a uniform structure, and for the p-side, they formed a columnar structure. This p-side did develop a positive potential and Ohl noted that the boundary between the n and p-sides seemed to be where the "photo-EMF" effect occurred [12].

In 1953 and 1954, using doped Silicon, Bell Laboratories achieved a 4.5% and 6% efficiency solar cell respectively after developing diffused junctions. Since then, cell efficiencies began to increase rapidly reaching 14.5% in 1961, by fabricating cells on a phosphorus-doped substrate [13]. Cells with a boron-doped substrate, which were needed for use in space due to their resistance to radiation, also reached 14.5% efficiency in the 1970s [13].

In 1961 William Shockley and Hans J. Queisser argued that the accepted theoretical efficiency limit for p-n junction solar cells at the time was not theoretically justified [14]. They named this limit the 'semiempirical limit' and presented a more justifiable limit which they termed the 'detailed balance limit'. The detailed balance limit assumes that all electron-

hole recombination in the cell is radiative, and thus amount of photons absorbed in the cell corresponds to the total photons and electrons emitted by the cell. It should be noted that detailed balance gives a rough, upper limit for the efficiency of a flat, planar solar cell, and the authors note that a solar cell that is able to concentrate solar radiation using reflectors or other means could theoretically have an efficiency up to the thermodynamic limit $(T_s - T_c)/T_c$ (here T_s denotes the Sun's temperature, and T_c is the solar cell's temperature) [14], implying we are modelling the solar cell as an ideal Carnot Engine. At the time the paper was written, the maximum experimental efficiency of the SC was about 14% [14]. The semi-empirical limit would limit solar cell efficiency to 21.7% and the detailed balance limit sets the max efficiency at about 30%, assuming the cell is a blackbody. Shockley and Queisser note that the true maximum efficiency for a Silicon p-n junction cell would be somewhere between those two numbers, as Silicon is guaranteed to have some nonradiative transitions [14].

In "The Path to 25% Silicon Solar Cell Efficiency: History of Silicon Cell Evolution" [13], Martin A. Green briefly recounts major milestones in solar cell development. In this article, published in 2009, Green reports the achievement of a 25% efficiency Silicon solar cell. Known as a passivated emitter, rear locally diffused (PERL) cell, the solar cell's high efficiency comes from its very strong response at red and blue wavelengths. A lot of factors contribute to the PERL cell's high efficiency, most notably the top oxide layer moulded into an inverted pyramid "tiler's" pattern for better light trapping, which contributes to the strong red response of the cell. The strong blue response is a result of a combination of a double layer antireflective coating, a thin annealed oxide layer and a lightly p-doped top surface [13].

In "A detailed study on loss processes in solar cells" [8] by Ao Wang and Yimin Xuan, 2018, the authors give a detailed review of all the factors that decrease power conversion efficiency (PCE) in an SC (as discussed in Section 1.1). Losses can be broken down into intrinsic (optical loss, below bandgap, thermalisation, emission, Carnot and angle mismatch loss) and extrinsic (non-radiative recombination loss, series resistance loss, shunt resistance loss, and parasitic absorption loss). The intrinsic losses depend on the type of SC used, while the extrinsic losses may be mitigated by improving the production process or reducing the amount of structural defects in the SC. The authors modelled the intrinsic losses for a crystalline Silicon (c-Si) SC and a perovskite SC, at concentration ratios (ratio of sunlight intensity) of both n=1 and n=5 Suns. For c-Si at n=1 they determine a maximum efficiency of 33.52%, which is in good agreement with Shockley and Queisser's detailed balance limit. Specifically, for the c-Si solar cell at n=1 and an incident power of 1000.37W/m^2, below bandgap loss accounted for 194.60W/m^2, thermalisation loss 315.16W/m^2 - already this is half of the power lost due to spectral mismatch - and angle mismatch loss 113.54W/m^2. All of these processes result in SC thermalisation, and the authors find that in total, the SC lost 649.63W/m^2 to heat. i.e. almost all of the PCE loss resulted in heat.

The article "Solar cell simulations based on ab initio methods" [1] by Alexander Quandt and Robert Warmbier, 2021, gives an overview of several ways in which SC's are simulated on a computer, but the article also describes the concept of "ab initio" simulation. To illustrate how standard SC device simulations are carried out, the authors divide a typical

p-n junction SC into three regions: region I is the depletion region, where the p-type and n-type semiconductors meet and free charge carriers are generated; region II is the portion of the semiconductors that the charge carriers travel through to reach the contacts; region III is at the metal contacts on either side of the SC where charge carriers are extracted, leading to a current. The processes in region I can be modelled using the diode equation, augmented by subtracting the SC light current (current generated under light illumination) density. For region II, the current density is modelled using Beer's law and decays exponentially as we move further away from the depletion region. The extraction of charge carriers in region III is modelled by relating the transmitted current density to the incoming current density, which depends on the absorption coefficient and the width of the barrier. The electrostatic potential of the device and the current densities in the p- and n-type regions can also be determined using the Poisson and continuity equations, however the authors point out that to solve these differential equations, boundary conditions need to be specified. Typically, this is the point where the metal contacts are, and this implies that carrier extraction also needs to be modelled. These models may lead to inaccurate results, and the authors propose ab initio simulation as a viable alternative. Quantum mechanical "ab initio" simulations would allow researchers to calculate many of the parameters that are used by the other models, but ab initio models can also be used as an alternative to the standard models. The article then gives a very brief overview of the fundamental theory and equations used for Density Functional Theory (DFT), the basis of ab initio simulation. DFT reformulates the many-body Schrödinger equation to be a functional of the electron density at a point, rather than a function of many electron coordinates. This allows for the quantum mechanical problem to be feasibly modelled on a computer. These ab initio methods can help reduce the need for physical experiments, however they often rely on many simplifications, such as assuming ideal structures and approximating the exchange-correlation functional (a functional that represents any energy effects on the system unaccounted for by other, more explicit terms). Also, since DFT relies on the electron density, the results are much more trustworthy for ground-state densities and energies, rather than excited states, since unoccupied states do not contribute to the electron density. This leads to the common problem of ab initio simulations inaccurately predicting the band gap of materials. Aside from that, DFT is often used for simulating elastic and surface properties of materials. The authors reinstate that ab initio methods are still not suitable for modelling many macroscopic properties of SCs, but could be used in conjunction with device simulations.

A detailed discussion on electron-phonon interactions and how they are modelled with ab initio methods can be found in "Electron-phonon interactions from first principles" [15] by Feliciano Giustino, 2017. In semiconductors, the electron-phonon interaction governs charge carrier mobility. The article cautions that using DFT to study electron-phonon interactions may result in inaccuracies, as the theory relies on both an approximate exchange-correlation functional as well as the Born-Oppenheimer approximation. The article covers a broad range of theory related to electron-phonon interactions, including calculating electron-phonon matrix elements using Density Functional Perturbation Theory to determine electron-phonon interaction self-energy, electron and phonon Green's functions, and calculating the Fan-Midgal and Debye-Waller terms for electron self energy. While many current difficulties with ab initio calculations are outlined, the author concludes that ab initio calculations of

electron-phonon interactions have an extremely wide variety of applications in condensed matter physics.

Ab initio simulations are typically carried out using one of the several software packages currently available. One of these packages is Quantum ESPRESSO, discussed in "QUANTUM ESPRESSO: a modular and open-source software project for quantum simulations of materials" [16] by Paolo Giannozzi et al. This software performs DFT calculations using the plane-wave basis set and pseudopotentials. The Quantum Espresso project aims to be an open distribution, allowing for auxiliary components to be implemented by a wider user community. It has a great advantage in that it is open source and thus freely available. Another freely available DFT software package is GPAW, discussed in "Electronic structure calculations with GPAW: a real-space implementation of the projector augmented-wave method" [17] by J Enkovaara et al. GPAW performs electronic structure calculations using the Projector Augmented Wave (PAW) method, which the authors of [17] note has advantages in terms of scalability and convergence properties. GPAW also allows for the use of the Local Combination of Atomic Orbitals (LCAO) basis set. Another ab initio software package is yambo, discussed in "yambo: an ab initio tool for excited state calculations" [18] by A. Marini et al. Like Quantum Espresso, yambo also uses the plane-wave method. Yambo carries out excited state calculations using many body perturbation theory and time-dependent DFT. The authors state that the software is both user-friendly and that the numerical methods are implemented efficiently.

2.2. Semiconductors

When a crystal is formed, the energy levels of the individual atoms overlap and form what are known as **energy bands**. Electrons of the crystal atoms essentially move freely within these energy bands. At 0K, the energy bands which are filled are called **valence bands**. Empty bands with higher energy are called the **conduction bands**. The energy difference between the *lowest* conduction band and *highest* valence band is known as the **band gap** of a material. A material is an **intrinsic semiconductor** if at room temperature some of its valence band electrons can transition to the conduction band. More electrons gain energy and are promoted as temperature is increased further. We can add an impurity to an intrinsic semiconductor, thereby "doping" it. If the element used as the impurity has more valence electrons than the semiconductor, the excess electrons are weakly bound and may be promoted to the conduction band with less thermal energy. We call the resulting product an **n-type semiconductor**. Similarly, when we dope with an element with fewer valence electrons, the product is a **p-type semiconductor**.

The **Fermi level** of electrons in a solid is the amount of work needed to add an electron to the solid. It is visualised as a hypothetical energy "level" that lies between the conduction and valence bands. At 0K, the states below the Fermi Level are filled and the states above it are empty and the material's Fermi level is called the **Fermi Energy**. If the value of the Fermi level is near the conduction band (as is the case with n-type semiconductors, the opposite being true for p-type), then at temperatures slightly above 0K, there is already

a higher probability of finding some electrons in the conduction band. This probability is given by the **Fermi Function** (from Fermi-Dirac statistics) [19]:

$$f(E) = \frac{1}{1 + e^{(E-E_F)/k_B T))}} \tag{1}$$

Where k_B is the Boltzmann constant. We see that the probability of a state $E = E_F$ being occupied is 50%, with energies below the Fermi Level having a higher probability of being occupied, and energies above it having a lower probability.

As thermal energy is applied to an intrinsic semiconductor, it produces an equal number of electrons in the conduction band and holes in the valence band, with the probability of generating an electron-hole pair being:

$$P(T) = e^{-E_B/k_B T} \tag{2}$$

Where E_B is the band gap of the semiconductor.

At this stage, the number of electrons (n_0) is equal to the number of holes (p_0) which is equal to the quantity n_i, which we call **the intrinsic density of carriers**. Then, n_i at a temperature T is proportional to the probability $P(T)$, and trivially $p_0 n_0 = n_i^2$. The relation $p_0 n_0 = n_i^2$ always holds at equilibrium for a semiconductor (where n_i is fixed for a temperature for the non-doped semiconductor), even a doped one.

2.3. p-n Junctions and Solar Cells

When an n-type and p-type semiconductor are placed side by side to form one system, this is called a **p-n junction**, and it allows us to separate charge carriers. Hence it is one way to make a solar cell more efficiently than using a pristine semiconductor (and the most common kind). Although the p-type and n-type semiconductors can have different Fermi levels, when they are joined, that system can only have one common Fermi level. However, "band bending" occurs, where the p-doped region will have a conduction band bent to be higher and further away from the Fermi level than the n-doped region, and the opposite is true of the valence band (see Figure 1). Hence, in a p-n junction, there is one constant Fermi Level, but the levels of the conduction and valence bands are not constant within the system. The area in the centre of the junctions where the n-type and p-type semiconductors meet is called the **Depletion region** [19]. The depletion region is where the conduction and valence bands are transitioning from one value to another, and so neither band is close to the Fermi level in this area. The depletion region contains very few charge carriers as holes diffuse toward the n-side and electrons towards the p-side, leaving a kind of 'gap' with few carriers but a strong electric field, as the p-side becomes negatively charged and vice-versa.

A positive voltage develops on the n-doped side of the p-n junction (and vice versa on the p-side). This is the **built-in potential of the p-n junction**, here denoted V_{bi}. However no potential difference will be measured across the p-n junction. Potential difference is the work per charge needed to move a charge between two points. Hence we see that the potential

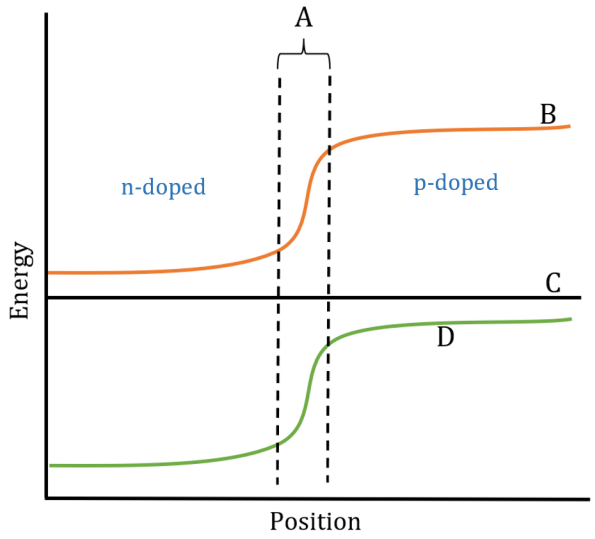

Figure 1: An energy band diagram of a p-n junction. On the left side is the n-doped semiconductor and the p-doped semiconductor is on the right. Label A shows the depletion region, B the conduction band, C the Fermi Level, and D the valence band. The gradient of the bands in the depletion region is directly proportional to the magnitude of the electric field.

difference across the p-n junction will be zero as there is no difference in Fermi level across it.

Even though the electrons and holes are separated by a strong electric field in the depletion region, at equilibrium there is still a small probability of an electron moving to the n-side, or a hole jumping to the p-side. This probability is given by:

$$P_{eq}(T) = e^{-E_b/k_B T} \tag{3}$$

Where $E_b = qV_{bi}$ is the change in energy band level across the depletion region, and q is the charge of an electron. V_{bi} is determined using the donor and acceptor impurity concentrations of the p- and n-doped regions respectively [19].

$$V_{bi} = \frac{k_B T}{q} \ln\left(\frac{N_a N_d}{n_i^2}\right) \tag{4}$$

N_a is the acceptor impurity concentration and N_d is the concentration of donor impurities. In physical p-n junctions at room temperature for typical impurity concentrations, $V_{bi} \sim 1V$. This leads to $P_{eq} \sim e^{-40}$, which is minuscule. However, one could increase this probability by applying a positive voltage V_{app} to the p-side. This is known as a **forward bias**. This would lower both the energy bands and the Fermi level, and effectively "narrow" the depletion region. The new probability of charges overcoming the potential barrier of the depletion region becomes:

$$P_{fb}(T) = e^{-q(V_{bi}-V_{app})/k_B T} \tag{5}$$

If V_{app} is high enough, this would allow for movement of charge carriers and a current through the p-n junction. The current density is given by the ideal Diode equation:

$$J = J_s(e^{\frac{qV_{app}}{nk_BT}} - 1) \tag{6}$$

where n is the diode ideality factor. For an ideal diode, $n = 1$. J_s is typically called the **saturation current density**, and represents the density of the charge carriers generated by the forward bias.

When electrons reach the p-side, they recombine with holes. The average distance that they travel before they recombine is called the **diffusion length** of the p-n junction. To maintain equilibrium, another electron is separated from a hole on the p-side, which eventually recombines, and the process continues. This creates a flow of electrons from the n-side towards the junction, and a flow of holes from the p-side towards the junction.

We can now apply the above discussion of p-n junctions to determine J-V characteristics in the context of (p-n junction-type) solar cells. A solar cell of this type would typically have p-type and n-type semiconductor layers sandwiched between two metal contacts. In a real SC, there is typically series resistance which, with applied voltage, would cause for a small current called the **dark current** to be present even when not under light illumination. When light is incident on the SC, it excites electrons in the valence band, causing them to transition to the conduction band thereby creating an electron-hole pair in the p-n junction. Electrons travel through the metal contact on the n-side (to create a current that powers a lamp or resistor, etc.), called the **light current** of the solar cell. But this results in a positive potential difference V_p on the p-side, which creates a forward bias. As discussed before, this decreases the potential barrier in the p-n junction, allowing electrons to cross over to the p-side giving rise to some current in the opposite direction. Hence, the net current flowing through the diode (the solar cell) is given by the current due to the forward bias, minus the light current density J_l:

$$J = J_s(e^{\frac{qV_p}{nk_BT}} - 1) - J_l \tag{7}$$

For an SC, J_s represents minority charge carriers while the electron-hole pairs generated by light are majority carriers. $J_s \sim 10^{-8}\text{A/m}^2$, approximately twelve orders of magnitude less than the typically expected value for J_l [1]. Note, however, that at higher temperatures excess thermal energy will excite the valence electrons in the p-n junction, giving them a higher probability of overcoming the band gap. This will increase the saturation current density, and lower the current output of the SC. This causes SCs to be less efficient in hot weather, or as the SC itself heats up due to the various efficiency loss processes.

Equation 7 would result in an overall negative current. Since the voltage in the solar cell is positive, this results in a negative power value - this implies that the diode is generating power. To simulate the J-V characteristics of an SC, we can write the light current density in terms of the charge-carrier generation rate $\mathcal{G}(\omega, z)$ [1]:

$$\begin{gathered} J_l = q \cdot \mathcal{G}(\omega, z) \cdot d \\ \text{Where:} \\ \mathcal{G}(\omega, z) = \alpha(\omega)\Phi(\omega)e^{-\alpha(\omega)z} \end{gathered} \tag{8}$$

Where d is the depletion region width, ω is the frequency of the incident photons, z is the vertical distance from the top, light-facing layer of the SC, $\alpha(\omega)$ is the attenuation coefficient for the bulk semiconductor material, and $\Phi(\omega)$ is the photon flux density [1]. With all of these quantities, one can model the J-V characteristics of the SC.

It is necessary for the absorption layer of an SC not to be too thick, because if it is significantly thicker than the diffusion length for the SC, electrons may recombine with holes before reaching the p-n junction. The energy lost as electrons shift from the conduction band to the valence band may then be converted to heat. These electrons then cannot contribute to the current given by the SC, and this lowers the SC efficiency. The charge-carrier **collection efficiency** in a solar cell is simply the ratio of current produced to the amount of current possible when the maximum number of electron-hole pairs that can be generated.

2.4. Losses and Thermalisation

As described in Sections 1.1 and 2.1 there are many factors that lead to Power Conversion Efficiency (PCE) loss in an SC, but the majority of losses occur from intrinsic losses due to spectral mismatch. Furthermore, almost all the power lost from all factors results in thermalisation of the SC.

The band gap E_g of a semiconductor is the difference between the energy of the valence band and the conduction band. Hence it represents how much energy a valence band electron must gain in order to be promoted to the conduction band and contribute to a current. In a solar cell, this energy is provided by solar radiation. However, some photons incident on the SC will have energy $E > E_g$. When these photons excite charge carriers, those charge carriers will have an excess energy $E_{ex} = E - E_g$, which will be transmitted to phonons (atomic vibrations) in the SC, which will result in heat. Hence the energy E_{ex} carried by the photons is wasted and not used to generate current. The power lost due to this **thermalisation loss** is given by [8]:

$$P_{th} = n \int_{E_g}^{\infty} (1 - R_c - T_c)\Phi_{\mathrm{AM1.5}}(E)(E - E_g)\mathrm{d}E \tag{9}$$

Where n is concentration ratio, that is ratio of sunlight intensity measured in number of suns (for the surface of the Earth, this is simply equal to 1), R_c and T_c are the reflectance and transmittance of the solar cell respectively, and $\Phi_{\mathrm{AM1.5}}(E)$ is the photon flux density under standard conditions (AM1.5 stands for Air Mass 1.5) in terms of the photon energy E [8]. In other words, the above equation integrates over all photon energies higher than E_g: the term $(1 - R_c - T_c)$ ensures only the fraction of photons absorbed by the SC are considered, not those reflected or transmitted; we multiply this by the photon flux density, the total number of photons with energy E per unit area per unit time; finally this is multiplied by the excess energy. This yields the total power lost due to excess photon energy.

Just as photons with energy higher than the band gap are incident on the solar cell, so too are photons with lower energy than the band gap. However, in the latter case since the photon has insufficient energy to generate an electron-hole pair, *all* of its energy is wasted.

The equation for the power lost [8] reads similarly as before, but now for all photon energies below E_g:

$$P_{low} = n \int_0^{E_g} (1 - R_c - T_c)\Phi_{\mathrm{AM1.5}}(E)E\mathrm{d}E \tag{10}$$

Both P_{th} and P_{low} contribute to thermalisation in the SC. All the different loss processes described in Section 1.1 contribute to PCE loss: optical loss, loss from below band gap photon energy, emission loss, thermalisation loss, emission loss, Carnot loss, angle mismatch loss, non-radiative recombination, series resistance, shunt resistance, and parasitic absorption loss. Of these below band gap loss, thermalisation loss, Carnot loss, non-radiative recombination, series resistance and shunt resistance contribute to heat generation in the SC [8]. But, among them P_{th} and P_{low} are the largest sources of loss.

So, clearly thermalisation of the SC is a crucial process involved in efficiency loss. If we wish to understand this process and how it arises, quantum mechanical ab initio simulations can provide insight into thermalisation at a more fundamental level. These simulations can reveal more complex and poorly understood dynamics of electron-phonon interactions that lead to thermalisation, and once we have a deep understanding of thermalisation in SCs, we may be able to find new ways to optimise them.

2.5. Summary

In this section we introduced some literature showing the history of solar cells and how their efficiency has improved over the years, as well as the detailed balance limit and loss processes that limit an SC's efficiency. Included also was literature about modern day DFT based ab initio simulations, their use on modelling electron-phonon interactions which are crucial for thermalisation, and the assorted software that can be used for such simulations.

Following that was a discussion of semiconductors and p-n junctions: the Fermi function of a material shows the probability of certain electronic states being occupied. When a p-type and n-type semiconductor are joined, a p-n junction is formed. The centre of a p-n junction forms a strong electric field, called the depletion region, and one can increase the probability of charge carriers crossing over the depletion region by applying a positive voltage to the p-side - this is called forward bias. We can find the forward-biased current density using the diode equation. For a solar cell, a light current is formed under illumination, and we can subtract that from the diode equation to find the current produced by the SC. Writing the light current density in terms of the charge-carrier generation rate allows one to model the J-V characteristics of the SC. When electrons cross the p-n junction to the p-side, they travel an average distance equal to the diffusion length before recombining with holes. The diffusion length thus affects the optimal thickness of an SC absorption layer.

Lastly, we reviewed the two most relevant causes of PCE loss in an SC: incident photons having energy below the band gap, and incident photons having energy higher than the band gap. Any energy that is not used to excite electrons to cross the band gap is essen-

tially wasted. The amount of power lost depends on the difference between photon energy and the band gap, the reflectance and transmittance of the solar cell, and the photon flux density of the incoming photons. Both of these loss processes result in thermalisation of the SC. Therefore, studying the quantum mechanical process that causes thermalisation (the electron-phonon interaction) could provide great insight into SC efficiency loss.

3. Ab Initio Methods Theory

The aim of ab initio methods is to predict macroscopic properties of materials from basic principles, i.e. that of quantum mechanics. Knowing only the quantum mechanical nature of electrons and ions and microscopic properties such as atomic positions, ab initio simulations intend to predict macroscopic, observable properties of materials.

Concepts such as Density Functional Theory provide an exciting practical application of quantum mechanics. When only the quantum properties of a material are required to simulate it, a researcher could theoretically be free to explore any possible scenario governed by the laws of physics. Furthermore, the following section on Density Functional Theory assumes no particularly advanced knowledge of quantum mechanics, only familiarity with the Schrödinger equation and mathematical principles related to the many-electron wavefunction.

3.1. Fundamentals of Density Functional Theory

Density Functional Theory is a reformulation of Quantum Mechanics which aims to make using quantum mechanical principles more computationally feasible for many-body systems.

For instance, in a bulk crystal, there are many atoms arranged in a lattice. If the lattice has N electrons, and each of these has a position in 3-dimensional space, then the many-body Schrödinger equation is a function of $3N$ variables. To solve this problem, Hohenberg and Kohn proposed in [20] that the energy of a quantum mechanical system of electrons can be written as a functional of the **electron density**, which is a function of position (that is, 3 variables) instead of a wavefunction of N electrons. Below, this thesis will go over this method of reformulating the many body problem using functionals of the electron density.

3.1.1. Defining the Electron Density

The necessary first step in formulating Density Functional Theory is to define the electron density $n(\mathbf{r})$ of a many-particle wavefunction.

The electron density $n(\mathbf{r})$ can be treated as an observable quantity in quantum mechanics, i.e as the expectation value of some density operator $\hat{n}$. For some many-electron wavefunction

$\Psi(\mathbf{r}_1, s_1, \mathbf{r}_2, s_2, ...\mathbf{r}_N, s_N)$, where $\mathbf{r}_i$ and s_i denote the position and spin of the i'th electron respectively, the electron density is given by:

$$n(\mathbf{r}) = \langle \Psi | \hat{n} | \Psi \rangle \tag{11}$$

The electron density operator, to yield an electron density as a function of $\mathbf{r}$, must find the probability for each electron position $\mathbf{r}_i$ to be at $\mathbf{r}$. Hence $\hat{n}$ is defined as:

$$\hat{n} = \sum_{i=1}^{N} \delta(\mathbf{r} - \mathbf{r}_i) \tag{12}$$

The Dirac Delta function in the operator ensures that to contribute to the density at $\mathbf{r}$, the i'th electron must have $\mathbf{r}_i = \mathbf{r}$. We can now derive the electron density for the multi-electron wavefunction:

$$\begin{aligned} n(\mathbf{r}) &= \int ... \int \Psi^*(\mathbf{r}_1, s_1, ...\mathbf{r}_N, s_N) \sum_{i=1}^{N} \delta(\mathbf{r} - \mathbf{r}_i) \Psi(\mathbf{r}_1, s_1, ...\mathbf{r}_N, s_N) \mathrm{d}\mathbf{r}_1 ... \mathrm{d}\mathbf{r}_N \\ &= \int ... \int \left[\sum_{i=1}^{N} \delta(\mathbf{r} - \mathbf{r}_i) \right] |\Psi(\mathbf{r}_1, s_1, ...\mathbf{r}_N, s_N)|^2 \mathrm{d}\mathbf{r}_1 ... \mathrm{d}\mathbf{r}_N \\ &= \int ... \int |\Psi(\mathbf{r}, s_1, ...\mathbf{r}_N, s_N)|^2 \mathrm{d}\mathbf{r}_2 ... \mathrm{d}\mathbf{r}_N \\ &\quad + \int ... \int \left[\sum_{i=2}^{N} \delta(\mathbf{r} - \mathbf{r}_i) \right] |\Psi(\mathbf{r}_1, s_1, ...\mathbf{r}_N, s_N)|^2 \mathrm{d}\mathbf{r}_1 ... \mathrm{d}\mathbf{r}_N \end{aligned} \tag{13}$$

The equation becomes a sum of N integrals, each containing a delta function. However, electrons are indistinguishable particles, and so the labels $\mathbf{r}_1, \mathbf{r}_2$ etc are arbitrary and interchangeable. Hence every integral in the sum will yield the same result as the first. As a final answer, we can write:

$$n(\mathbf{r}) = N \int ... \int |\Psi(\mathbf{r}, s_1, \mathbf{r}_2, s_2 ... \mathbf{r}_N, s_N)|^2 \mathrm{d}\mathbf{r}_2 ... \mathrm{d}\mathbf{r}_N \tag{14}$$

Now, in Density Functional Theory, the electrons of a many-electron system are modelled as single electrons inside an external potential (these are the Kohn-Sham equations that are discussed further on in this section). Because of this, it is necessary to express the many-electron wavefunction (and hence the density) in terms of single-electron states. To that end, we write the many-particle wavefunction Ψ as a Slater determinant. This formulation was derived by Slater in 1929 in [21]. In DFT, this approximation is known as the Hartree-Fock approximation [22]. A wavefunction expressed as a Slater determinant reads:

$$\Psi \approx \Phi = \frac{1}{\sqrt{N!}} \begin{vmatrix} \phi_1(\mathbf{r}_1, s_1) & \phi_2(\mathbf{r}_1, s_1) & \cdots & \phi_N(\mathbf{r}_1, s_1) \\ \phi_1(\mathbf{r}_2, s_2) & \phi_2(\mathbf{r}_2, s_2) & \cdots & \phi_N(\mathbf{r}_2, s_2) \\ \vdots & \vdots & \ddots & \vdots \\ \phi_1(\mathbf{r}_N, s_N) & \phi_2(\mathbf{r}_N, s_N) & \cdots & \phi_N(\mathbf{r}_N, s_N) \end{vmatrix} \tag{15}$$

The functions ψ_i are called **spin-orbitals**. If we assume there is no spin-orbit interaction, the spin-orbitals can be written as products of a spatial function and a spin-dependent function.

The Slater determinant formulation will allow us to not only simplify the expression for electron density, but also to easily work out expectation values for any many-particle Hermitian operators that are a sum of single particle operators (such as the Coulomb interactions which will be encountered further in this section). We will illustrate this for the case $N = 3$ below, but the same argument can be applied for arbitrary N.

Suppose we have a Hermitian operator that is a sum of single particle operators, $\hat{H} = \sum_i^N \hat{h}$ - the operator $\hat{n}$ defined earlier would fit into this category. We consider $N = 3$, with 3 single particle states $\alpha(\mathbf{r}_1), \beta(\mathbf{r}_2)$ and $\gamma(\mathbf{r}_3)$ such that a many particle wavefunction can be expressed as the Slater determinant:

$$\begin{aligned}\Psi(\mathbf{r}_1, \mathbf{r}_2, \mathbf{r}_3) \approx &\frac{1}{\sqrt{6}}[\alpha(\mathbf{r})_1\beta(\mathbf{r}_2)\gamma(\mathbf{r}_3) - \alpha(\mathbf{r}_1)\beta(\mathbf{r}_3)\gamma(\mathbf{r}_2) \\ &- \alpha(\mathbf{r}_2)\beta(\mathbf{r}_1)\gamma(\mathbf{r}_3) + \alpha(\mathbf{r}_2)\beta(\mathbf{r}_3)\gamma(\mathbf{r}_1) \\ &+ \alpha(\mathbf{r}_3)\beta(\mathbf{r}_1)\gamma(\mathbf{r}_2) - \alpha(\mathbf{r}_3)\beta(\mathbf{r}_2)\gamma(\mathbf{r}_1)] \\ = &\frac{1}{\sqrt{6}}\det(\alpha, \beta, \gamma)\end{aligned} \tag{16}$$

Where $\det(\alpha, \beta, \gamma)$ is a shorthand notation for the determinant expressed above. Now, we can evaluate the expectation value:

$$\langle\Psi|\hat{H}|\Psi\rangle = \frac{1}{6}\int\int\int \det(\alpha, \beta, \gamma)^*\hat{H}\det(\alpha, \beta, \gamma)\mathrm{d}\mathbf{r}_1\mathrm{d}\mathbf{r}_2\mathrm{d}\mathbf{r}_3 \tag{17}$$

Due to orthonormality, this integral yields $N!$ times the first term. This is shown explicitly in Appendix A in the case of two states for simplicity. Hence, we are left with two simple products in the integral:

$$\langle\Psi|\hat{H}|\Psi\rangle = \int\int\int \left(\alpha(\mathbf{r}_1)\beta(\mathbf{r}_2)\gamma(\mathbf{r}_3)\right)^* \hat{H}\left(\alpha(\mathbf{r}_1)\beta(\mathbf{r}_2)\gamma(\mathbf{r}_3)\right)\mathrm{d}\mathbf{r}_1\mathrm{d}\mathbf{r}_2\mathrm{d}\mathbf{r}_3 \tag{18}$$

We now have an expectation value with a product of single particle wavefunctions, and an operator which is a sum of single particle operators, which can be expressed as a trace over single-particle operators, $\langle\Psi|\hat{H}|\Psi\rangle = \sum_i^N \langle\psi_i|\hat{h}|\psi_i\rangle$.

We now return to the electron density. It can now be expressed as:

$$\begin{aligned}n(\mathbf{r}) &= \langle\Psi|\hat{n}|\Psi\rangle \\ &= \left\langle \alpha(\mathbf{r}_1)\beta(\mathbf{r}_2)\gamma(\mathbf{r}_3)\left|\sum_{i=1}^{3}\delta(\mathbf{r}-\mathbf{r}_i)\right|\alpha(\mathbf{r}_1)\beta(\mathbf{r}_2)\gamma(\mathbf{r}_3)\right\rangle \\ &= \langle\alpha(\mathbf{r}_s)|\delta(\mathbf{r}-\mathbf{r}_s)|\alpha(\mathbf{r}_s)\rangle + \langle\beta(\mathbf{r}_s)|\delta(\mathbf{r}-\mathbf{r}_s)|\beta(\mathbf{r}_s)\rangle + \langle\gamma(\mathbf{r}_s)|\delta(\mathbf{r}-\mathbf{r}_s)|\gamma(\mathbf{r}_s)\rangle \\ &= \int\delta(\mathbf{r}-\mathbf{r}_s)|\alpha(\mathbf{r}_s)|^2\mathrm{d}\mathbf{r}_s + \int\delta(\mathbf{r}-\mathbf{r}_s)|\beta(\mathbf{r}_s)|^2\mathrm{d}\mathbf{r}_s + \int\delta(\mathbf{r}-\mathbf{r}_s)|\gamma(\mathbf{r}_s)|^2\mathrm{d}\mathbf{r}_s \\ &= |\alpha(\mathbf{r})|^2 + |\beta(\mathbf{r})|^2 + |\gamma(\mathbf{r})|^2\end{aligned} \tag{19}$$

When the integral was separated into a sum of 3 integrals, the labels $\mathbf{r}_1, \mathbf{r}_2, \mathbf{r}_3$ became arbitrary - electrons are indistinguishable and each of those labels represent electronic position - hence they were replaced with a single variable $\mathbf{r}_s$.

Similarly, for the case of an arbitrary N, if we express a multi-particle wavefunction $\Psi(\mathbf{r}_1, \mathbf{r}_2, ...\mathbf{r}_N)$ as a Slater determinant of single particle states $\psi_1, \psi_2 ... \psi_N$, the electron density is given by:

$$n(\mathbf{r}) = \sum_{i=1}^{N} |\psi_i(\mathbf{r})|^2 \tag{20}$$

The expression above will be the most relevant in this thesis' discussion of DFT. If the single-electron wavefunctions $\psi_i(\mathbf{r})$ are normalised, we can see that:

$$\int n(\mathbf{r}) \mathrm{d}\mathbf{r} = N \tag{21}$$

Intuitively, this makes sense - if density of particles is the number of particles per unit volume, then the total number of particles over the entire volume should be N, the total number of electrons in the system.

We can also use the definition of the electron density in Equation 20 to express integrals over all the electronic variables as integrals of the electron density. If we consider a potential $V(\mathbf{r}) = \sum_i v(\mathbf{r}_i)$, the expectation value is:

$$\begin{aligned} \langle \Psi | V(\mathbf{r}) | \Psi \rangle &= \sum_{i}^{N} \langle \psi_i | v(\mathbf{r}) | \psi_i \rangle \\ &= \sum_{i}^{N} \int \psi_i^* v(\mathbf{r}) \psi_i \mathrm{d}\mathbf{r} \\ &= \int \sum_{i}^{N} |\psi_i|^2 v(\mathbf{r}) \mathrm{d}\mathbf{r} \\ &= \int n(\mathbf{r}) v(\mathbf{r}) \mathrm{d}\mathbf{r} \end{aligned} \tag{22}$$

The property above, as well as the definitions of electron density will be vital in the formulation of DFT that is presented in the following sections.

3.1.2. The Hohenberg-Kohn Theorems and their Proofs

In order to reformulate the many-body problem in terms of the electron density, it must first be proven that this is a valid and unique approach.

1. Suppose we have an electronic many-particle Hamiltonian:

$$\hat{H} = \hat{T} + \hat{W} + V_{ext}(\mathbf{r}) \tag{23}$$

Where $\hat{W}$ represents any additional potential terms that are not a part of the external potential. Define $\mathfrak{r} = \{\mathbf{r}_i\} = \mathbf{r}_1, \mathbf{r}_2, ...\mathbf{r}_N$. The first Hohenberg-Kohn theorem states that [20] *no two different external potentials $V_{ext}(\boldsymbol{r})$ (except by an additive constant) can yield the same ground state electron density, $n(\boldsymbol{r})$.* There is a one-to-one correspondence between the set of all $n(\mathbf{r})$ and the set of all $V_{ext}(\mathbf{r})$. This theorem can be proven by contradiction. For ease of notation, let $\Psi_0(\mathfrak{r}) = \Psi_0$ and $\Psi_0'(\mathfrak{r}) = \Psi_0'$, where Ψ_0 and Ψ_0' represent ground state many particle wavefunctions. The electron density is defined according to Equation 14. Suppose we have two different external potentials such that:

$$\begin{aligned} \hat{H}|\Psi_0\rangle &= \left(\hat{T} + \hat{W} + V_{ext}(\mathbf{r})\right)|\Psi_0\rangle = E_0|\Psi_0\rangle \\ \hat{H}'|\Psi_0'\rangle &= \left(\hat{T} + \hat{W} + V_{ext}'(\mathbf{r})\right)|\Psi_0'\rangle = E_0'|\Psi_0'\rangle \end{aligned} \tag{24}$$

That is, the Hamiltonian $\hat{H}$ yields the ground state energy E_0 and the ground state electron wavefunction $|\Psi_0\rangle$, and similarly, the Hamiltonian $\hat{H}'$ yields the ground state energy E_0' and the ground state electron wavefunction $|\Psi_0'\rangle$. We are also assuming that for any constant C,

$$V_{ext}'(\mathbf{r}) \neq V_{ext}(\mathbf{r}) + C \tag{25}$$

Also,

$$V_{ext}(\mathbf{r}) = \sum_i v_{ext}(\mathbf{r}_i) \tag{26}$$

For our proof, assume that the first Hohenberg-Kohn theorem is wrong and that both potentials, that is both Hamiltonians yield ground state wavefunctions with the same electron density. The electron density is defined as the squared modulus of the wavefunction, so we assume that

$$n(\mathbf{r}) = N\int |\Psi_0(\mathbf{r}, \mathbf{r}_2...\mathbf{r}_N)|^2 \mathrm{d}\mathbf{r}_2...\mathrm{d}\mathbf{r}_N = N\int |\Psi_0'(\mathbf{r}, \mathbf{r}_2...\mathbf{r}_N)|^2 \mathrm{d}\mathbf{r}_2...\mathrm{d}\mathbf{r}_N \tag{27}$$

We know that for a given Hamiltonian, assuming non-degenerate ground states, the ground state energy given by a ground state wavefunction will always be less than the energy given by some other, trial wavefunction $\Psi_T \neq \Psi_0$ (the variational principle of quantum mechanics - the ground state energy is the minimum energy of the system). Hence:

$$\begin{aligned} & E_0 = \langle\Psi_0|\hat{H}|\Psi_0\rangle < \langle\Psi_T|\hat{H}|\Psi_T\rangle \\ \implies\ & E_0 < \langle\Psi_0'|\hat{H}|\Psi_0'\rangle \\ \text{Similarly:}\ & \\ & E_0' < \langle\Psi_0|\hat{H}'|\Psi_0\rangle \end{aligned} \tag{28}$$

We can now expand the inequalities:

$$\begin{aligned}
E_0 &< \langle \Psi_0' | \hat{H} | \Psi_0' \rangle \\
E_0 &< \langle \Psi_0' | \left(\hat{T} + \hat{W} + V_{ext}(\mathbf{r}) \right) | \Psi_0' \rangle \\
E_0 &< \langle \Psi_0' | \left(\hat{T} + \hat{W} + V_{ext}(\mathbf{r}) + V'_{ext}(\mathbf{r}) - V'_{ext}(\mathbf{r}) \right) | \Psi_0' \rangle \\
E_0 &< \langle \Psi_0' | \hat{H}' | \Psi_0' \rangle + \langle \Psi_0' | \left(V_{ext}(\mathbf{r}) - V'_{ext}(\mathbf{r}) \right) | \Psi_0' \rangle \\
E_0 &< E_0' + \int \left[\Psi_0'^* \left(V_{ext}(\mathbf{r}) - V'_{ext}(\mathbf{r}) \right) \Psi_0' \right] \mathrm{d}\mathbf{r}_1 \mathrm{d}\mathbf{r}_2 ... \mathrm{d}\mathbf{r}_N \\
E_0 &< E_0' + \int n(\mathbf{r}) \left(v_{ext}(\mathbf{r}) - v'_{ext}(\mathbf{r}) \right) \mathrm{d}\mathbf{r} \qquad \text{(See Eq.22)}
\end{aligned} \tag{29}$$

Similarly:

$$E_0' < E_0 + \int n(\mathbf{r}) \left(v'_{ext}(\mathbf{r}) - v_{ext}(\mathbf{r}) \right) \mathrm{d}\mathbf{r}$$

If we sum the two inequalities for E_0 and E_0', we get:

$$E_0 + E_0' < E_0' + E_0 \tag{30}$$

This is a contradiction. Hence our assumption that the potentials yield the same electron density is wrong, that is the two integrals in Equation 27 are infact not equal. The ground state electron density uniquely determines the external potential.

2. The second Hohenberg-Kohn theorem states that [20] *the energy of a system is a unique functional of the electron density, it can be written as* $E[n(\boldsymbol{r})]$. *There exists a "universal functional"* $F[n(\boldsymbol{r})]$ *such that for the ground state electron density,* $E[n(\boldsymbol{r})]$ *is minimised and yields the ground state energy.* $E[n(\boldsymbol{r})]$ *is the defined in the form:*

$$E[n(\mathbf{r})] = F[n(\mathbf{r})] + \int n(\mathbf{r}) v_{ext}(\mathbf{r}) \mathrm{d}\mathbf{r} \tag{31}$$

To derive the definition of $E[n(\mathbf{r})]$, we write out the expression for the energy of a many-body system, with $\hat{T}$ representing the kinetic energy operator and $\hat{U}$ representing the potential experienced from particles interacting with each other:

$$\begin{aligned}
E[n(\mathbf{r})] &= \left\langle \Psi \left| \hat{T} + \hat{U} + V_{ext}(\mathbf{r}) \right| \Psi \right\rangle \\
E[n(\mathbf{r})] &= \left\langle \Psi \left| \hat{T} + \hat{U} \right| \Psi \right\rangle + \int n(\mathbf{r}) v_{ext}(\mathbf{r}) \mathrm{d}\mathbf{r} \\
E[n(\mathbf{r})] &= F[n(\mathbf{r})] + \int n(\mathbf{r}) v_{ext}(\mathbf{r}) \mathrm{d}\mathbf{r}
\end{aligned} \tag{32}$$

The functional $F[n(\mathbf{r})]$ does not depend on a system's unique external potential and so is the same for any many-electron system.

Now, to prove that the ground-state electron density minimises the energy functional: consider a ground-state wavefunction Ψ_0 that yields a ground state electron density n,

and a trial wavefuction Ψ_T that yields a different electron density n_T. Because of the variational principle,

$$\begin{aligned} E[n] &= \left\langle \Psi_0 \left| \hat{T} + \hat{U} + V_{ext}(\mathbf{r}) \right| \Psi_0 \right\rangle \\ E[n_T] &= \left\langle \Psi_T \left| \hat{T} + \hat{U} + V_{ext}(\mathbf{r}) \right| \Psi_T \right\rangle \\ \implies E[n] &< E[n_T] \end{aligned} \tag{33}$$

Hence, the energy functional is minimised by the ground-state electron density.

The two theorems above form the foundation of DFT. In practice, for many-body systems, $F[n(\mathbf{r})]$ is approximated with the Kohn-Sham equations, which will be discussed further on in this section. The ground state electron density in the variational principle is typically characterised by imposing normalisation using the Lagrange Multiplier method [23].

3.1.3. The Dynamical Matrix and the Kohn-Sham Equations

We wish to model a crystal lattice, a system of many interacting nuclei and electrons in order to study the lattice dynamical and electronic properties of the system. The general first step taken is the **adiabatic** or **Born-Oppenheimer (BO) approximation**, initially outlined by by Born and Oppenheimer in [24]. The approximation assumes that, since nuclei have much higher mass and move at much lower velocities than electrons, electrons respond to changes in their environment much more quickly and can be modeled as moving in a field where the nuclei are at fixed positions. First we solve the many-electron Schrödinger equation for specific nuclear configurations, then the electronic energies contribute to a fixed potential energy surface (PES) for the nuclei. Then the nuclear Schrödinger equation can be solved and analysed for the (global) minimum of the PES, which allows one to calculate the vibrational properties of the system.

One should note that the BO approximation would be highly inaccurate in systems where the nuclear and electronic motion is strongly coupled. An example of this would be in certain chemical reactions [23], or systems containing light elements such as H, He, or Li.

Suppose we have a system where the BO approximation is valid, such as a crystal lattice. Let $\mathbf{R} = \{\mathbf{R}_1, \mathbf{R}_2, ...\mathbf{R}_{N_A}\} = \{\mathbf{R}_I\}$ be the set of all nuclear positions, or the nuclear configuration (with N_A the total number of nuclei), and $\mathbf{R}_I$ represents the position of nucleus I. The nuclear Schrödinger equation reads:

$$\left(-\sum_I \frac{\hbar^2}{2M_I} \frac{\partial^2}{\partial \mathbf{R}_I^2} + E(\mathbf{R}) \right) \Phi(\mathbf{R}) = \mathcal{E}\Phi(\mathbf{R}) \tag{34}$$

Where M_I is the mass of the I'th nucleus. $E(\mathbf{R})$ is the external potential that arises from the field of electrons surrounding the nuclei. It is called the **Born-Oppenheimer (BO) energy surface** or the **clamped-ion energy** [23]. $E(\mathbf{R})$ is in fact the ground state energy

for the system of electrons moving in the field of "fixed" nuclei. The electronic Schrödinger equation reads:

$$\hat{H}^{BO}_{\mathbf{R}}(\mathbf{r})\Psi_{\mathbf{R}}(\mathfrak{r}) = E(\mathbf{R})\Psi_{\mathbf{R}}(\mathfrak{r}) \tag{35}$$

The electronic wavefunction $\Psi_{\mathbf{R}}(\mathfrak{r})$ is a function of the electronic positions $\mathfrak{r} = \{\mathbf{r}_i\}$, for some fixed nuclear configuration $\mathbf{R}$, that is it depends parametrically on $\mathbf{R}$. The same is true for the Hamiltonian $\hat{H}^{BO}$, which represents the net energy of the system of electrons. It is called the Born-Oppenheimer Hamiltonian, and has the form:

$$\hat{H}^{BO} = -\frac{\hbar^2}{2m}\sum_i \frac{\partial^2}{\partial \mathbf{r}_i^2} + \frac{1}{2}\frac{e^2}{4\pi\varepsilon_0}\sum_i\sum_{j\neq i}\frac{1}{|\mathbf{r}_i - \mathbf{r}_j|} + \sum_i V_{\mathbf{R}}(\mathbf{r}_i) + E_N(\mathbf{R})$$

Where:

$$V_{\mathbf{R}}(\mathbf{r}_i) = -\frac{1}{4\pi\varepsilon_0}\sum_I \frac{Z_I e^2}{|\mathbf{r}_i - \mathbf{R}_I|} \tag{36}$$

$$E_N(\mathbf{R}) = \frac{1}{2}\frac{e^2}{4\pi\varepsilon_0}\sum_I\sum_{J\neq I}\frac{Z_I Z_J}{|\mathbf{R}_I - \mathbf{R}_J|}$$

The terms in the above Hamiltonian simply represent the kinetic energy and the electrostatic interaction energy that result from the electrons. The last two terms are labelled for ease of notation later on. To be consistent with other sources and for ease of notation, we will use atomic units such that the Coulomb constant $1/4\pi\varepsilon_0 = 1$. Z_I is the atomic number of the I'th nucleus, and $\mathbf{r}_i$ is the position of the i'th electron.

The system of nuclei will be at its equilibrium geometry when the net force F_I acting on each nucleus I is zero. Hence, at equilibrium,

$$F_I \equiv -\frac{\partial E(\mathbf{R})}{\partial \mathbf{R}_I} = 0 \tag{37}$$

Since $E(\mathbf{R})$ is a scalar function of multiple variables, its second derivative is a matrix, called the Hessian.

$$\mathbf{H} = \frac{\partial^2 E(\mathbf{R})}{\partial \mathbf{R}_I \partial \mathbf{R}_J} \tag{38}$$

This Hessian describes the dynamical behaviour and the interatomic forces of the system. It is called the **matrix of Interatomic Force Constants (IFCs)**, while its Fourier transform (used in the discussion for crystal lattices later on in this thesis) is called the **Dynamical Matrix**. The eigenvalues of the (scaled) matrix of IFCs are the **phonon frequencies**, denoted ω. A phonon is a collective atomic vibration, that can be modeled as a bosonic particle in Quantum Mechanics. It has an energy, momentum/wavevector, and polarization. Phonons are classified into **phonon modes**, which are given by the different eigenvectors of the matrix of IFCs. Hence to determine the phonon frequencies, we need to solve:

$$\det\left(\frac{1}{\sqrt{M_I M_J}}\frac{\partial^2 E(\mathbf{R})}{\partial \mathbf{R}_I \mathbf{R}_J} - \omega^2 \delta_{IJ}\right) = 0 \tag{39}$$

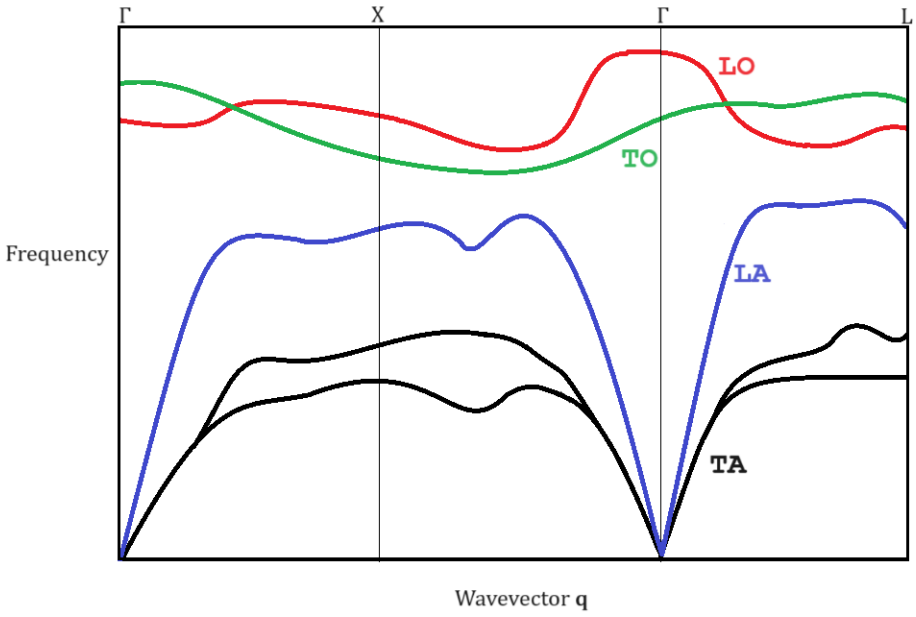

Figure 2: A schematic diagram of a phonon dispersion relation. The different phonon modes are labelled. Phonon frequency is depicted on the vertical axis, while the horizontal axis depicts wavevector. The labels Γ, X, L indicate specific points in the lattice, with Γ being $\mathbf{q} = (0, 0, 0)$. This format of the diagram allows us to visualise the magnitude of the phonon frequency along different paths, for example $\Gamma \to X \to \Gamma \to L$. It is worth noting that at Γ, acoustic phonon frequency vanishes.

Where δ_{IJ} is the identity matrix, and the matrix of IFCs is scaled by dividing it by the square roots of the nuclear masses.

When the phonon frequencies for a periodic crystal lattice are calculated numerically, they are typically plotted as a function of reciprocal space wavevectors $\mathbf{q}$. This is because working in reciprocal space (the Fourier transform of real space) is more convenient numerically as it coincides with the application of Bloch's theorem on the electronic wave function and on the lattice vibrations. The plot of $\omega(\mathbf{q})$ for each phonon mode is called the **Phonon Dispersion Relation** and typically looks like Fig 2. Points Γ, X and L are points on the first Brillouin Zone (BZ) (a primitive unit cell of a crystal defined in reciprocal space) of a cubic lattice.

Phonon modes which have zero frequency at the point Γ are called acoustic modes. Acoustic phonons which have a polarisation parallel to their wavevector $\mathbf{q}$ are called Longitudinal Acoustic (LA) phonons, and if their polarisation is perpendicular to the wavevector, they are called Transverse Acoustic (TA) phonons. Phonon modes which have non-zero frequency at the Γ point are called optical, and can be further split in semiconductors to Transverse Optical (TO) and Longitudinal Optical (LO) [25].

We now return to the task of finding the first and second derivatives of the BO energy surface, $E(\mathbf{R})$. The derivative can be found by using the Hellmann-Feynman (HF) Theorem. The

HF theorem has in fact been derived and proven independently by several physicists [26], including Wolfgang Pauli in 1922 in [27], however it is named after Hans Hellmann who proved it in 1937 in [28] and Richard Feynman who proved it in 1939 in [29].

The HF Theorem states that *for a Hamiltonian that depends on a parameter λ, the partial derivative of the expectation value is the expectation value of the partial derivative of the Hamiltonian.* So,

$$\begin{aligned} &\text{Given:} \\ &E_\lambda = \left\langle \Psi_\lambda \middle| \hat{H}_\lambda \middle| \Psi_\lambda \right\rangle \\ &\text{Then:} \\ &\frac{\partial E_\lambda}{\partial \lambda} = \left\langle \Psi_\lambda \middle| \frac{\partial \hat{H}_\lambda}{\partial \lambda} \middle| \Psi_\lambda \right\rangle \end{aligned} \tag{40}$$

Where Ψ_λ is an eigenfunction of the Hamiltonian corresponding to the eigenvalue E_λ. A proof of this theorem is as follows:

$$\begin{aligned} \frac{\partial E_\lambda}{\partial \lambda} &= \frac{\partial}{\partial \lambda} \left\langle \Psi_\lambda \middle| \hat{H}_\lambda \middle| \Psi_\lambda \right\rangle \\ &= \left\langle \frac{\partial \Psi_\lambda}{\partial \lambda} \middle| \hat{H}_\lambda \middle| \Psi_\lambda \right\rangle + \left\langle \Psi_\lambda \middle| \frac{\partial \hat{H}_\lambda}{\partial \lambda} \middle| \Psi_\lambda \right\rangle + \left\langle \Psi_\lambda \middle| \hat{H}_\lambda \middle| \frac{\partial \Psi_\lambda}{\partial \lambda} \right\rangle \\ &= \left\langle \frac{\partial \Psi_\lambda}{\partial \lambda} \middle| E_\lambda \Psi_\lambda \right\rangle + \left\langle \Psi_\lambda \middle| \frac{\partial \hat{H}_\lambda}{\partial \lambda} \middle| \Psi_\lambda \right\rangle + \left\langle \Psi_\lambda E_\lambda \middle| \frac{\partial \Psi_\lambda}{\partial \lambda} \right\rangle \\ &= E_\lambda \left[\left\langle \frac{\partial \Psi_\lambda}{\partial \lambda} \middle| \Psi_\lambda \right\rangle + \left\langle \Psi_\lambda \middle| \frac{\partial \Psi_\lambda}{\partial \lambda} \right\rangle \right] + \left\langle \Psi_\lambda \middle| \frac{\partial \hat{H}_\lambda}{\partial \lambda} \middle| \Psi_\lambda \right\rangle \\ &= E_\lambda \frac{\partial}{\partial \lambda} \left\langle \Psi_\lambda \middle| \Psi_\lambda \right\rangle + \left\langle \Psi_\lambda \middle| \frac{\partial \hat{H}_\lambda}{\partial \lambda} \middle| \Psi_\lambda \right\rangle \\ &= \left\langle \Psi_\lambda \middle| \frac{\partial \hat{H}_\lambda}{\partial \lambda} \middle| \Psi_\lambda \right\rangle \end{aligned} \tag{41}$$

This occurs because we assume Ψ_λ is normalised, hence $\langle \Psi_\lambda | \Psi_\lambda \rangle = 1$ and so its partial derivative yields zero.

Using the Hellman-Feynman Theorem we can now calculate the first derivative of the BO energy surface, the negative of which yields the force on each nucleus. Only the terms containing $V_{\mathbf{R}}(\mathbf{r})$ and $E_N(\mathbf{R})$ depend on $\mathbf{R}$, so only those terms are left when the partial derivative with respect to $\mathbf{R}_I$ is taken. Assuming that the wavefunction and electron density

are normalised:

$$\begin{aligned} F_I \equiv -\frac{\partial E(\mathbf{R})}{\partial \mathbf{R}_I} &= -\left\langle \Psi_{\mathbf{R}}(\mathfrak{r}) \left| \frac{\partial \hat{H}^{BO}_{\mathbf{R}}(\mathbf{r})}{\partial \mathbf{R}_I} \right| \Psi_{\mathbf{R}}(\mathfrak{r}) \right\rangle \\ &= -\left\langle \Psi_{\mathbf{R}}(\mathfrak{r}) \left| \sum_i \frac{\partial V_{\mathbf{R}}(\mathbf{r}_i)}{\partial \mathbf{R}_I} + \frac{\partial E_N(\mathbf{R})}{\partial \mathbf{R}_I} \right| \Psi_{\mathbf{R}}(\mathfrak{r}) \right\rangle \\ &= -\left\langle \Psi_{\mathbf{R}}(\mathfrak{r}) \left| \sum_i \frac{\partial V_{\mathbf{R}}(\mathbf{r}_i)}{\partial \mathbf{R}_I} \right| \Psi_{\mathbf{R}}(\mathfrak{r}) \right\rangle - \left\langle \Psi_{\mathbf{R}}(\mathfrak{r}) \left| \frac{\partial E_N(\mathbf{R})}{\partial \mathbf{R}_I} \right| \Psi_{\mathbf{R}}(\mathfrak{r}) \right\rangle \\ &= -\int \Psi^*_{\mathbf{R}}(\mathfrak{r}) \sum_i \frac{\partial V_{\mathbf{R}}(\mathbf{r}_i)}{\partial \mathbf{R}_I} \Psi_{\mathbf{R}}(\mathfrak{r}) \mathrm{d}\mathbf{r}_1 ... \mathrm{d}\mathbf{r}_N - \int \Psi^*_{\mathbf{R}}(\mathfrak{r}) \frac{\partial E_N(\mathbf{R})}{\partial \mathbf{R}_I} \Psi_{\mathbf{R}}(\mathfrak{r}) \mathrm{d}\mathbf{r}_1 ... \mathrm{d}\mathbf{r}_N \\ &= -\int n_{\mathbf{R}}(\mathbf{r}) \frac{\partial V_{\mathbf{R}}(\mathbf{r})}{\partial \mathbf{R}_I} \mathrm{d}\mathbf{r} - \frac{\partial E_N(\mathbf{R})}{\partial \mathbf{R}_I} \end{aligned} \tag{42}$$

Next, we compute the second derivative, given simply by the product rule for derivatives:

$$\frac{\partial^2 E(\mathbf{R})}{\partial \mathbf{R}_I \partial \mathbf{R}_J} = \int \frac{\partial n_{\mathbf{R}}(\mathbf{r})}{\partial \mathbf{R}_J} \frac{\partial V_{\mathbf{R}}(\mathbf{r})}{\partial \mathbf{R}_I} \mathrm{d}\mathbf{r} + \int n_{\mathbf{R}}(\mathbf{r}) \frac{\partial^2 V_{\mathbf{R}}(\mathbf{r})}{\partial \mathbf{R}_I \partial \mathbf{R}_J} \mathrm{d}\mathbf{r} + \frac{\partial E_N(\mathbf{R})}{\partial \mathbf{R}_I \partial \mathbf{R}_J} \tag{43}$$

This shows that the matrix of IFCs can be computed using the electron density, as opposed to the electronic wavefunction. This is in fact a special case of the second Hohenberg-Kohn theorem described earlier. In particular, the matrix of IFCs requires both the ground-state electron density $n_{\mathbf{R}}(\mathbf{r})$ and the partial derivative $\partial n_{\mathbf{R}}(\mathbf{r})/\partial \mathbf{R}_J$, the **linear response** of the density due to a change in nuclear configuration. The problem now remains to calculate these quantities.

This problem to determine $n_{\mathbf{R}(\mathbf{r})}$ is addressed by the theory of Walter Kohn and Leu Jeu Sham in [30], where they described a set of self-consistent equations to solve the Schrödinger equation for a system of interacting electrons. This is anologous to the Hartree-Fock method, first described by Douglas Rayner Hartree in [31] and [32].

Consider the system of interacting electrons. According to the Hohenberg-Kohn theorems, the system's ground state energy can be expressed as:

$$E[n(\mathbf{r})] = F[n(\mathbf{r})] + \int n(\mathbf{r}) V(\mathbf{r}) \mathrm{d}\mathbf{r} \tag{44}$$

Where the universal functional $F[n(\mathbf{r})]$ accounts for energy resulting from the electron's interacting amongst themselves, and $V(\mathbf{r})$ here denotes the external potential that interacts with the electron density (abbreviated from $n_{\mathbf{R}}(\mathbf{r})$ to $n(\mathbf{r})$ for ease of notation). In the case of our system of many nuclei and electrons (in a crystal lattice), the external potential acting on the electrons arises from the Coulomb forces due to the nuclei, which are assumed frozen in place in the BO approximation. The universal functional then includes the kinetic energy term as well as the electron-electron interaction. The electron-electron interaction can be

expressed as an integral over the electron density, however in doing so the term will now include an interaction of the electron with itself. This term is called the Hartree term, E_H.

$$F[n(\mathbf{r})] = T_0[n(\mathbf{r})] + E_H[n(\mathbf{r})] + E_{xc}[n(\mathbf{r})] \tag{45}$$

A term $E_{xc}[n(\mathbf{r})]$, called the **exchange-correlation functional**, is also added to the universal functional. It is simply a place-holder term that represents any other possible effects on the energy that have been unaccounted for, because their explicit form as functionals of $n(\mathbf{r})$ is not known. However, it is named the exchange-correlation functional because in practice, it represents electron "exchange" and "correlation" effects: "exchange" is a quantum mechanical effect that can cause two electrons to swap (exchange) wavefunctions, which causes a decrease in electron-electron repulsion; "correlation" refers to how an electron's motion may be influenced by other electrons.

We can now express the ground state energy, with the Hartree term written out explicitly:

$$E[n(\mathbf{r})] = T_0[n(\mathbf{r})] + \frac{e^2}{2}\int\int \frac{n(\mathbf{r})n(\mathbf{r}')}{|\mathbf{r}-\mathbf{r}'|}\mathrm{d}\mathbf{r}\mathrm{d}\mathbf{r}' + E_{xc}[n(\mathbf{r})] + \int n(\mathbf{r})V(\mathbf{r})\mathrm{d}\mathbf{r} \tag{46}$$

In the above equation, $\mathbf{r}$ can be thought of as $\mathbf{r}_i$ and $\mathbf{r}'$ can be thought of as $\mathbf{r}_j$ written in the definition of $\hat{H}^{BO}$, Equation 36. In numerical simulations, $E_{xc}[n(\mathbf{r})]$ needs to be approximated.

It was discussed in Section 3.1.1 that if the wavefunction $\Psi_{\mathbf{R}}(\mathfrak{r})$ of N electrons is approximated as a Slater determinant of many single particle spin-orbitals $\psi_n(\mathbf{r})$, we can write the electron density as a sum of the moduli of the single-particle states.

$$n(\mathbf{r}) = \sum_n^N |\psi_n(\mathbf{r})|^2 \tag{47}$$

Hence we can determine the approximate electron density by determining these single-particle states.

Let us a consider one single electron, with wavefunction $\psi_n(\mathbf{r})$ in our original system of interacting electrons that was expressed with $\Psi_{\mathbf{R}}(\mathfrak{r})$. The concept proposed by Kohn and Sham is to treat the electron-electron interaction term as part of the "external" potential acting on a single electron in the non-interacting reference system. The single electron Schrödinger equation can be written as:

$$\left(-\frac{\hbar^2}{2m}\frac{\partial^2}{\partial\mathbf{r}^2} + V_{SCF}(\mathbf{r})\right)\psi_n(\mathbf{r}) = \varepsilon_n\psi_n(\mathbf{r}) \tag{48}$$

For a single electron with wavefunction $\psi_n(\mathbf{r})$ in our original system of many electrons and many nuclei, the potential term $V_{SCF}(\mathbf{r})$ now incorporates the effects of other electrons, nuclei, and exchange and correlation.

$$V_{SCF}(\mathbf{r}) = V(\mathbf{r}) + e^2\int \frac{n(\mathbf{r}')}{|\mathbf{r}-\mathbf{r}'|}\mathrm{d}\mathbf{r}' + v_{xc}(\mathbf{r})$$

Where: (49)

$$v_{xc}(\mathbf{r}) = \frac{\delta E_{xc}[n(\mathbf{r})]}{\delta n(\mathbf{r})}$$

The term $v_{xc}(\mathbf{r})$ is called the **exchange-correlation potential** and is the functional derivative of the exchange-correlation energy.

The form of V_{SCF} is very similar to the functional derivative of Equation 46. We can write $T_0[n(\mathbf{r})] = \sum_n \left\langle \psi_n(\mathbf{r}) \left| -\frac{\hbar^2}{2m}\frac{\partial^2}{\partial \mathbf{r}} \right| \psi_n(\mathbf{r}) \right\rangle$, and shift all possible corrections into E_{xc}. Then:

$$\frac{\delta E[n(\mathbf{r})]}{\delta n(\mathbf{r})} = V_{SCF}(\mathbf{r}) + \frac{e^2}{2}\int \frac{n(\mathbf{r}')}{|\mathbf{r}-\mathbf{r}'|}\mathrm{d}\mathbf{r}' \tag{50}$$

In practice, the extra term containing the double integral can be incorporated into E_{xc}, such that $\delta E[(\mathbf{r})]/\delta n(\mathbf{r}) = V_{SCF}$.

Hence, we have modelled the electrons in the many electron system as single electrons under an external potential, V_{SCF}, which represents the same effects a single electron would experience if it were in a many-electron system. The one-electron Schrödinger equation can be solved for the wavefunctions $\psi_n(\mathbf{r})$, which are called the **auxilliary Kohn-Sham orbitals**, and their corresponding eigenvalues are given by ε_n (see Equation 48).

Equations 47, 48, and 49 form what are known as the **Kohn-Sham equations**. When these equations are solved numerically, one starts with an initial estimate for the electron density. That is then used to solve for V_{SCF}, which in turn is used to solve for the orbitals $\psi_n(\mathbf{r})$. The orbitals are then used to calculate a new value for the density. This process is repeated iteratively until the value for the density converges (becomes self-consistent). This is often referred to as Self-Consistent Field (SCF) calculation.

We can also find the relation between the single electron ground state energies, and the energy functional $E[n(\mathbf{r})]$, the BO energy surface. Note that the sum over all the single electron states n can also be taken as double the sum from states 1 to $N/2$, accounting for electrons of different spins occupying the same state. Otherwise, one can simply define ε_n in such a way that it is implied that each value arises twice, as opposed to each state and each ε_n being unique.

$$\begin{aligned}
\sum_n^N \varepsilon_n &= 2\sum_{n=1}^{N/2}\varepsilon_n = 2\sum_{n=1}^{N/2}\left\langle \psi_n(\mathbf{r}) \left| \left(-\frac{\hbar^2}{2m}\frac{\partial^2}{\partial \mathbf{r}} + V_{SCF}(\mathbf{r})\right)\right| \psi_n(\mathbf{r})\right\rangle \\
&= 2\sum_{n=1}^{N/2}\int \psi_n^*(\mathbf{r})\left(-\frac{\hbar^2}{2m}\frac{\partial^2}{\partial \mathbf{r}}\right)\psi_n(\mathbf{r})\mathrm{d}\mathbf{r} + 2\sum_{n=1}^{N/2}\int \psi_n^*(\mathbf{r})\psi_n(\mathbf{r})V_{SCF}(\mathbf{r})\mathrm{d}\mathbf{r} \\
&= T_0[n(\mathbf{r})] + \int n(\mathbf{r})V_{SCF}(\mathbf{r})\mathrm{d}\mathbf{r} \\
&= T_0[n(\mathbf{r})] + \int n(\mathbf{r})V(\mathbf{r})\mathrm{d}\mathbf{r} + \int n(\mathbf{r})\left(e^2\int \frac{n(\mathbf{r}')}{|\mathbf{r}-\mathbf{r}'|}\mathrm{d}\mathbf{r}'\right)\mathrm{d}\mathbf{r} + \int n(\mathbf{r})v_{xc}(\mathbf{r})\mathrm{d}\mathbf{r}
\end{aligned} \tag{51}$$

So the energy functional in terms of the Kohn-Sham orbital energies is:

$$E[n(\mathbf{r})] = 2\sum_{n=1}^{N/2}\varepsilon_n - \frac{e^2}{2}\int\int \frac{n(\mathbf{r})n(\mathbf{r}')}{|\mathbf{r}-\mathbf{r}'|}\mathrm{d}\mathbf{r}'\mathrm{d}\mathbf{r} + E_{xc}[n(\mathbf{r})] - \int n(\mathbf{r})v_{xc}\mathrm{d}\mathbf{r} \tag{52}$$

3.1.4. Application to crystals

Most Ab Initio software for crystalline systems such as Quantum Espresso use a Plane-Wave basis set [33] where the single electron wave function is expanded into Plane Waves using Bloch's theorem. Since the calculations in this thesis are presented for bulk crystalline silicon and Gallium Arsenide, the nuclei are arranged periodically, hence the potential which acts on the single electrons in the Kohn-Sham Schrödinger equation, V_{SCF} is periodic. Hence, the single electron wavefunctions can be expressed as plain waves multiplied by a lattice periodic amplitude function, as according to Bloch's Theorem, shown by Felix Bloch in [34].

$$\psi_n(\mathbf{r}) = e^{i\mathbf{k}\cdot\mathbf{r}} u_n(\mathbf{r}) \tag{53}$$

Here $\mathbf{k}$ indicates a point in reciprocal space, also called the wavevector, and $u_n(\mathbf{r})$ is a periodic function with the same periodicity as V_{SCF} and the bulk crystal. Recall that the electron wavefunction and hence the periodic function $u_n(\mathbf{r})$ depends parametrically on $\mathbf{R}$.

It was shown that the matrix of IFC's is given by $\frac{\partial^2 E(\mathbf{R})}{\partial \mathbf{R}_I \partial \mathbf{R}_J}$ and we can solve for the phonon frequencies using Equation 39, and the the IFC matrix can be found with Equation 43. We can break up Equation 43 into an electronic contribution (the first two terms), and an ionic contribution (the third term). Next, we wish to convert Equations 39 and 43 to reciprocal coordinate space for the numerical calculation. The following theory to carry out these steps can be found in [23]. We define the position of the I-th atom in terms of the the unit cell l and atom s within a unit cell.

$$\mathbf{R}_I \equiv \mathbf{R}_l + \mathbf{p}_s + \mathbf{z}_s(l) \tag{54}$$

Where $\mathbf{R}_l$ indicates the position of the l-th unit cell, $\mathbf{p}_s$ is the position of the s-th nucleus in said unit cell at equilibrium, and $\mathbf{z}_s(l)$ is the deviation from equilibrium of the s-th nucleus. Similarly, we can define $\mathbf{R}_J \equiv \mathbf{R}_m + \mathbf{p}_t + \mathbf{z}_t(m)$. We can see that $\partial \mathbf{R}_I = \partial \mathbf{z}_s$, hence the matrix of IFCs can be written, with respect to the components of $\mathbf{z}_s(l)$ and $\mathbf{z}_t(m)$:

$$C_{st}^{\alpha\beta}(l,m) \equiv \frac{\partial^2 E}{\partial z_s^\alpha(l) \partial z_t^\beta(m)} \tag{55}$$

Where α, β are the row and column indices of the matrix respectively. If we write the total number of unit cells in the lattice as N_c, the Fourier transform of $C_{st}^{\alpha\beta}(l,m)$ is given by:

$$\begin{aligned} \tilde{C}_{st}^{\alpha\beta}(\mathbf{q}) &\equiv \sum_{\mathbf{R}_I} e^{-i\mathbf{q}\cdot\mathbf{R}_I} C_{st}^{\alpha\beta}(l,m) \\ &= \frac{1}{N_c} \frac{\partial^2 E}{\partial z_s^{*\alpha}(\mathbf{q}) \partial z_t^\beta(\mathbf{q})} \end{aligned} \tag{56}$$

The term $\mathbf{z}_s(\mathbf{q})$ comes from the following expression for the position vector (or "distortion pattern") $\mathbf{R}_I$:

$$\mathbf{R}_I\left[\mathbf{z}_s(\mathbf{q})\right] = \mathbf{R}_l + \mathbf{p}_s + \mathbf{z}_s(\mathbf{q}) e^{i\mathbf{q}\cdot\mathbf{R}_l} \tag{57}$$

Now we can use the transformed matrix of IFCs to obtain the phonon frequencies (as a function of coordinates in reciprocal space) using the same determinant as before.

$$\det\left(\frac{1}{\sqrt{M_s M_t}}\tilde{C}_{st}^{\alpha\beta}(\mathbf{q}) - \omega^2(\mathbf{q})\right) = 0 \tag{58}$$

Similarly to how $\frac{\partial^2 E(\mathbf{R})}{\partial \mathbf{R}_I \partial \mathbf{R}_J}$ was derived, we can calculate for $\tilde{C}_{st}^{\alpha\beta}(\mathbf{q})$

$$\begin{aligned}
\tilde{C}_{st}^{\alpha\beta}(\mathbf{q}) &= \frac{1}{N_c}\left[\int \frac{\partial n_{\mathbf{R}}(\mathbf{r})}{\partial z_t^{\beta}(\mathbf{q})}\frac{\partial V_{\mathbf{R}}(\mathbf{r})}{\partial z_s^{\alpha}(\mathbf{q})}\mathrm{d}\mathbf{r} + \int n_{\mathbf{R}}(\mathbf{r})\frac{\partial^2 V_{\mathbf{R}}(\mathbf{r})}{\partial z_s^{\alpha}(\mathbf{q})\partial z_t^{\beta}(\mathbf{q})}\mathrm{d}\mathbf{r} + \frac{\partial^2 E_N(\mathbf{R})}{\partial z_s^{\alpha}(\mathbf{q})\partial z_t^{\beta}(\mathbf{q})}\right] \\
\tilde{C}_{st}^{\alpha\beta}(\mathbf{q}) &= \frac{1}{N_c}\left[\int \frac{\partial n_{\mathbf{R}}(\mathbf{r})}{\partial z_t^{\beta}(\mathbf{q})}\frac{\partial V_{\mathbf{R}}(\mathbf{r})}{\partial z_s^{\alpha}(\mathbf{q})}\mathrm{d}\mathbf{r} + \int n_{\mathbf{R}}(\mathbf{r})\frac{\partial^2 V_{\mathbf{R}}(\mathbf{r})}{\partial z_s^{\alpha}(\mathbf{q})\partial z_t^{\beta}(\mathbf{q})}\mathrm{d}\mathbf{r}\right] + {}^{ion}\tilde{C}_{st}^{\alpha\beta}(\mathbf{q})
\end{aligned} \tag{59}$$

The term ${}^{ion}\tilde{C}_{st}^{\alpha\beta}(\mathbf{q})$ is calculated from the nuclei-nuclei interaction energy and is independent of the electron density. An explicit derivation of the term in reciprocal space coordinates can be found in [23].

All that is needed now to calculate the remainder of the matrix of IFCs is the derivative of $V_{\mathbf{R}}(\mathbf{r})$ and of the electron density. The derivative of the electron density is given by the variation of the electron density, which needs to be determined using Density Functional Perturbation theory. This prodecure is carried out in Section 3.2. The term $V_{\mathbf{R}}(\mathbf{r})$ is the electron-nucleus interaction energy. It is often approximated by defining some "pseudopotential", v_s, such that [23]:

$$\begin{aligned}
V_{\mathbf{R}}(\mathbf{r}) &= \sum_I v_s(\mathbf{r} - \mathbf{R}_I) \\
V_{\mathbf{R}}(\mathbf{r}) &= \sum_l \sum_s v_s(\mathbf{r} - \mathbf{R}_l - \mathbf{p}_s - \mathbf{z}_s(l))
\end{aligned} \tag{60}$$

A pseudopotential is an approximation for the true electron-ion interaction energy. The pseudopotential assumes that the inner electrons of the atom are fixed, and accounts for their contribution as part of a potential that acts only on the valence electrons.

The final obstacle that remains to solving the Kohn-Sham system is finding suitable approximations for the exchange correlation functional.

3.1.5. Exchange-Correlation Functionals

An in-depth discussion of various exchange-correlation functionals is beyond the scope of this thesis, but we will indroduce the main types that are most commonly used.

The **Local Density Approximation** (LDA) was initially introduced by Kohn and Sham in 1965 in [30]. The system is divided into several small, equal volumes which are each assumed

to contribute the same exchange-correlation energy. Each volume is small enough such that the electron density within is approximated to be constant. Then at each coordinate $\mathbf{r}$, the constant density contributes an exchange-correlation energy $\varepsilon_{xc}(n)$. The total exchange-correlation energy is given by:

$$E_{xc}^{LDA} = \int \varepsilon_{xc}(n) n(\mathbf{r}) \mathrm{d}\mathbf{r} \tag{61}$$

The energy $\varepsilon_{xc}(n)$ is calculated numerically, and is typically written as a sum of exchange and correlation parts $\varepsilon_{xc}(n) = \varepsilon_x(n) + \varepsilon_c(n)$ Clearly in the case of the uniform electron gas, where the electron density is constant everywhere, the LDA is exact and no longer an approximation. However even for more complex systems, it has proven to be surprisingly accurate when calculating some properties (structure, phonon frequency, bulk modulus, bond length) for materials with weak correlation [23].

The LDA approximation can also be written as a function of densities for spin-up and spin-down electrons explicitly, where it is called the Local Spin Density Approximation (LDSA).

The **Generalized Gradient Approximation** was introduced by Axel D. Becke in 1988 [35], Perdew et al in 1993 [36] and Langreth and Mehl in 1984 [37]. It supposes that the exchange-correlation energy for a coordinate $\mathbf{r}$ is a function of both the electron density as well as the gradient of the electron density, in order to account for a system with non-uniform electron density.

$$E_{xc}^{GGA} = \int \varepsilon_{xc}(n, \nabla n) n(\mathbf{r}) \mathrm{d}\mathbf{r} \tag{62}$$

The energy $\varepsilon_{xc}(n, \nabla n) n(\mathbf{r})$ also needs to be calculated numerically. One type of GGA functional that is used later in this thesis is the "Perdew-Burke-Ernzerhof" (PBE) functional, introduced in [38].

GGA functionals generally have more accurate correlation energies than LDA functionals [23].

The third most common type of exchange-correlation functionals are **Hybrid Functionals**. These were presented and analysed by Axel D. Becke in 1993 in [39]. To construct the hybrid functional, we first define an exchange-correlation potential U_{xc}^{λ}, where λ represents electron-electron coupling strength. The exchange correlation energy is the integral of the potential, and this integral is then approximated by linear interpolation:

$$\begin{aligned} E_{xc}^{Hy} &= \int_0^1 U_{xc}^{\lambda} \mathrm{d}\lambda \\ &\approx \frac{1}{2} U_{xc}^{0} + \frac{1}{2} U_{xc}^{1} \end{aligned} \tag{63}$$

But, at $\lambda = 0$, there is no electron-electron coupling. Hence U_{xc}^{0} represents exchange energy only, and can be represented exactly by the Hartree-Fock exchange energy functional:

$$E_x^{HF} = -\frac{1}{2} \int \int \frac{\psi_i(\mathbf{r})^* \psi_j(\mathbf{r}')^* \psi_j(\mathbf{r}) \psi_i(\mathbf{r}')^*}{|\mathbf{r} - \mathbf{r}'|} \mathrm{d}\mathbf{r} \mathrm{d}\mathbf{r}' \tag{64}$$

E_x needs to be solved for numerically. Next, the term U_{xc}^1 is approximated by any other approximations for the exchange-correlation energy. In [39], Becke proposes using the LSDA functional. For increased accuracy, the factors of $1/2$ can be replaced with some parameters C_0 and C_1 which are adjusted according to whichever gives the best accuracy when compared to experiment. Hence, the hybrid functional reads:

$$E_{xc}^H = C_0 E_x^{HF} + C_1 E_{xc}^{LSDA} \tag{65}$$

The hybrid functional has been shown to give very accurate results for the exchange correlation energy when compared to experiment [39].

A type of hybrid functional that is be used later in this thesis is the Heyd–Scuseria–Ernzerhof (HSE) functional, presented by Jochen Heyd, Gustavo E. Scuseria and Matthias Ernzerhof in 2003 in [40]. In 2006 some corrections were made to parameters used by the HSE functional [41, 42], and this new version is labelled as HSE06.

3.2. DFPT and the Variation of the Electron Density

The procedure to calculate the matrix of IFCs using DFT is called **Density Functional Perturbation Theory** (DFPT) [23]. The process of combining the Hartree-Fock method with the Perturbation Theory of Quantum Mechanics was first done by R. M. Sternheimer in 1954 in [43] to calculate electronic polarizabilities.

In Equation 43 it was seen that the matrix of IFCs requires both the electron density, and the linear response of the electron density, $\partial n(\mathbf{r})/\partial \mathbf{R}_J$. To find the derivative of the electron density, the Kohn-Sham equations must be linearised. In order to do this, we must first define the "finite-difference operator": suppose we have a function $\mathcal{F}(x)$ which depends parametrically on λ, we define a finite-difference operator Δ^λ as [23]:

$$\Delta^\lambda \mathcal{F}_\lambda(x) = \sum_i \frac{\partial \mathcal{F}_\lambda}{\partial \lambda_i} \Delta^\lambda \lambda_i \tag{66}$$

Using the operator, we can linearise Equation 47, the electron density. Applying the finite-difference operator to the electron density will yield the change in the density at each $\mathbf{r}$, due to variations in nuclear configuration $\mathbf{R}$.

$$\begin{aligned}
\Delta^{\mathbf{R}} n_{\mathbf{R}}(\mathbf{r}) &= \Delta^{\mathbf{R}} \left[2 \sum_{n=1}^{N/2} |\psi_n(\mathbf{r})|^2 \right] \\
&= 2 \sum_{n=1}^{N/2} \sum_I \left[\frac{\partial}{\partial \mathbf{R}_I} (\psi_n^*(\mathbf{r}) \psi_n(\mathbf{r})) \Delta^{\mathbf{R}} \mathbf{R}_I \right] \\
&= 2 \sum_{n=1}^{N/2} \sum_I \left[\left(\psi_n^*(\mathbf{r}) \frac{\partial \psi_n(\mathbf{r})}{\partial \mathbf{R}_I} + \psi_n(\mathbf{r}) \frac{\partial \psi_n^*(\mathbf{r})}{\partial \mathbf{R}_I} \right) \Delta^{\mathbf{R}} \mathbf{R}_I \right]
\end{aligned} \tag{67}$$

We can see above that the two terms in the round brackets are complex conjugates of each other, that is $\psi_n^*(\mathbf{r})\frac{\partial\psi_n(\mathbf{r})}{\partial\mathbf{R}_I} = \left(\psi_n(\mathbf{r})\frac{\partial\psi_n^*(\mathbf{r})}{\partial\mathbf{R}_I}\right)^*$. Now we can use the fact that for an arbitrary complex number $\phi = a + ib$, the sum of it and its complex conjugate $\phi + \phi^* = 2a = 2\text{Re}(\phi)$. Hence:

$$\begin{aligned}\Delta^{\mathbf{R}} n_{\mathbf{R}}(\mathbf{r}) &= 2\sum_{n=1}^{N/2}\sum_I \left[2\text{Re}\left(\psi_n^*(\mathbf{r})\frac{\partial\psi_n(\mathbf{r})}{\partial\mathbf{R}_I}\right)\Delta^{\mathbf{R}}\mathbf{R}_I\right] \\ &= 4\sum_{n=1}^{N/2}\left[\text{Re}\left(\psi_n^*(\mathbf{r})\sum_I\frac{\partial\psi_n(\mathbf{r})}{\partial\mathbf{R}_I}\right)\Delta^{\mathbf{R}}\mathbf{R}_I\right]\end{aligned} \tag{68}$$

Finally, the variation in the electron density can be expressed as:

$$\Delta^{\mathbf{R}} n_{\mathbf{R}}(\mathbf{r}) = 4\text{Re}\left[\sum_{n=1}^{N/2}\psi_n^*(\mathbf{r})\Delta^{\mathbf{R}}\psi_n(\mathbf{r})\right] \tag{69}$$

This means that to find the variation in the electron density, we need $\Delta^{\mathbf{R}}\psi_n(\mathbf{r})$, the variation of the auxiliary KS orbitals. This is solved by writing the problem in terms of first order Quantum Mechanical perturbation theory.

Suppose we have a ground state Hamiltonian $\hat{H}_0$, state $|n^0\rangle$ and energy E_n^0. Then suppose that the Hamiltonian is perturbed by a potential, or perturbation $\hat{V}$, which yields the eigenvectors $|n\rangle$ and eigenvalues E_n. The first order perturbation theory equation reads [44]:

$$\hat{H}_0\left|n^{(1)}\right\rangle + \hat{V}\left|n^0\right\rangle = E_n^0\left|n^{(1)}\right\rangle + E_n^{(1)}\left|n^{(0)}\right\rangle \tag{70}$$

Where $\left|n^{(1)}\right\rangle$ and $E_n^{(1)}$ are the first order variations of $\left|n^{(0)}\right\rangle$ and E_n^0 respectively. Higher order terms have been neglected.

In the notation used for our Kohn-Sham system, the ground state $\left|n^{(0)}\right\rangle$ is written as the KS orbital ψ_n, and its first order variation is represented by $\Delta^{\mathbf{R}}\psi_n$. The orbital's corresponding eigenvalue is ε_n and its variation can be expressed as $\Delta^{\mathbf{R}}\varepsilon_n$. The Kohn-Sham Hamiltonian, $\hat{H}_{KS}$ is given by Equation 48. Suppose that the Kohn-Sham system is perturbed by some variation $\hat{V} = \Delta^{\mathbf{R}}V_{SCF}$. Then:

$$\begin{aligned}\hat{H}_{KS}\left|\Delta^{\mathbf{R}}\psi_n\right\rangle + \Delta^{\mathbf{R}}V_{SCF}\left|\psi_n\right\rangle &= \varepsilon_n\left|\Delta^{\mathbf{R}}\psi_n\right\rangle + \Delta^{\mathbf{R}}\varepsilon_n\left|\psi_n\right\rangle \\ \left(\hat{H}_{KS} - \varepsilon_0\right)\left|\Delta^{\mathbf{R}}\psi_n\right\rangle &= -\left(\Delta^{\mathbf{R}}V_{SCF} - \Delta^{\mathbf{R}}\varepsilon_n\right)\left|\psi_n\right\rangle\end{aligned} \tag{71}$$

Equation 71 above is the first order perturbation theory equation for the Kohn-Sham system [23]. This equation is analogous to the Sternheimer Equation used in atomic physics, derived by Sternheimer in [43].

The variation (first order correction) of the ground state energy ε_n is also given by first-order perturbation theory.

$$\Delta^{\mathbf{R}}\varepsilon_n = \left\langle\psi_n\left|\Delta^{\mathbf{R}}V_{SCF}\right|\psi_n\right\rangle \tag{72}$$

The variation in the SCF potential is simply the sum of the variation of all the terms:

$$\begin{aligned}\Delta^{\mathbf{R}}V_{SCF} =&\Delta^{\mathbf{R}}V(\mathbf{r}) + e^2\int\frac{\Delta^{\mathbf{R}}n(\mathbf{r}')}{|\mathbf{r}-\mathbf{r}'|}\mathrm{d}\mathbf{r}' + \Delta^{\mathbf{R}}v_{xc}(n(\mathbf{r}))\\ =&\Delta^{\mathbf{R}}V(\mathbf{r}) + e^2\int\frac{\Delta^{\mathbf{R}}n(\mathbf{r}')}{|\mathbf{r}-\mathbf{r}'|}\mathrm{d}\mathbf{r}' + \sum_I\frac{\partial v_{xc}[n(\mathbf{r})]}{\partial\mathbf{R}_I}\Delta^{\mathbf{R}}\mathbf{R}_I\\ =&\Delta^{\mathbf{R}}V(\mathbf{r}) + e^2\int\frac{\Delta^{\mathbf{R}}n(\mathbf{r}')}{|\mathbf{r}-\mathbf{r}'|}\mathrm{d}\mathbf{r}' + \frac{\mathrm{d}v_{xc}}{\mathrm{d}\,(n(\mathbf{r}))}\sum_I\frac{\partial n(\mathbf{r})}{\partial\mathbf{R}_I}\Delta^{\mathbf{R}}\mathbf{R}_I\\ =&\Delta^{\mathbf{R}}V(\mathbf{r}) + e^2\int\frac{\Delta^{\mathbf{R}}n(\mathbf{r}')}{|\mathbf{r}-\mathbf{r}'|}\mathrm{d}\mathbf{r}' + \frac{\mathrm{d}v_{xc}}{\mathrm{d}\,(n(\mathbf{r}))}\Delta^{\mathbf{R}}n(\mathbf{r})\end{aligned} \tag{73}$$

So:

$$\Delta^{\mathbf{R}}V_{SCF} = \Delta^{\mathbf{R}}V(\mathbf{r}) + e^2\int\frac{\Delta^{\mathbf{R}}n(\mathbf{r}')}{|\mathbf{r}-\mathbf{r}'|}\mathrm{d}\mathbf{r}' + \left.\frac{\mathrm{d}v_{xc}}{\mathrm{d}n}\right|_{n=n(\mathbf{r})}\Delta^{\mathbf{R}}n(\mathbf{r}) \tag{74}$$

Equations 69, 71 and 74 can be solved iteratively/self-consistently to find the variation of the electron density, in the same way that the Kohn-Sham equations can be solved to find the electron density.

The equations above are the approach used to calculate the phonon dispersion in Section 5. However, using perturbation theory, it is possible to derive further expressions for the variation of the wavefunction, and by extension for the variation of the density. Suppose we have some state $\psi_m(\mathbf{r})$, $m \neq n$. Then from first order perturbation theory, it is given that:

$$\Delta^{\mathbf{R}}\psi_n(\mathbf{r}) = \sum_{m\neq n}\psi_m\frac{\langle\psi_m|\Delta^{\mathbf{R}}V_{SCF}|\psi_n\rangle}{\varepsilon_n-\varepsilon_m} \tag{75}$$

It follows with Equation 69:

$$\Delta^{\mathbf{R}}n(\mathbf{r}) = 4\mathrm{Re}\sum_{n=1}^{N/2}\sum_{m\neq n}\psi_n^*\psi_m\frac{\langle\psi_m|\Delta^{\mathbf{R}}V_{SCF}|\psi_n\rangle}{\varepsilon_n-\varepsilon_m} \tag{76}$$

The sum above can be simplified since for all m which correspond to occupied states (the same states that are denoted by n), the states will cancel out. Let us denote the values of m and n as $n = 1, 2, 3, ...i, ...j, ...N$ and $m = 1, 2, 3...i, ...j, ...N, N+1, ...M$. The states ψ_n denote ground states and hence all occupied or valence states. The states ψ_m denote all possible states, so for $m \geq N+1$, ψ_m denotes a conduction, or unoccupied state. Consider the case where m represents a valence state, that is consider the case where $n = i$ and $m = j$, and vice versa. We can see that, since $\Delta^{\mathbf{R}}V_{SCF}$ is Hermitian (since it is simply real-valued):

$$\psi_i^*\psi_j\frac{\langle\psi_j|\Delta^{\mathbf{R}}V_{SCF}|\psi_i\rangle}{\varepsilon_i-\varepsilon_j} = -\left(\psi_j^*\psi_i\frac{\langle\psi_i|\Delta^{\mathbf{R}}V_{SCF}|\psi_j\rangle}{\varepsilon_j-\varepsilon_i}\right)^* \tag{77}$$

And for any complex number, the difference between it and its complex conjugate yields twice the imaginary part of the complex number, that is:

$$\psi_i^*\psi_j\frac{\langle\psi_j|\Delta^{\mathbf{R}}V_{SCF}|\psi_i\rangle}{\varepsilon_i-\varepsilon_j} + \psi_j^*\psi_i\frac{\langle\psi_i|\Delta^{\mathbf{R}}V_{SCF}|\psi_j\rangle}{\varepsilon_j-\varepsilon_i} = 2\mathrm{Im}\left(\psi_i^*\psi_j\frac{\langle\psi_j|\Delta^{\mathbf{R}}V_{SCF}|\psi_i\rangle}{\varepsilon_i-\varepsilon_j}\right) \tag{78}$$

But Equation 76 takes only the real part of the summation, which means that the imaginary part above is equal to zero. Hence, for all m which denote a valence state, ψ_m will cancel out in the sum. Therefore we can shorten the sum by setting ψ_m to represent conduction states only, that is $m = N + 1, ...M$.

This method of determining the electron density variation given by Equation 76 requires knowing both the conduction and valence states of a system, which is significantly more computationally expensive than determining only the valence states, so it is used less in practice [23].

3.3. The Electron-Phonon Interaction

As mentioned before, we can model collective atomic vibrations as particles, and these particles are named **phonons**. In a crystalline semiconductor, electrons will lose energy through inelastic scattering with phonons. The phonons will then transfer energy to the lowest energy phonons (these are the acoustic phonons) which leads to thermalisation. It is well known that thermalisation of the solar cell lowers the conversion efficiency of the PV device [45]. In order to study how phonons affect the conductivity of a PV device, we study the **electron-phonon interaction**. It is complicated to simulate the dissipation to lower-energy phonons, so this thesis will assume that this process is very fast compared to the lifetimes related to electron-phonon interactions.

Phonons arise from variations in atomic positions, $\Delta^R \mathbf{R}_I$. To study them, first we define the position of the I-th atom in terms of the the unit cell l and atom s within a unit cell.

$$\mathbf{R}_I \equiv \mathbf{R}_l + \mathbf{p}_s + \mathbf{z}_s(l) \tag{79}$$

Here, $\mathbf{R}_l$ indicates the position of the l-th unit cell, $\mathbf{p}_s$ is the equilibrium position of the s-th nucleus in each unit cell, and $\mathbf{z}_s(l)$ is the deviation from equilibrium of the s-th nucleus in the l-th unit cell, that is $\mathbf{z}_s(l)$ is the displacement of the I-th nucleus. The index I can be defined as $I = \{l, s\}$. Let $\mathbf{R}_I^0$ be the equilibrium position of the I-th atom, where $\mathbf{z}_s(l) = 0$.

The Fourier Transform of the displacement is:

$$f(\mathbf{q}) = \frac{1}{\sqrt{N_l}} \sum_I \mathbf{z}_s(l) e^{-\mathbf{q}\cdot\mathbf{R}_I^0} \tag{80}$$

So the inverse Fourier Transform is:

$$\mathbf{z}_s(l) = \frac{1}{\sqrt{N_l}} \sum_{\mathbf{q}} f(\mathbf{q}) e^{\mathbf{q}\cdot\mathbf{R}_I^0} \tag{81}$$

Where N_l is the number of unit cells, and $\mathbf{q}$ signifies points in the reciprocal lattice.

In order to proceed, we need to make one crucial approximation - that is that the atomic vibrations can be modelled as harmonic oscillators. For some vibration with wavevector $\mathbf{q}$,

we indicate a vibration with the same magnitude but opposite direction with wavevector -**q**. Then, the Fourier Transform of the displacement is written simply the same way a position operation is written in terms of the creation and annihilation operators of the quantum harmonic oscillator (in reciprocal space) [44, 46].

$$f(\mathbf{q}) = \sqrt{\frac{\hbar}{2M\omega_\eta(\mathbf{q})}}\mathfrak{e}_\eta(\mathbf{q})(a^\dagger_{-\mathbf{q},\eta} + a_{\mathbf{q},\eta}) \tag{82}$$

Where $\mathfrak{e}_\eta(\mathbf{q})$ is the eigenvector along the direction of $\mathbf{q}$ for phonon mode η, M is the mass contained in the unit cell, and $\omega_\eta(\mathbf{q})$ is the frequency of the atomic vibration. There are several types of phonon modes η, so we consequently take an additional sum over η, and the final expression for the atomic displacements is then:

$$\mathbf{z}_s(l) = \sum_{\mathbf{q},\eta}\sqrt{\frac{\hbar}{2M\omega_\eta(\mathbf{q})N_l}}\mathfrak{e}_\eta(\mathbf{q})e^{\mathbf{q}\cdot\mathbf{R}^0_I}(a^\dagger_{-\mathbf{q},\eta} + a_{\mathbf{q},\eta}) \tag{83}$$

The atomic displacement $\mathbf{z}_s(l)$ is synonymous with the variation in atomic positions $\Delta^{\mathbf{R}}\mathbf{R}_I$.

We can now see that the expression for the atomic displacement contains information about phonons, such as their wavevectors and frequencies. In order to determine the electron-phonon interaction, we can look at how atomic displacement affects electronic energies.

First, we must recall the Hamiltonian for our electronic system, the Kohn-Sham Schrödinger equation shown in Equation 48. The potential V_{SCF} represents all interactions of electrons with each other as well as with nuclei. The next step is to expand V_{SCF} as a Taylor series about the equilibrium nuclear configuration, $\mathbf{R}^0$ [15]. Note that previously, we treated V_{SCF} as a function of the electronic positions $\mathbf{r}$, and it only depended parametrically on the nuclear configuration $\mathbf{R}$. In the discussion below, the dependence of V_{SCF} on $\mathbf{R}$ is what is relevant, and so it is written as a function of $\mathbf{R}$.

$$V_{SCF}(\mathbf{R}) = V_{SCF}(\mathbf{R}^0) + \Delta^{\mathbf{R}}V_{SCF} + \frac{1}{2}\frac{\partial^2 V_{SCF}}{\partial\mathbf{R}_I^2}\left(\Delta^{\mathbf{R}}\mathbf{R}_I\right)^2 + ... \tag{84}$$

The first term, $V_{SCF}(\mathbf{R}^0)$ does not contain any phonon-inducing effects, as no phonons are created when the atoms are simply fixed at their equilibrium positions. This term also contains the electron-electron interaction, while the other terms do not as the electron-electron interaction does not depend explicitly on $\mathbf{R}$ (within the context of the adiabatic approximation). Hence, the electron-phonon interaction contained within V_{SCF} is a result of the first order and higher order terms. We will yet again approximate and consider only the first order term. Hence we can write:

$$\hat{H}_{ep} \approx \Delta^{\mathbf{R}}V_{SCF} \tag{85}$$

Where $\hat{H}_{ep}$ is defined as an electron-phonon interaction Hamiltonian. To derive the expression for the electron-phonon interaction potential, we model an electron interacting with a phonon as single particle, or **quasiparticle**, often called a "polaron".

Suppose an electron is in state $|\mathbf{k}, \sigma\rangle$, where $\mathbf{k}$ is its wavevector and its band index is denoted by σ. The electron scatters a phonon of some phonon mode η = LA, TA, TO or LO with wave vector $\mathbf{q}$. This causes the electron to change momentum (it may or may not change band index well) to $|\mathbf{k}+\mathbf{q}, \sigma\rangle$. The electron-phonon interaction for this process is:

$$V_{ep} = \sum_{\mathbf{k}} \left\langle \mathbf{k}+\mathbf{q}, \sigma \left| \hat{H}_{ep} \right| \mathbf{k}, \sigma \right\rangle c^{\dagger}_{\mathbf{k}+\mathbf{q},\sigma} c_{\mathbf{k},\sigma} \tag{86}$$

We can now evaluate:

$$\begin{aligned} V_{ep} &= \sum_{\mathbf{k}} \left\langle \mathbf{k}+\mathbf{q}, \sigma \left| \Delta^{\mathbf{R}} V_{SCF} \right| \mathbf{k}, \sigma \right\rangle c^{\dagger}_{\mathbf{k}+\mathbf{q},\sigma} c_{\mathbf{k},\sigma} \\ &= \sum_{\mathbf{k}} \left\langle \mathbf{k}+\mathbf{q}, \sigma \left| \sum_{I} \frac{\partial V_{SCF}(\mathbf{R})}{\partial \mathbf{R}_I} \mathbf{z}_s(l) \right| u^{\mathbf{k}}_{\sigma} \right\rangle c^{\dagger}_{\mathbf{k}+\mathbf{q},\sigma} c_{\mathbf{k},\sigma} \end{aligned} \tag{87}$$

Hence the final expression for the electron-phonon interaction potential, V_{ep}, is defined to have the form [47]:

$$V_{ep} = \sum_{\eta \mathbf{k}\mathbf{q}} M_{\eta}(\mathbf{k}+\mathbf{q}, \mathbf{k}) \left(a_{\mathbf{q},\eta} + a^{\dagger}_{\text{-}\mathbf{q},\eta} \right) c^{\dagger}_{\mathbf{k}+\mathbf{q},\sigma} c_{\mathbf{k},\sigma} \tag{88}$$

The matrix element $M_{\eta}(\mathbf{k}+\mathbf{q}, \mathbf{k})$ (from now on abbreviated as M_{η}) is the matrix element for some phonon mode η, and it given by:

$$M_{\eta} = A_{\eta}(\mathbf{q}) \left\langle u^{\mathbf{k}+\mathbf{q}}_{\sigma} \left| \Delta^{\mathbf{q},\eta} v^{\mathbf{q}}_{SCF} \right| u^{\mathbf{k}}_{\sigma} \right\rangle \tag{89}$$

Where $v^{\mathbf{q}}_{SCF}$ is the periodic part of the Fourier Series expansion of V_{SCF}, and $u^{\mathbf{k}+\mathbf{q}}_{\sigma}$ $u^{\mathbf{k}}_{\sigma}$ a the periodic function that arises when an electron state is written as a Bloch State,

$$|\mathbf{k}, \sigma\rangle = u^{\mathbf{k}}_{\sigma} e^{i\mathbf{k}\cdot\mathbf{r}} \tag{90}$$

The representation of the matrix element shown in Equation 89 is relevant when attempting to calculate the electron-phonon matrix elements numerically using the plane-wave basis set in DFT software, though this is not the approach used to calculate the matrix element in the practical implementation portion of this thesis. The factor $A_{\eta}(\mathbf{q})$ is:

$$A_{\eta}(\mathbf{q}) = \sqrt{\frac{\hbar}{2 N_l M \omega_{\eta}(\mathbf{q})}} \mathfrak{e}_{\eta}(\mathbf{q}) \tag{91}$$

3.4. Summary

In this Section we first discussed Density Functional Theory, a way to make quantum mechanical simulations of many body systems computationally feasible by reformulating the problem in terms of an electron density at a point, instead of using functions of many electronic positions. The foundation of DFT are the two Hohenberg-Kohn theorems: the first

theorem states that for a many body system, the external potential will correspond to a unique electron density; the second theorem states that the total energy of the system is a unique functional of the electron density, and there exists a universal functional such that the ground state density minimises the total energy. Both of these theorems can be proved using the variational principle. We also showed that when a many particle wavefunction is approximated as a Slater determinant, the electron density for the many particle system can be written as the sum of the moduli of single particle spin-orbitals.

Next, to determine the lattice dynamical properties of a many electron system such as a bulk crystalline semiconductor, we employed the Born-Oppenheimer approximation. In this approximation, it is assumed that electrons respond much more quickly to changes in the environment than nuclei. Hence the problem can be separated into two: solving a system of many, interacting electrons in a field of fixed nuclei, followed by solving a system of nuclei where the potential is a fixed Potential Energy Surface due to the electrons. The PES, or BO energy surface is the ground state energy of the electron system. The second derivative of this energy surface yields the matrix of Interatomic Force Constants, and the eigenvalues of the scaled matrix yield the phonon (collective atomic vibration) frequencies for the nuclear system. The eigenvectors are labelled as different phonon modes - transverse optical, longitudinal optical, transverse acoustic and longitudinal acoustic. A plot of phonon frequencies vs wavevector is called a phonon dispersion relation. Using the Hellman-Feynman theorem, the second derivative of the BO energy surface can be written in terms of the electron density, the derivative of the density, and the electron-electron and electron-nucleus Coulomb interactions.

To find the matrix of IFCs, the electron density is needed - this can be expressed as a sum of single electron wavefunction moduli. The Kohn-Sham equations model the many-electron system as a collection of single electrons under an external potential which includes all the effects due to other electrons and fixed nuclei. The single electron wavefunctions are called the auxiliary Kohn-Sham orbitals. By solving these single electron Schrödinger equations, we can find the electron density of the many-body system. The energy of the many electron system is written as a sum of the universal functional and any external potential acting on the system. The universal functional also contains an exchange-correlation energy term, which accounts for effects that aren't yet explicitly known as functionals of the electron density, and so the exchange-correlation energy needs to be approximated. The most common types of exchange correlation functions are the Local Density Approximation, Generalised Gradient Approximations, and hybrid functionals.

Ab initio software often uses the plane-wave basis set to determine the electronic energies and phonon frequencies numerically. This means that the electronic wavefunctions are written as Bloch states. The Fourier transform of the matrix of IFCs is taken and the electron-nucleus interaction is approximated with a pseudopotential. The Dynamical matrix (the Fourier transform of the IFC matrix) also requires the variation of the electron density, which is calculated using Density Functional Perturbation Theory. The variation of the density is written in terms of the variations in the electron wavefunctions, which can be determined using quantum mechanical first order perturbation theory.

Lastly, this section gave an overview of the electron-phonon interaction, the process which leads to thermalisation of the bulk material. First, the atomic displacements are expressed in terms of the creation and annihilation operators. Next, when we expand the Kohn-Sham potential about the equilibrium nuclear configuration, we see that only its first and higher order derivatives contain phonon effects. Approximating to the first order gives the electron-phonon interaction Hamiltonian. Next, we consider an electron in one state which shifts to another state by scattering a phonon. We find the expectation value of the interaction Hamiltonian for an electron going from one state to the other, which leads us to an expression for the electron-phonon interaction potential. Contained within this expression is the electron phonon matrix element, a key quantity for determining electron-phonon self energy and thus electron-phonon interaction lifetimes.

4. Self-Energy and the LA Phonon Matrix Element

As mentioned, we have modelled the electrons interacting with phonons as quasiparticles. If we want to find meaningful information, such as the duration of the interaction - or in other words, the lifetime of the quasiparticle, we need to first derive the quasiparticle **self-energy**. The self-energy of a particle is defined as the energy that the particle gains due to the changes it causes in its own environment, and the resulting interactions with its environment. The next step then in studying the electron-phonon interaction is to determine its contribution to the electron's self energy.

4.1. Green's Functions and Electron-Phonon Self-Energy

The quantity of self-energy arises within the theory of Green's Functions [48]. This thesis will briefly discuss how Green's Functions and the Dyson Equation are used to derive a self-energy term for a specific potential. In particular, the theory of Matsubara Green's Functions and representing the statistical mechanics of quantum systems in terms of imaginary time and frequency are presented in detail by Takeo Matsubara in [49]. A comprehensive explanation of Green's Functions and electron-phonon interactions can also be found in [46] and [15].

First, we suppose that the electronic creation and annihilation operators are dependant on some imaginary time variable, τ, and can be written as $c_{\mathbf{k},\sigma}(\tau)$. Writing quantum mechanical operators with dependencies on time is also known as the Heisenberg representation [50]. Suppose we start at $\tau = 0$ and end at time τ. The time-dependent Green's function for a fermionic particle can be written as:

$$G(\mathbf{k}, \tau) = -\langle \hat{T}_W c_{\mathbf{k},\sigma}(\tau) c^{\dagger}_{\mathbf{k},\sigma}(0) \rangle \tag{92}$$

In words, the function above can simply be seen as the probability amplitude that an electron with wavevector $\mathbf{k}$ and band σ is created at time = 0 and annihilated at time τ. The equation has an additional operator, $\hat{T}_W$, called Wick's time ordering operator [15]. $\hat{T}_W$

orders the operators such that they have increasing time from left to right. The electronic Green's function represented above does not account for spin index as for the purposes of our discussion, we assume we are dealing with non-magnetic states.

Consider the Hamiltonian for the electronic system - the Hamiltonian accounts for electronic interactions as well as electron-nucleus interaction. We can express the Hamiltonian as a sum of contributions from electrons, lattice vibrations (phonons), and electron-phonon interactions.

$$\hat{H} = \hat{H}_e + \hat{H}_p + \hat{H}_{ep} \tag{93}$$

The term $\hat{H}_{ep}$ is also interpreted as a perturbation imposed on a Hamiltonian $\hat{H} = \hat{H}_e + \hat{H}_p$.

The time dependent annihilation/creation operators of the electrons are defined in the Heisenberg picture as:

$$c_{\mathbf{k},\sigma}(\tau) = e^{i\hat{H}\tau/\hbar} c_{\mathbf{k},\sigma} e^{-i\hat{H}\tau/\hbar} \tag{94}$$

The imaginary time τ is varied from $-\beta$ to β, where $\beta = 1/T$; T is the (finite) temperature of the system in Kelvin. This is a commonly used definition which allows for a broader connection between a system's statistical mechanics and thermodynamics. This means that imaginary time is large for low temperatures and small for high temperatures.

Similarly, we can define the Green's function for bosons - including bosonic quasiparticles such as phonons. Since the displacement $\mathbf{z}_s(l)$ is a function of $\mathbf{q}$, we can write it as $\mathbf{z}_{s,\mathbf{q}}$. The Green's function can be written in terms of the displacement vector $\mathbf{z}_{s,\mathbf{q}}$, then reformulated using 83 in terms of the phonon creation and annihilation operators as follows:

$$\begin{aligned} U(\mathbf{q},\tau) &= -\langle \hat{T}_W \mathbf{z}_{s,\mathbf{q}}(\tau) \mathbf{z}_{s,-\mathbf{q}}(0) \rangle \\ &= \sum_{\eta} A_\eta(\mathbf{q}) A_\eta(-\mathbf{q}) D(\mathbf{q},\eta,\tau) \end{aligned} \tag{95}$$

Where the Green's function $D(\mathbf{q},\eta,\tau)$ is:

$$D(\mathbf{q},\eta,\tau) = -\langle \hat{T}_W [a^\dagger_{-\mathbf{q},\eta}(\tau) + a_{\mathbf{q},\eta}(\tau)][a_{-\mathbf{q},\eta}(0) + a^\dagger_{\mathbf{q},\eta}(0)] \rangle \tag{96}$$

Next, many-body perturbation theory is applied to the Hamiltonian (Eqn. 93). The interacting Green's functions $G(\mathbf{k},\tau)$ and $D(\mathbf{q},\eta,\tau)$ are expressed as an infinite series of Feynman diagrams [46].

$$G(\mathbf{k},\tau) = -\sum_{n=0}^{\infty} (-1)^n \int_0^\beta \dots \int_0^\beta \langle T_W c_{\mathbf{k},\sigma}(\tau) V_{ep}(\tau_1) \dots V_{ep}(\tau_n) c^\dagger_{\mathbf{k},\sigma}(0) \rangle \mathrm{d}\tau_1 \dots \mathrm{d}\tau_n \tag{97}$$

And similarly for $D(\mathbf{q},\eta,\tau)$. $G(\mathbf{k},\tau)$ and $D(\mathbf{q},\eta,\tau)$ are by definition periodic functions such that:

$$\begin{aligned} G(\mathbf{k},\tau+\beta) &= -G(\mathbf{k},\tau) \\ D(\mathbf{q},\eta,\tau+\beta) &= D(\mathbf{q},\eta,\tau) \end{aligned} \tag{98}$$

To express the Green's functions in the frequency domain, their Fourier transforms are taken:

$$\begin{aligned} G(\mathbf{k}, ip_n) &= \int_0^\beta G(\mathbf{k}, \tau) e^{ip_n \tau} \mathrm{d}\tau \\ D(\mathbf{q}, \eta, i\nu_m) &= \int_0^\beta D(\mathbf{q}, \eta, \tau) e^{i\nu_m \tau} \mathrm{d}\tau \end{aligned} \tag{99}$$

The values ω_n and ν_m are called Matsubara frequencies for fermions and bosons respectively. They form a discrete set of imaginary frequencies, where n and m are integers. The frequencies are:

$$\begin{aligned} p_n &= (2n+1)\pi T \\ \nu_m &= 2m\pi T \end{aligned} \tag{100}$$

To proceed, we will also need the fermionic and bosonic time-dependent Green's functions for the unperturbed Hamiltonian $\hat{H} = \hat{H}_e + \hat{H}_p$ (i.e. without any electron-phonon interaction), which read [46]:

$$\begin{aligned} G_0(\mathbf{k}, ip_n) &= \frac{1}{ip_n - \varepsilon(\mathbf{k})} \\ D_0(\mathbf{q}, \eta, i\nu_m) &= \frac{1}{i\nu_m - \omega_\eta(\mathbf{q})} - \frac{1}{i\nu_m + \omega_\eta(\mathbf{q})} \end{aligned} \tag{101}$$

Taking a partial sum of each of the series of Feynman diagrams yields what is known as the Dyson equation [51]. For fermionic and bosonic Green's functions, the Dyson equation reads, respectively:

$$\begin{aligned} G(\mathbf{k}, ip_n) &= \frac{G_0(\mathbf{k}, ip_n)}{1 - G_0(\mathbf{k}, ip_n)\Sigma(\mathbf{k}, ip_n)} \\ D(\mathbf{q}, \eta, i\nu_m) &= \frac{D_0(\mathbf{q}, \eta, i\nu_m)}{1 - D_0(\mathbf{q}, \eta, i\nu_m)\Pi(\mathbf{q}, \eta, i\nu_m)} \end{aligned} \tag{102}$$

Where Σ is the electron self-energy and Π is the phonon self-energy. Multiplying by the denominator and dividing each term in the fermionic equation by GG_0 (and DD_0 for the bosonic Green's function), we can cast the Dyson equations into the form:

$$\begin{aligned} G(\mathbf{k}, ip_n)^{-1} &= G_0(\mathbf{k}, ip_n)^{-1} - \Sigma(\mathbf{k}, ip_n) \\ D(\mathbf{q}, \eta, i\nu_m)^{-1} &= D_0(\mathbf{q}, \eta, i\nu_m)^{-1} - \Pi(\mathbf{q}, \eta, i\nu_m) \end{aligned} \tag{103}$$

The Dyson equation has allowed us to express the interacting Green's function in terms of the unperturbed Green's function and particle self-energy. The self-energies are the sum of all single-particle, irreducible Feynman diagrams and Σ includes the effects of both electron-electron and electron-phonon interactions. Similarly, Π includes both electron-phonon and phonon-phonon interactions.

In the Feynman diagram series for the electronic Green's function, the lowest order diagram represents an electron emitting and reabsorbing a phonon. More detail on how this evaluation

is done can be found in [46, 49]. We can hence write out the electron-phonon self-energy term as:

$$\Sigma_{ep}(\mathbf{k}, ip_n) = -\frac{1}{\beta}\sum_{\mathbf{q},\eta}\sum_{m'}|M_\eta(q)|^2 D_0(\mathbf{q}, i\nu_{m'})G_0(\mathbf{k}-\mathbf{q}, ip_n - i\nu_{m'}) \tag{104}$$

The summations over the frequency index for different combinations of unperturbed Matsubara Green's Functions are known. In particular for the Green's functions above [46]:

$$-\frac{1}{\beta}\sum_{m'} D_0(\mathbf{q}, i\nu_{m'})G_0(\mathbf{p}, ip_n + i\nu_{m'}) = \frac{N_\eta(\mathbf{q}) + n_F(\varepsilon(\mathbf{p}))}{ip_n - \varepsilon(\mathbf{p}) + \hbar\omega_\eta(\mathbf{q})} + \frac{N_\eta(\mathbf{q}) + 1 - n_F(\varepsilon(\mathbf{p}))}{ip_n - \varepsilon(\mathbf{p}) - \hbar\omega_\eta(\mathbf{q})} \tag{105}$$

Hence, the contribution to the self-energy arising from the electron-phonon interaction is:

$$\Sigma_{ep}(\mathbf{k}, ip_n) = \sum_{\mathbf{q},\eta}|M_\eta(\mathbf{q})|^2\left\{\frac{N_\eta(\mathbf{q}) + n_F(\varepsilon(\mathbf{k}+\mathbf{q}))}{ip_n - \varepsilon(\mathbf{k}+\mathbf{q}) + \hbar\omega_\eta(\mathbf{q})} + \frac{N_\eta(\mathbf{q}) + 1 - n_F(\varepsilon(\mathbf{k}+\mathbf{q}))}{ip_n - \varepsilon(\mathbf{k}+\mathbf{q}) - \hbar\omega_\eta(\mathbf{q})}\right\} \tag{106}$$

The first term represents the emission of a phonon with wavevector $\mathbf{q}$, and the second term represents absorption of a phonon with wavevector $\mathbf{q}$ (not necessarily the same phonon that was emitted). The values $N_\eta(\mathbf{q})$ and $n_F(\varepsilon(\mathbf{k}+\mathbf{q}))$ are the phonon and electron occupation numbers given by the Bose-Einstein and Fermi-Dirac distributions respectively:

$$N_\eta(\mathbf{q}) = \frac{1}{e^{\hbar\omega_\eta(\mathbf{q})/k_BT} - 1} \qquad n_F(\varepsilon(\mathbf{k}+\mathbf{q})) = \frac{1}{e^{\{\varepsilon(\mathbf{k}+\mathbf{q})-\mu\}/k_BT} + 1} \tag{107}$$

We have now arrived at an expression for the electron-phonon interaction self-energy. Visually, we can show the electronic and phonon self energies in a Feynman diagram, see Figure 3.

There is another method for deriving the quantity in Equation 106 which is to apply second order perturbation theory to the Hamiltonian, Eqn. 93 [46]. From second order perturbation theory, the second order correction for the eigenvalue E of the Hamiltonian is:

$$\Sigma_{ep} = \Delta E^{(2)} = \sum_I \frac{\langle I|\hat{H}_{ep}|in\rangle}{E_I - E_{in}} \tag{108}$$

Where $|in\rangle$ represents the initial state of the system. This leads to the expression [47]:

$$\Sigma_{ep}(\mathbf{k}) = \sum_{\mathbf{q},\eta}|M_\eta(\mathbf{q})|^2\left\{\frac{N_\eta(\mathbf{q}) + 1 - n_F(\varepsilon(\mathbf{k}+\mathbf{q}))}{\varepsilon(\mathbf{k}) - \varepsilon(\mathbf{k}+\mathbf{q}) - \hbar\omega_\eta(\mathbf{q})} + \frac{N_\eta(\mathbf{q}) - n_F(\varepsilon(\mathbf{k}+\mathbf{q}))}{\varepsilon(\mathbf{k}) - \varepsilon(\mathbf{k}+\mathbf{q}) + \hbar\omega_\eta(\mathbf{q})}\right\} \tag{109}$$

This representation is slightly different from the one that arose from Green's function theory - that is, the initial energy of the electron is represented as $\varepsilon(\mathbf{k})$ instead of using the frequency, ip_n.

In the context of a solar cell: as photons are incident on the solar cell, they are absorbed forming electron-hole pairs. The electron then proceeds to lose energy as some contributes to atomic vibrations (which will cause the cell to thermalise) - i.e this is the electron-phonon

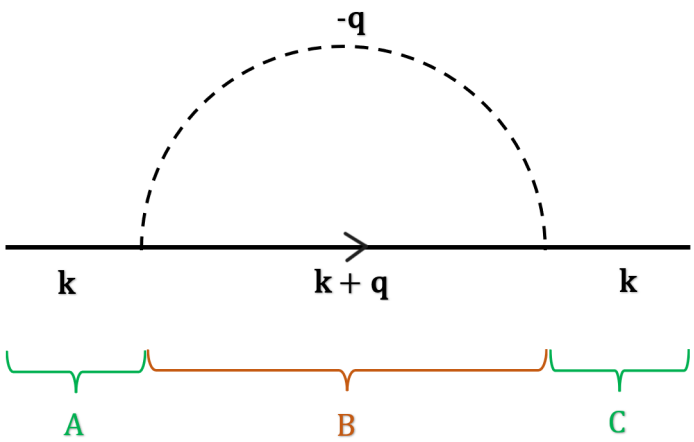

Figure 3: Feynman diagram showing the electron self energy (shown by the solid line) and phonon self energy (shown by the dashed line). The area labelled A shows the electron with wavevector $\mathbf{k}$. Area B shows the electron-phonon interaction - the electron has wavevector $\mathbf{k}+\mathbf{q}$ after emitting a phonon with wavevector $-\mathbf{q}$. In area C the electron has re-absorbed the phonon and once again has the wavevector $\mathbf{k}$.

interaction. We can consider the intermediate state in Figure 3 as a single quasiparticle, a polaron. Once this interaction is over, and the polaron ceases to exist, the electron will be reabsorbed into a hole and will no longer have the energy to reach the contacts of the solar PV device and create current. Hence, the lifetime of the polaron determines the conductivity of the solar cell (a similar procees exists for holes instead of electrons). When the lifetime is known, along with the electronic velocity, we would have a crucial piece of information needed to determine an optimal thickness for the absorption layer of a solar cell.

To determine quasiparticle properties and how they are affected by their interactions with the environment, the "advanced" and "retarded" (i.e. delayed) Green's functions need to be defined. The retarded Green's function describes particles propagating forward in time, whereas the advanced Green's Function describes particles propagating with time reversed - it can be used to study the possible effects of future events on past events. All measurable quantities (conductivity, susceptibility etc.) are in fact retarded response functions [47].

By the method of analytic continuation, we change $ip_n \to p + i\delta$ for the retarded Green's function, and $ip_n \to p - i\delta$ for the advanced Green's function, where δ is the Dirac-delta function. Note that the advanced function and retarded function are complex conjugates of each other.

$$\begin{aligned} G(\mathbf{k}, ip_n)\big|_{ip_n \to p+i\delta} &= G^{ret}(\mathbf{k}, p) \\ G(\mathbf{k}, ip_n)\big|_{ip_n \to p-i\delta} &= G^{adv}(\mathbf{k}, p) \end{aligned} \tag{110}$$

The **spectral function** is defined as:

$$A(\mathbf{k}, p) = -2\mathrm{Im}[G^{ret}(\mathbf{k}, p)] \tag{111}$$

The retarded Green's function can be written as:

$$\begin{aligned} G^{ret}(\mathbf{k}, p) &= \frac{1}{p + E_n - E_{n'} + i\delta} \\ &= P\frac{1}{p + E_n - E_{n'}} - i\pi\delta(p + E_n - E_{n'}) \end{aligned} \tag{112}$$

The symbol P is used to denote the principal value and is used to separate the real and imaginary parts of the retarded Green's Function. Using the definition of the non-interacting Green's function in Equation 101, we can find the retarded function:

$$G_0^{ret}(\mathbf{k}, p) = \frac{1}{p - i\delta - \varepsilon(\mathbf{k})} \tag{113}$$

Now, combining the Dyson Equation (Eqn 102) and the expression for G_0 in Equation 101, we can write the Green's function as:

$$G(\mathbf{k}, ip_n) = \frac{1}{ip_n - \varepsilon(\mathbf{k}) - \Sigma(\mathbf{k}, ip_n)} \tag{114}$$

We can apply the analytic continuation $ip_n \to E + i\delta$ on both the Dyson equation and the self-energy $\Sigma(\mathbf{k}, ip_n)$.

$$\Sigma^{ret}(\mathbf{k}, E) = \mathrm{Re}\Sigma^{ret}(\mathbf{k}, E) + i\mathrm{Im}\Sigma^{ret}(\mathbf{k}, E) \tag{115}$$

$$G^{ret}(\mathbf{k}, E) = \frac{1}{E + i\delta - \varepsilon(\mathbf{k}) - \Sigma^{ret}(\mathbf{k}, E)} \tag{116}$$

Finally, we can determine the quasiparticle lifetime - the lifetime of the electron-phonon interaction, $\tau(\mathbf{k})$.

$$-\frac{\hbar}{2\tau(\mathbf{k})} = \mathrm{Im}\Sigma^{ret}(\mathbf{k}, E) \tag{117}$$

In this case, $E = \varepsilon(\mathbf{k})$. Hence, the duration of the electron-phonon interaction, that is the lifetime $\tau(\mathbf{k})$ of the phonon scattering and absorption, is given by:

$$\begin{aligned} \frac{\hbar}{\tau(\mathbf{k})} = 2\pi \sum_{\mathbf{q},\eta} |M_\eta(\mathbf{q})|^2 \{ &[N_\eta(\mathbf{q}) + 1 - n_F(\varepsilon(\mathbf{k} + \mathbf{q}))]\delta[\varepsilon(\mathbf{k}) - \varepsilon(\mathbf{k} - \mathbf{q}) - \hbar\omega_\eta(\mathbf{q})] \\ &+ [N_\eta(\mathbf{q}) + n_F(\varepsilon(\mathbf{k} + \mathbf{q}))]\delta[\varepsilon(\mathbf{k}) - \varepsilon(\mathbf{k} - \mathbf{q}) + \hbar\omega_\eta(\mathbf{q})]\} \end{aligned} \tag{118}$$

For the purpose of this thesis, we wish to find the electron-phonon interaction lifetimes for materials used for Solar PV cells, specifically GaAs and Si, which are semiconductors. In semiconductors and insulators, the conduction band is typically unoccupied. So, should an electron shift to the conduction band, its lifetime in the conduction band would be very short. Because of this, for semiconductors and insulators we can approximate that the electron occupation number $n_F(\varepsilon(\mathbf{k} + \mathbf{q})) \approx 0$. This leads us to our final expression for the electron-phonon interaction lifetime for semiconductors:

$$\begin{aligned} \frac{\hbar}{\tau(\mathbf{k})} = 2\pi \sum_{\mathbf{q},\eta} |M_\eta(\mathbf{q})|^2 \{ &[N_\eta(\mathbf{q}) + 1]\delta[\varepsilon(\mathbf{k}) - \varepsilon(\mathbf{k} - \mathbf{q}) - \hbar\omega_\eta(\mathbf{q})] \\ &+ [N_\eta(\mathbf{q})]\delta[\varepsilon(\mathbf{k}) - \varepsilon(\mathbf{k} - \mathbf{q}) + \hbar\omega_\eta(\mathbf{q})]\} \end{aligned} \tag{119}$$

4.2. Deformation Potential Theory and the LA Phonon Matrix Element

In this section, we discuss how the concept of a "deformation potential" can be used to simplify the process of calculating an approximate lifetime of the electron-phonon interaction. The deformation potential discussed here is also referred to as the "hydrostatic deformation potential" in some sources. The following argument is discussed in [47].

Semiconductors and insulators have a band gap, but most electrons will have an energy close to the conduction band minimum while holes will have energy close to the valence band maximum. When the particles gain heat, they gain kinetic energy. Hence the kinetic energy of the particles is approximately equal to their thermal energy:

$$\varepsilon_K(k) = \frac{\hbar^2 k^2}{2m^*} \approx k_B T \tag{120}$$

Where k is the particle wavevector and m^* is the particle's effective mass.
Now, when an electron interacts with a phonon, it gains/loses kinetic energy equal to the phonon energy $\hbar\omega_\eta(q)$, where $\omega_\eta(q)$ is the phonon frequency and η symbolises the phonon mode (LA, TA, LO or TO). Hence,

$$\varepsilon_K(k+q) = \varepsilon_K(k) \pm \hbar\omega_\eta(q) \tag{121}$$

This symbolises an electron being scattered from wavevector k to wavevector $k+q$. Since the wavevector is so small, we can approximate the energy of acoustical phonons using the Debye model ($\omega_\eta(q) = c_\eta q$, where c_η is phonon group velocity), and optical phonons using the Einstein model ($\omega_\eta(q) = \omega_\eta(0) = \omega_0$). For the scope of this thesis, only the electron-phonon interaction involving the Longitudinal Acoustic (LA) phonons will be studied. This approximation will be useful when deriving the LA phonon Matrix element.

An acoustical phonon corresponds to local lattice compression/dilations. If hydrostatic pressure is applied to a solid such as a bulk crystal, the lattice constant decreases, also causing the band energies to change. For very small pressures, the change in lattice constant (and by extension cell volume) is directly proportional to the change in band energy. To find this relationship, we begin with the continuity equation from fluid dynamics. Taking $\mathbf{v}$ as fluid velocity and ρ as its density, the continuity equation reads:

$$\begin{aligned} 0 &= \frac{\partial \rho}{\partial t} + \nabla \cdot (\mathbf{v}\rho) \\ &= \frac{\partial \rho}{\partial t} + \rho \nabla \cdot \mathbf{v} + \mathbf{v} \cdot \nabla \rho \\ &\approx \frac{\partial \rho}{\partial t} + \rho \nabla \cdot \mathbf{v} \end{aligned} \tag{122}$$

We can neglect the term $\mathbf{v} \cdot \nabla\rho$ as it is very small.

Suppose that the atoms of the solid have the positions $\mathbf{R}_I$. We rewrite the velocity in terms

of the derivative of the displacement:

$$\begin{aligned} \frac{\partial \rho}{\partial t} &= -\rho \nabla \cdot \mathbf{v} \\ \frac{\partial \rho}{\partial t} &= -\rho \nabla \cdot \frac{\partial \mathbf{R}_I}{\partial t} \\ \delta \rho &= -\rho \nabla \cdot \mathbf{R}_I \end{aligned} \tag{123}$$

Hence

$$\frac{\delta \rho}{\rho} = -\nabla \cdot \mathbf{R}_I = -\Delta \tag{124}$$

In the above equation, the term Δ is called the **dilation** [47], but it can also be written in terms of the fractional change in volume. If we take the density as the number of particles N per unit volume (the argument is the same if we define the density as mass per volume),

$$\begin{aligned} \rho &= \frac{N}{V} \\ \frac{\delta \rho}{\delta V} &= -\frac{N}{V^2} \\ \implies \frac{\delta \rho}{\rho} &= -\frac{N/V^2}{N/V} \delta V \\ \frac{\delta \rho}{\rho} &= -\frac{\delta V}{V} \\ \implies \frac{\delta V}{V} &= \Delta \cdot \mathbf{R}_I \end{aligned} \tag{125}$$

The dilation or the fractional change in volume, as briefly mentioned before, is proportional to the change in band energy. The constant of proportionality, denoted D, is called the **deformation potential constant** [47]. Hence we write:

$$D \frac{\delta V}{V} = \delta E_b \tag{126}$$

Where E_b denotes the band energy. In a discrete form, it can be written:

$$E_i - E_0 = D \frac{V_i - V_0}{V_0} \tag{127}$$

Where E_i denotes the band energy of a band at some unit cell volume V_i, and E_0 is the energy of the same band at equilibrium cell volume V_0.

Hence, if band energies and cell volumes are known, one should be able to plot a linear relationship between the change in band energy and fractional change in cell volume, and determine the deformation potential. This is the approach that is taken in the following section of this thesis.

The deformation potential will allow us to approximate the LA phonon matrix element. The electron-acoustic phonon interaction Hamiltonian can be written as follows:

$$\hat{H}_{ep}^{ac} = D \nabla \cdot \mathbf{R}_I \tag{128}$$

However, we had already derived an expression for the atomic displacement $\nabla \cdot \mathbf{R}_I = \mathbf{z}_s(l)$ in Equation 83. In this following, η can only be used to represent an acoustic phonon mode. Thus the Hamiltonian can be written as:

$$\hat{H}_{ep}^{ac} = D \sum_{\mathbf{q},\eta} \sqrt{\frac{\hbar}{2M_s \omega_\eta(\mathbf{q}) N_l}} \mathbf{q} \cdot \mathfrak{e}_\eta(\mathbf{q}) e^{\mathbf{q}\cdot\mathbf{R}_I^0} (a_{-\mathbf{q},\eta}^\dagger + a_{\mathbf{q},\eta}) \tag{129}$$

Using Equation 86, we can derive the electron-LA phonon interaction potential as:

$$V_{ep}^{ac} = \sum_{\mathbf{k}\mathbf{q}\eta} D \sqrt{\frac{\hbar}{2M_s \omega_\eta(\mathbf{q}) N_l}} \mathbf{q} \cdot \mathfrak{e}_\eta(\mathbf{q}) \left(a_{\mathbf{q},\eta} + a_{\mathbf{-q},\eta}^\dagger\right) c_{\mathbf{k}+\mathbf{q},\sigma}^\dagger c_{\mathbf{k},\sigma} \tag{130}$$

Now, from the form of the interaction potential shown in Equation 88, we can deduce the LA phonon matrix element from the above equation.

$$M_\eta^{ac}(\mathbf{q}) = D \sqrt{\frac{\hbar}{2M_s \omega_\eta(\mathbf{q}) N_l}} \mathbf{q} \cdot \mathfrak{e}_\eta(\mathbf{q}) \tag{131}$$

This expression can be simplified further when we consider that acoustic phonons have long wavelengths, and at long wavelength LA phonon displacements are parallel in direction to the wavevector - $\mathfrak{e}_{LA}(\mathbf{q})||\mathbf{q}$, while TA phonon displacements are perpendicular. This would cause the dot product in the matrix element to equal zero. Hence only the Longitudinal Acoustic phonons experience the deformation potential interaction, while TA phonons do not.

As discussed previously, we can use the Debye model for acoustic phonons such that $\omega_{LA}(\mathbf{q}) = c_{LA} q$. We also consider one unit cell such that $N_l = 1$. We let $M_s = M$ where M is the mass of the unit cell in question. The final expression for the LA phonon matrix element is thus:

$$M_{LA}(q) = D \sqrt{\frac{\hbar}{2M c_{LA}}} \sqrt{q} \tag{132}$$

In the following section, this thesis will propose calculating an approximate electron-phonon interaction lifetime by accounting only for the LA phonon contribution, as a way to make the entire process of determining self-energy much cheaper computationally compared to attempting to compute the various other matrix elements numerically.

4.3. Summary

In this section we wrote out the time-dependent fermionic Green's function, using the time-dependent electron creation and annihilation operators. The Green's function represents the probability amplitude that an electron is created at one time and annihilated at another. The Hamiltonian for the many-electron system is then rewritten as a sum of electron, phonon, and electron-phonon interaction terms, and we then define a bosonic Green's function to

represent the phonons. We apply many-body perturbation theory to the Hamiltonian, and the interacting Green's function is derived from an infinite series of Feynman diagrams. Taking a partial sum of these series yields the Dyson equation which contains a term for electron self-energy. Self-energy is the change in a particle's energy due to it interacting with its environment. The lowest order Feynman diagram represents an electron emitting and reabsorbing a phonon. With all of this information, one can write out an expression for the electron-phonon self energy as a summation of the non-interacting phonon and electron Green's functions, and the electron-phonon matrix element. The electron-phonon interaction lifetime is determined by the inverse of the imaginary part of the retarded (delayed) self energy. For semiconductors, we make the approximation that the electron occupation number, given by the Fermi-Dirac distribution is zero.

We then argue that the electron-phonon interaction can be modelled as involving acoustic phonons only, as they are the lowest energy phonons and higher energy phonons would transition to lower energy. Since an acoustical phonon corresponds to lattice compression, we treat the crystal lattice as if it is under hydrostatic pressure. Using the continuity equation from fluid dynamics, we derive a relation between the density of the unit cell and the atomic displacements. We find that the fractional change in unit cell volume is proportional to the change in band energy, and the constant of proportionality is called the deformation potential. In this case, the electron-phonon interaction Hamiltonian is simply a product of the deformation potential and atomic displacements. From here we determine the electron-acoustic phonon matrix element. However, due to TA phonon modes being perpendicular to the wavevector, their contribution to the matrix element vanishes, leaving only the LA phonon contribution. The final expression for the electron-LA phonon matrix element depends only on the deformation potential, the LA phonon group velocity, and the phonon wavenumber.

5. Implementation

In this Section, we will discuss how ab initio methods can be used to obtain an approximate electron-phonon interaction lifetime using the Deformation Potential method. This is then implemented for bulk Silicon and bulk Gallium Arsenide, typical materials used to construct solar cells.

The theory of the previous sections will need to be written in a way that makes it possible for DFT software to run calculations, that is it needs to be possible to run iterations using discrete "basis sets". The calculations below were run using the software Quantum Espresso, which uses the Plane-Wave (PW) basis set to calculate the phonon dispersion relation [33], and the python package GPAW to calculate the electronic band energies.

The GPAW package is able to use both the Plane-Wave basis set and the Linear Combination of Atomic Orbitals (LCAO) basis set, using the Projector Augmented Wave (PAW) method. However, for the calculations presented below, PW mode was used. More information on

the PAW method can be found in [17, 52, 53].

Below is a description of how DFT software was used to determine band energies and phonon dispersions, followed by approximate electron-phonon interaction lifetimes for bulk Si and GaAs using deformation potentials. The electron-phonon interaction lifetime is significant in determining how long electrons in a solar cell take to thermalise, that is lose their energy to heat, and can be used to determine an optimal thickness for a Solar PV material.

5.1. Outline of Methods

The following subsection describes the details of how the simulations were carried out, such as which energy band, pseudopotential and exchange-correlation functionals were used. Following that is the derivation of a simplified expression for the electron-phonon interaction lifetime using the deformation potential.

5.1.1. Phonon Dispersion and LA Phonon Group Velocity

One of the values required by the matrix element $M_{LA}(q)$ is the LA phonon group velocity, c_{LA}. This can be read off a material's respective phonon dispersion relation. A phonon dispersion relation of a system can be determined through ab initio numerical calculations. First the Kohn-Sham equations of the system are solved numerically to determine the ground-state configuration and orbital energies. Then, the phonon dispersion is determined through Density Functional Perturbation Theory [54].

For the phonon data presented below for Silicon and Gallium Arsenide, pseudopotentials were used for each element (Silicon, Gallium and Arsenic). Specifically, the pseudopotentials used were Optimal Norm-Conserving Vanderbilt (ONCV) pseudopotentials were used, and they were generated using the "Perdew-Burke-Ernzerhof" (PBE) exchange-correlation functional, an exchange-correlation functional based on the Generalised Gradient Approximation (GGA) method [38]. Further discussion on ONCV pseudopotentials can be found in [55].

Another type of pseudopotential is the ultra-soft pseudopotential, first introduced by David Vanderbilt in [56]. An ultra-soft pseudopotential involves writing the pseudopotential v_s as a product of a local and non-local potentials. It indroduces further approximations in order for the Plane Wave expansions of the inner electrons to converge more rapidly. A mathematical discussion of pseudopotentials and ultra-soft pseudopotentials is beyond the scope of this thesis but can be found in more detail in [23, 56].

The last quantity that is needed for the overall calculation is a form for the exchange-correlation functional for the original Kohn-Sham system. With that, the system can be solved in order to ultimately calculate a ground state electron density, which is used to calculate the matrix of IFCs. For this calculation, the exchange-correlation functional "PBEsol" is used, an improved version of PBE with slightly altered parameters [57].

Once the matrix of IFCs is calculated, Equation 58 can be solved, and the eigenvalues $\omega(\mathbf{q})$ are plotted for each phonon mode (eigenvector). The gradients of the lines $\omega(\mathbf{q})$ give the phonon velocities. The deformation potential is calculated using only the group velocity c_{LA} of the Longitudinal Acoustic (LA) phonons. We consider the LA phonon dispersion around the Γ point where the LA phonons have the lowest energy and q is very small - here the phonon dispersion is essentially linear, and the gradient c_{LA} is constant.

5.1.2. Deformation Potential Calculation

The deformation potential arises from:

$$E_i - E_0 = D\frac{V_i - V_0}{V_0} \tag{133}$$

Where D is the deformation potential, E_i represents the energy of an electronic band at cell volume V_i, and E_0 is the equilibrium energy of that same band, at equilibrium unit cell volume V_0

The band energies are given by the eigenvalues of the KS Hamiltonian - the ground state energies from the single electron Schrödinger equation given in Equation 48. The ground state single electron energy can now be calculated for each unit cell volume V_i. In principle, any band can be used. For the discussion below, band energies are calculated for the Lowest Unoccupied Molecular Orbital (LUMO), also known as the Conduction Band Minimum (CBM), i.e. the lowest energy conduction state. LUMO energies gave the most consistent results when compared to Highest Occupied Molecular Orbital (HOMO) energies for the simulations in this thesis. The measurement is then taken at the wavevector $\mathbf{k}$ where the energy of the band is the lowest (in the case of LUMO).

$$E_i = \min\left[\varepsilon^i_{LUMO}(\mathbf{k})\right] \tag{134}$$

To calculate the energies, the KS equations need to be solved using the plane wave basis set. To do so we simply write the state ψ_n as a Bloch State as in Equation 53, and take the Fourier series expansion of V_{SCF}:

$$V_{SCF}(\mathbf{r}) = \sum_{\mathbf{G}} v^{\mathbf{G}}_{SCF} e^{i\mathbf{G}\cdot\mathbf{r}}$$

Where: (135)

$$V_{SCF}(\mathbf{r}+\mathbf{R}) = V_{SCF}(\mathbf{r})$$

$$\mathbf{G}\cdot\mathbf{R} = 2\pi\delta_{ij}$$

Here $\mathbf{G}$ denotes the reciprocal lattice vector. The primitive unit cell volume of the Silicon and GaAs crystal lattices are 1/4 times the lattice constant cubed. As the lattice constant is altered, the distance between atoms $|\mathbf{R}_I - \mathbf{R}_J|$ is altered, resulting in some unit cell volume V_i. The resulting change in unit cell structure will affect the energy of the electronic bands, resulting in some band energy E_i. The equilibrium cell volume is known from experimental data, and can be determined in simulations as it is the volume V_0 that corresponds to the minimum total energy of the entire cell.

5.1.3. Calculating self-energy and lifetime

In the following, I made use of unpublished notes by my supervisor, Prof. Alexander Quandt. Starting with the Equation 119 for the electron-phonon interaction, we will now apply a series of approximations to reduce the number of steps needed to calculate the lifetime:

- As it was already stated, the term $n_F(\varepsilon(\mathbf{k}+\mathbf{q})) \approx 0$. This is the electron occupation number and is effectively zero for semiconductors and insulators.
- The phonon occupation number $N_\eta(\mathbf{q})$ can be approximated for high temperatures. Using the approximation $e^x \approx x+1$ for very small x, and T = 300K, we have that $\hbar\omega(\mathbf{q})/k_BT$ is very small. Hence $N_\eta(\mathbf{q})$ becomes

$$\begin{aligned} N_\eta(\mathbf{q}) &= \frac{1}{e^{\hbar\omega(\mathbf{q})/k_BT}-1} \\ &\approx \frac{1}{\frac{\hbar\omega(\mathbf{q})}{k_BT}+1-1} \\ &= \frac{k_BT}{\hbar\omega(\mathbf{q})} \end{aligned} \tag{136}$$

  Note that this term is much larger than 1, hence the +1 term in Equation 119 will also be discarded.
- Since this thesis will approximate the electron-phonon interaction as arising due to LA phonons only, $\eta = LA$. Hence the sum in Equation 119 is simplified to a sum over just q. Consequently, $\omega_\eta(\mathbf{q}) = \omega_{LA}(\mathbf{q}) = c_{LA}q$, using the Debye model, and $M_\eta(\mathbf{q}) = M_{LA}(\mathbf{q}) = C\sqrt{q}$ where $C = D\sqrt{\hbar/2Mc_{LA}}$. This was derived in Section 4.2.

For ease of notation, let $\delta_- = \delta[\varepsilon(\mathbf{k})-\varepsilon(\mathbf{k}-\mathbf{q})-\hbar\omega_\eta(\mathbf{q})]$ and $\delta_+ = \delta[\varepsilon(\mathbf{k})-\varepsilon(\mathbf{k}-\mathbf{q})+\hbar\omega_\eta(\mathbf{q})]$. Now Equation 119 is simplified to:

$$\begin{aligned} \frac{\hbar}{\tau(\mathbf{k})} &= 2\pi\sum_{\mathbf{q}} C^2 q\left(\frac{k_BT}{\hbar c_{LA}q}\delta_- + \frac{k_BT}{\hbar c_{LA}q}\delta_+\right) \\ \frac{\hbar}{\tau(\mathbf{k})} &= \frac{2\pi C^2 k_BT}{\hbar c_{LA}}\sum_{\mathbf{q}}(\delta_- + \delta_+) \\ \frac{\hbar}{\tau(\mathbf{k})} &= \frac{\pi D^2 k_BT}{c_{LA}^2 M}\sum_{\mathbf{q}}(\delta_- + \delta_+) \end{aligned} \tag{137}$$

Now all that is left to do is evaluate the sum. Firstly, the sum over the vector $\mathbf{q}$ can be evaluated as a volume integral.

$$\frac{\hbar}{\tau(\mathbf{k})} = \frac{\pi D^2 k_BT}{c_{LA}^2 M}\frac{\Omega_0}{(2\pi)^3}\int_V(\delta_- + \delta_+)d^3q \tag{138}$$

Where Ω_0 is the equilibrium volume of the unit cell. Next we want to rewrite δ_+ and δ_- as functions of q, by rewriting the energies ε. The choice of whether to consider valence band holes or conduction band electrons is arbitrary. In the following we consider the conduction band electrons. The kinetic energy of an electron in the conduction band is $\varepsilon(\mathbf{k}) = \hbar^2 k^2/2m_c$ where m_c is the effective mass of the electron. Hence

$$\begin{aligned}
\delta_- &= \delta[\varepsilon(\mathbf{k}) - \varepsilon(\mathbf{k}-\mathbf{q}) - \hbar\omega_\eta(\mathbf{q})] \\
&= \delta\left[\frac{\hbar^2 k^2}{2m_c} - \frac{\hbar^2|\mathbf{k}-\mathbf{q}|^2}{2m_c} - \hbar c_{LA} q\right] \\
&= \delta\left[\frac{\hbar^2 k^2}{2m_c} - \frac{\hbar^2(k^2 - 2\mathbf{k}\cdot\mathbf{q} + q^2)}{2m_c} - \hbar c_{LA} q\right] \\
&= \delta\left[\frac{\hbar^2}{2m_c}(2\mathbf{k}\cdot\mathbf{q} - q^2) - \hbar c_{LA} q\right] \\
&= \delta\left[\frac{\hbar^2}{2m_c}(2kq\cos\theta - q^2) - \hbar c_{LA} q\right] \\
&= \delta\left[\frac{\hbar^2}{2m_c}(2kq\cos\theta - q^2 - q_s q)\right] \\
&= \delta\left[\frac{\hbar^2}{2m_c} f(q)\right]
\end{aligned} \tag{139}$$

where θ is the angle between $\mathbf{k}$ and $\mathbf{q}$, and is chosen to be the polar angle when evaluating our volume integral $\mathrm{d}^3 q$ in spherical coordinates, $q_s = 2m_c c_{LA}/\hbar$, and $f(q) = 2kq\cos\theta - q^2 - q_s q$. Similarly for δ_+,

$$\begin{aligned}
\delta_+ &= \delta\left[\frac{\hbar^2}{2m_c}(2kq\cos\theta - q^2 + q_s q)\right] \\
&= \delta\left[\frac{\hbar^2}{2m_c} g(q)\right]
\end{aligned} \tag{140}$$

where $g(q) = 2kq\cos\theta - q^2 + q_s q$. We can now use the following property of the delta function,

$$\delta(\alpha x) = \frac{1}{|\alpha|}\delta(x) \tag{141}$$

Also, since $f(q)$ and $g(q)$ are clearly continuously differentiable, we can use the definition of the composition of $\delta(f(x))$

$$\delta(f(x)) = \sum_i \frac{\delta(x - x_i)}{|f'(x_i)|} \tag{142}$$

Where x_i are the roots of the continuously differentiable function $f(x)$. For $f(q)$, its roots q_i are at $q_1 = 0$ and $q_2 = 2k\cos\theta - q_s$. Note that q is always ≥ 0. Then,

$$\begin{aligned}
f'(q) &= 2k\cos\theta - 2q - q_s \\
f'(q_2) &= 2k\cos\theta - 2(2k\cos\theta - q_s) - q_s \\
&= -(2k\cos\theta - q_s) \\
&= -q_2 \\
f'(q_1) &= f'(0) = 2k\cos\theta - q_s = q_2
\end{aligned} \tag{143}$$

We can now simplify δ_-:

$$\begin{aligned}\delta_- &= \frac{2m_c}{\hbar^2}\delta\left[f(q)\right] \\ &= \frac{2m_c}{\hbar^2}\left[\frac{\delta(q)}{|f'(q_1)|} + \frac{\delta(q-q_2)}{|f'(q_2)|}\right]\end{aligned} \tag{144}$$

Similarly, considering δ_+, the roots q_i' of $g(q)$ are $q_1' = 0$ and $q_2' = 2k\cos\theta + 2q_s$. Then,

$$\delta_+ = \frac{2m_c}{\hbar^2}\left[\frac{\delta(q)}{|g'(q_1')|} + \frac{\delta(q-q_2')}{|g'(q_2')|}\right] \tag{145}$$

Where $g'(q_1') = 2k\cos\theta + q_s = q_2'$. We can now begin to evaluate the integral in equation 138, substituting these expansions for δ_+ and δ_-, and converting to spherical co-ordinates:

$$\begin{aligned}\frac{\hbar}{\tau(k)} &= \frac{\pi D^2 k_B T}{c_{LA}^2 M}\frac{2m_c}{\hbar^2}\frac{\Omega_0}{(2\pi)^3}\int_V\left(\frac{\delta(q)}{|f'(q_1)|} + \frac{\delta(q-q_2)}{|f'(q_2)|} + \frac{\delta(q)}{|g'(q_1')|} + \frac{\delta(q-q_2')}{|g'(q_2')|}\right)d^3q \\ &= \frac{2m_c\pi D^2 k_B T}{\hbar^2 c_{LA}^2 M}\frac{\Omega_0}{(2\pi)^3}\int_{\phi=0}^{2\pi}\int_{\theta=0}^{\pi}\int_{q=0}^{q_{max}}\left(\frac{\delta(q)}{q_2} + \frac{\delta(q-q_2)}{q_2} + \frac{\delta(q)}{q_2'}\right. \\ &\qquad\left. + \frac{\delta(q-q_2')}{q_2'}\right)q^2\sin\theta\ \mathrm{d}q\ \mathrm{d}\theta\ \mathrm{d}\phi \\ &= \frac{2m_c\pi D^2 k_B T}{\hbar^2 c_{LA}^2 M}\frac{\Omega_0}{(2\pi)^3}2\pi\int_{\theta=0}^{\pi}\int_{q=0}^{q_{max}}\left(\frac{\delta(q)q^2}{q_2} + \frac{\delta(q-q_2)q^2}{q_2} + \frac{\delta(q)q^2}{q_2'}\right. \\ &\qquad\left. + \frac{\delta(q-q_2')q^2}{q_2'}\right)\sin\theta\ \mathrm{d}q\ \mathrm{d}\theta \\ &= \frac{2m_c\pi D^2 k_B T}{\hbar^2 c_{LA}^2 M}\frac{\Omega_0}{(2\pi)^3}2\pi\int_0^{\pi}\left(0 + \frac{q_2^2}{q_2} + 0 + \frac{q_2'^2}{q_2'}\right)\sin\theta\ \mathrm{d}\theta \\ &= \frac{2m_c\pi D^2 k_B T}{\hbar^2 c_{LA}^2 M}\frac{\Omega_0}{(2\pi)^3}2\pi\int_0^{\pi}\left(q_2 + q_2'\right)\sin\theta\ \mathrm{d}\theta\end{aligned} \tag{146}$$

Here we made use of the sampling property of the delta function, i.e for some function $f(x)$:

$$\int f(x)\delta(x-a)\ \mathrm{d}x = f(a) \tag{147}$$

For simplification, we make the substitution $d(\cos\theta) = -\sin\theta\mathrm{d}\theta$. The upper and lower limit of the integral change accordingly:

$$\begin{aligned}\frac{\hbar}{\tau(k)} &= \frac{2m_c\pi D^2 k_B T}{\hbar^2 c_{LA}^2 M}\frac{\Omega_0}{(2\pi)^3}2\pi\int_1^{-1} -\left(q_2 + q_2'\right)\ \mathrm{d}(\cos\theta) \\ &= \frac{2m_c\pi D^2 k_B T}{\hbar^2 c_{LA}^2 M}\frac{\Omega_0}{(2\pi)^3}2\pi\int_{-1}^{1}\left(q_2 + q_2'\right)\ \mathrm{d}(\cos\theta) \\ &= \frac{2m_c\pi D^2 k_B T}{\hbar^2 c_{LA}^2 M}\frac{\Omega_0}{(2\pi)^3}2\pi\int_{-1}^{1}\left((2k\cos\theta - q_s) + (2k\cos\theta + q_s)\right)\ \mathrm{d}(\cos\theta) \\ &= \frac{2m_c\pi D^2 k_B T}{\hbar^2 c_{LA}^2 M}\frac{\Omega_0}{(2\pi)^3}2\pi\int_{-1}^{1}4k\cos\theta\ \mathrm{d}(\cos\theta)\end{aligned} \tag{148}$$

Now, $\cos\theta$ being negative is unphysical, as $q \geq 0$ and q_s is very small by assumption. Hence,

$$\begin{aligned}\frac{\hbar}{\tau(k)} &= \frac{2m_c\pi D^2 k_B T}{\hbar^2 c_{LA}^2 M}\frac{\Omega_0}{(2\pi)^3}2\pi\int_0^1 4k\cos\theta\ \mathrm{d}(\cos\theta) \\ &= \frac{2m_c\pi D^2 k_B T}{\hbar^2 c_{LA}^2 M}\frac{\Omega_0}{(2\pi)^3}2\pi\frac{4k}{2} \\ &= \frac{\Omega_0 m_c D^2 k_B T}{\hbar^2 c_{LA}^2 M\pi}k\end{aligned} \tag{149}$$

Hence, we have derived an expression for the lifetime of the electron-phonon interaction for LA phonons in terms of the deformation potential D and the phonon velocity c_{LA}:

$$\frac{\hbar}{\tau(k)} = \frac{\Omega_0}{\pi}\left[\frac{D^2 m_c k_B T}{\hbar^2 c_{LA}^2 M}\right]k \tag{150}$$

5.2. Bulk Silicon

In order to determine D from Equation 133 we must first determine the equilibrium cell volume V_0 and hence the corresponding equilibrium energy E_0 for the conduction band. In Figure 4 the volume of the primitive unit cell of Silicon is varied and plotted against the cell potential energy. The minimum of the graph corresponds to V_0. The cell potential energy was calculated using the GPAW package [58].

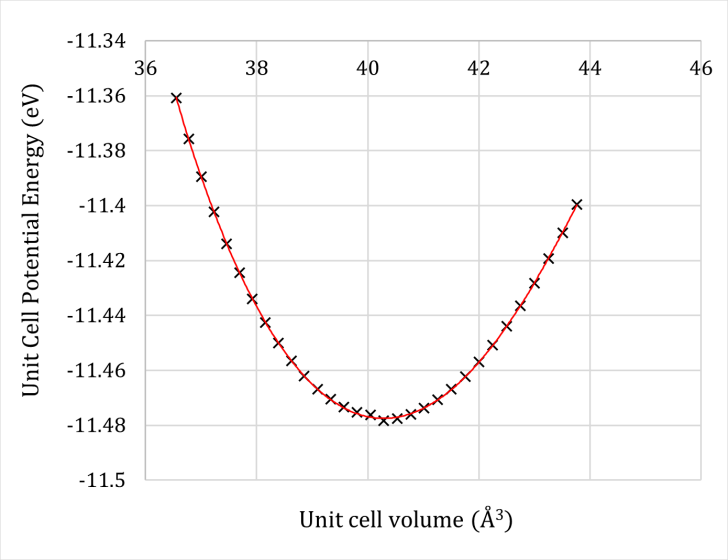

Figure 4: Potential Energy vs Primitive unit cell volume for Silicon, calculated using the GPAW package [58]. The minimum of the graph occurs at 40.25Å^3. This corresponds to a lattice constant of 5.44Å. In comparison, the known lattice constant for bulk Silicon is 5.431Å [59].

In Figure 4 we find V_0 for Si to be 40.25Å^3. When calculating the band energy in GPAW, the exchange-correlation functional HSE06 [40, 41, 42] was found to give the most consistent results. At equilibrium volume we find the corresponding LUMO E_0 for Si to be 8.23eV. Varying the lattice constant by 1.5% in both directions, the relationship in Equation 133 is plotted for Silicon in Figure 5.

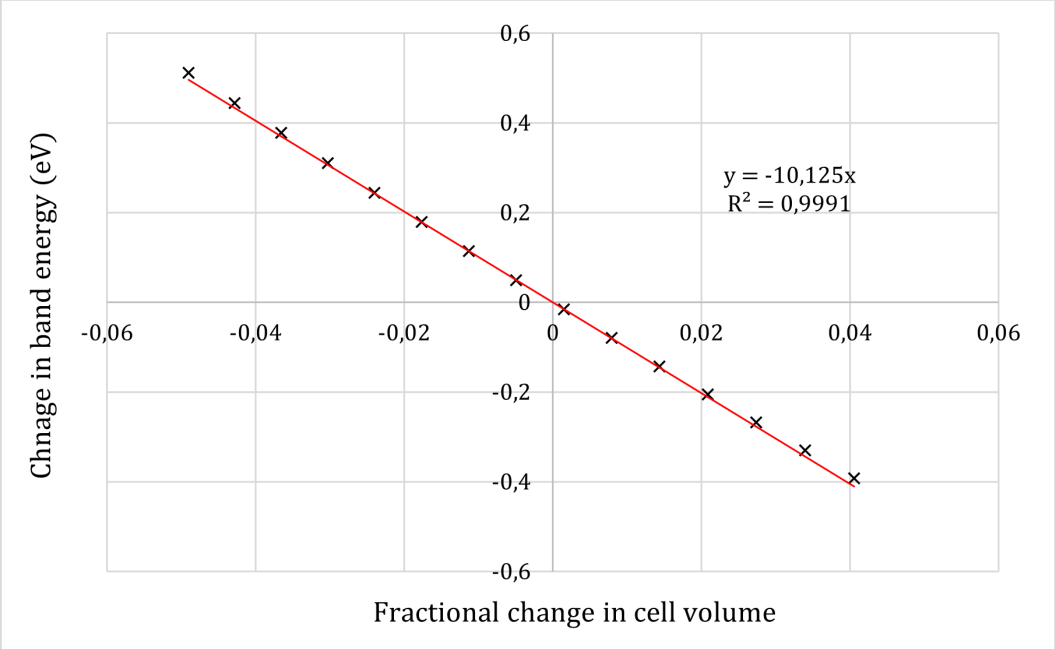

Figure 5: Graph showing the change in LUMO (Lowest Unoccupied Molecular Orbital) energy vs fractional change in volume for the Si. From the gradient we find that the deformation potential D is -10.125 eV. This is comparable to the value -10.0eV found in [60]

From Figure 5 we find a deformation potential D for Si to be -10.125eV. This is in very good agreement with the value of -10.0eV found by A. Blacha, H. Presting and M. Cardona in [60], and this value is recorded in the datasheets of [61], but not many other measurements of the Si deformation potential at the LUMO (CBM) can be found. The value of -10.0eV found by Blacha, Presting and Cardona was calculated using the empirical pseudopotential method, i.e through ab initio numerical simulations. One should note that in [60] the authors record two values for the Si deformation potential calculated using conduction bands - for s-like conduction bands (bands with spherical or near spherical symmetry) the authors record a deformation potential of -15.3eV, while for p-like conduction bands (bands with dumbbell/pear-like symmetry) the authors get the value of -10.0eV. Silicon is an indirect band gap semiconductor, and hence its conduction band minimum would have both s-like and p-like characteristics. It is therefore justifiable to compare the deformation potential determined using LUMO energy to the deformation potential of a p-like conduction band.

Next, in Figure 6 we have the phonon dispersion relation for Silicon which was studied, as well as the area around the second Γ point enlarged. In Figure 7 the gradient of the LA line from Fig. 6b is calculated to find the LA phonon group velocity, $c_{LA} = 1389.7\text{m} \cdot \text{s}^{-1}$. We now have everything necessary to calculate the electron-phonon interaction lifetime, given

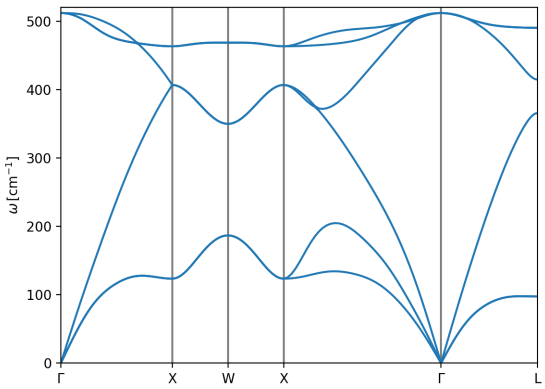

(a) Silicon Phonon Dispersion relation

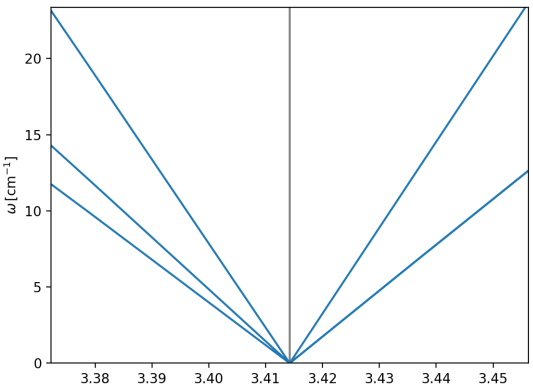

(b) Silicon Phonon Dispersion zoomed in around the Γ point, showing the acoustic phonon frequencies. The highest gradient line represents the LA phonons.

Figure 6: Figures showing the Phonon Dispersion relation for bulk Si, as calculated with Quantum Espresso [62]. Figure 6a shows the full dispersion, while Figure 6b shows a small area around the Γ point, where the acoustic phonon frequencies appear approximately linear. The x-axis depicts the wavevector q in units of $2\pi/a$, where a is the lattice constant of Silicon in au (or Bohr), with $a = 10.263$au.

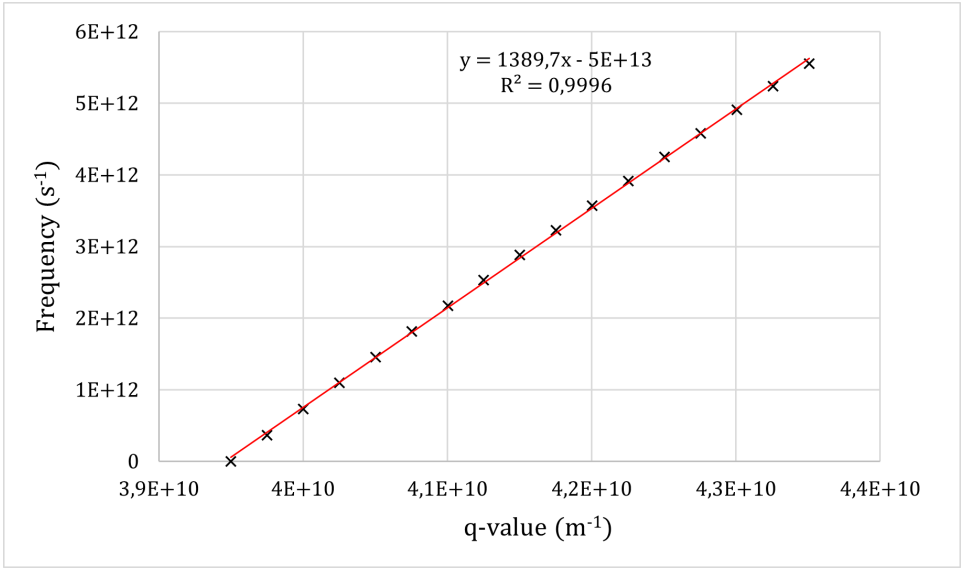

Figure 7: Close-up of the line representing the longitudinal acoustic (LA) phonon from the Silicon phonon dispersion relation. We can read off the phonon group velocity from the gradient, $c_{LA} = 1389.7$ m·s^{-1}.

by equation:

$$\frac{\hbar}{\tau(k)} = \frac{\Omega_0}{\pi}\left[\frac{D^2 m_c k_B T}{\hbar^2 c_{LA}^2 M}\right] k \tag{151}$$

Where $\tau(k)$ is the electron-phonon interaction lifetime, Ω_0 is the volume of the conventional unit cell at equilibrium, D is the deformation potential, and c_{LA} is the LA phonon group velocity. m_c is the effective electron mass assuming a parabolic conduction band. Here, it is approximated with the free electron mass, $m_e = 9.1094\times10^{-31}$ kg. M is taken as the mass of the conventional unit cell, given by equilibrium volume (40.247 Å^3, the primitive unit cell volume as given by Figure 4 multiplied by 4 to get the volume for the conventional unit cell), multiplied by the density of Si, 2.329g·cm^{-3} [61]. The values used are summarised in a table below.

Table 1: Calculated deformation potential, LA phonon group velocity, and other values used for bulk Silicon

Label	Value	Reference
Ω_0	1.6099×10^{-28} m^3	Fig. 4
D	-10.125 eV	Fig. 5
c_{LA}	1389.7 m/s	Fig. 7
T	300 K	-
M	3.7495×10^{-25} kg	Fig. 4 and [61]

Using Equation 150 and the values in Table 1 we can get a simplified relation for $\tau(k)$:

$$\tau(k) = 1.669 \times 10^{-6}\text{s}\cdot\text{m}^{-1}\cdot\frac{1}{k} \tag{152}$$

Where the wavenumber k is in units of m^{-1}. As a test value for k, we use the argument that $\hbar^2k^2/2m^* \approx k_BT$ as discussed in Equation 120 in Section 5. We can simplify this to

$$k \approx \sqrt{\frac{2k_BTm_e}{\hbar^2}} \approx 8.237 \times 10^8\text{m}^{-1} \tag{153}$$

We can now plot $\tau(k)$ vs k for Silicon, and vary k by $\pm$ 10% of the approximation above. This can be seen in Figure 8. Hence we calculate that the electron-phonon interaction lifetime τ in Si is of the order of 2.0×10^{-15} s. Recalling that $-\hbar/2\tau(k) = \text{Im}\Sigma_{ep}^{ret}$, in order to compare the result to other literature, we approximate $\Sigma_{ep} \sim \hbar/2\tau$. This yields an electron-phonon self-energy in the order of 160meV. We compare this to the result calculated by A. Marini in [63] of 20-50 meV for the Fan contribution of the e-p interaction in bulk Si, calculated using the DFT software package Yambo [64].

Yambo uses the Plane-Wave SCF method similarly to Quantum Espresso. We wish to compare ab initio results such as that of [63] to the simplified deformation potential approach used in this thesis to calculate the phonon mediated electron self-energy. Our result of

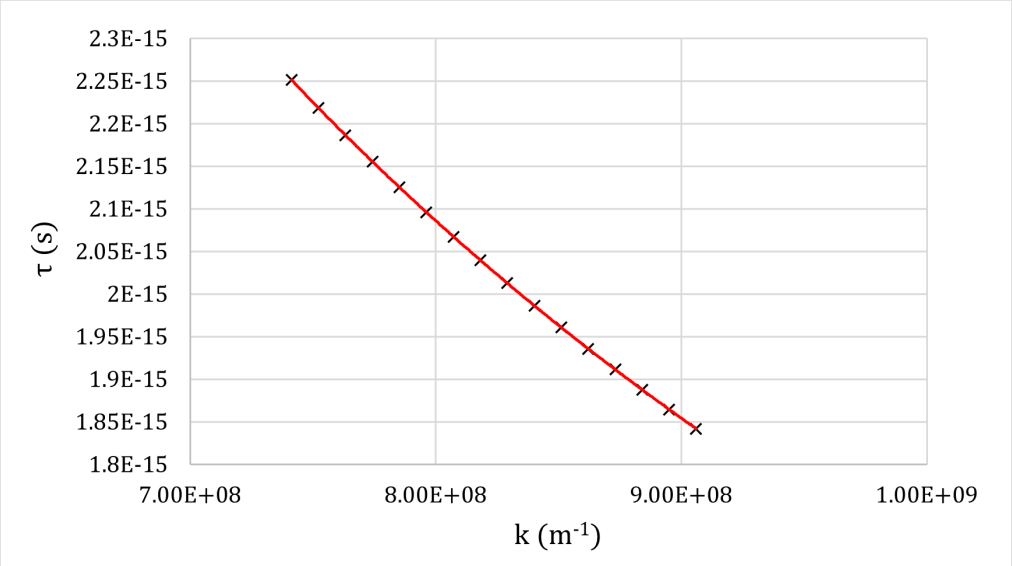

Figure 8: Graph showing the electron-phonon interaction lifetime τ vs the wavenumber k, for bulk Silicon. We can see that τ is of the order of 2.0×10^{-15} s.

160meV compares relatively well within the scope of this thesis to the Fan self energy term in [63]. One should note that to determine an accurate electron-phonon self energy, a DFT software would need to be able to calculate both the Fan-Midgal and Debye-Waller(DW) e-p matrix elements, however a detailed first principles implementation of the DW term is yet to be realised [15]. The detailed theory of electron-phonon interactions including the Debye-Waller matrix element is explained by Allen and Heine in [65] and by Feliciano Giustino in [15].

It would be interesting to see how this result for the electron-phonon interaction lifetime would compare to ab initio results which include the DW matrix element, as well as to possible future experiments. The level of accuracy of the above result would give insight into the extent of the LA phonon contribution to the total electron-phonon self energy.

5.3. Gallium Arsenide

Following the same process as for Silicon, below are figures indicating the equilibrium volume, deformation potential and LA phonon group velocity for GaAs. The values are summarised in Table 2. Once again, we will approximate m_c using the free electron mass. The density of Gallium Arsenide is taken to be 5.318 g·cm^{-3} [66].

In Figure 12 the deformation potential for GaAs is calculated to be -18.663eV. We compare this to the value of -18.3eV found in [60]. Unlike for Si, many sources have attempted to calculate the deformation potential of GaAs, but there appears to be more debate on what that value should be. In [60], the authors report a value of -18.3eV for GaAs for an s-like conduction band, and -7.3eV for a p-like conduction band. Since our data is for the LUMO

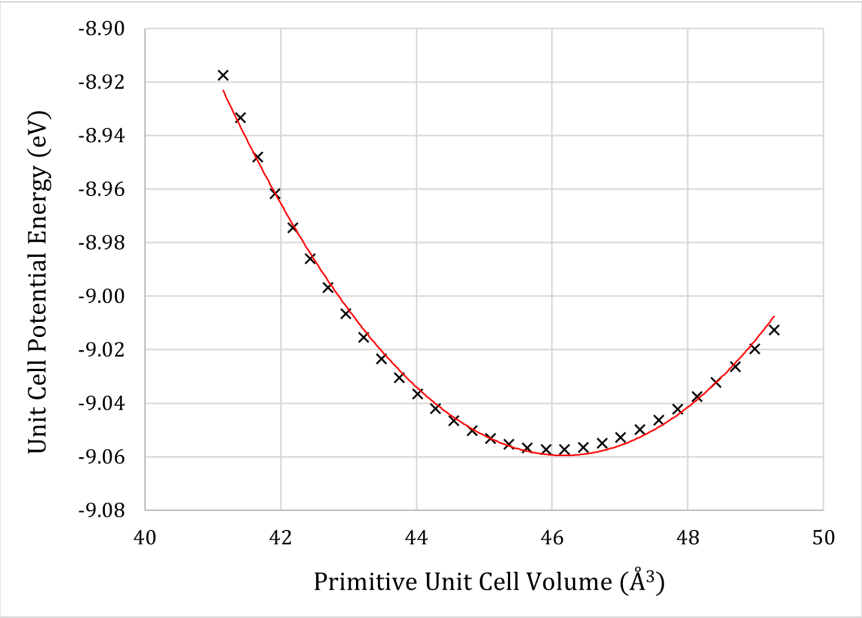

Figure 9: Potential Energy vs Primitive unit cell volume for Gallium Arsenide, calculated using the GPAW package [58]. The minimum of the graph occurs at V_0 =46.69Å^3 with a corresponding LUMO energy of $E_0 = 5.195$eV. This volume corresponds to a lattice constant of 5.72Å. In comparison, the known lattice constant for Gallium Arsenide is 5.65Å [67].

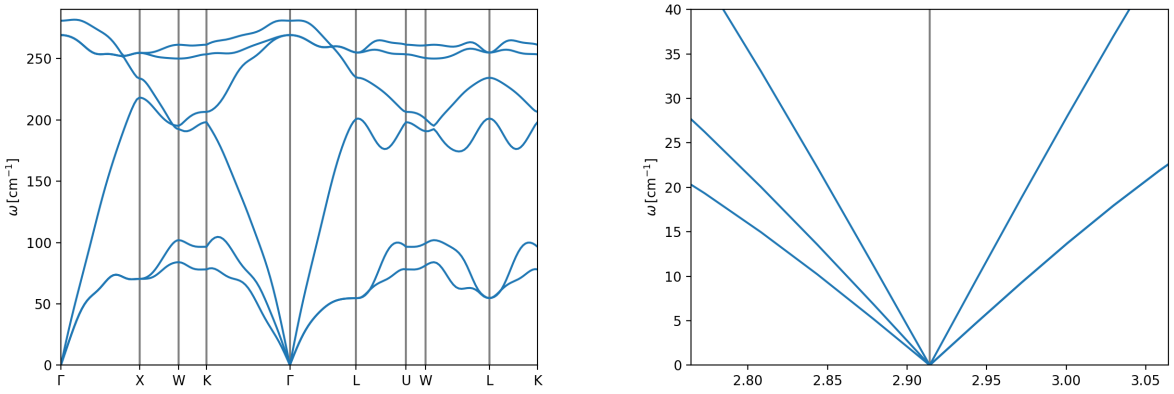

(a) GaAs Phonon Dispersion relation

(b) GaAs Phonon Dispersion zoomed in around the acoustic phonons at the Γ point

Figure 10: Figures showing the Phonon Dispersion relation for Gallium Arsenide, as calculated with Quantum Espresso [62]. Figure 10a shows the full dispersion, while Figure 10b shows a small area around the Γ point, where the acoustic phonon frequencies appear approximately linear. The wavevector q shown on the x-axis is in units of $2\pi/a$, where a is the lattice constant of GaAs in au (or Bohr), and $a = 10.68$au.

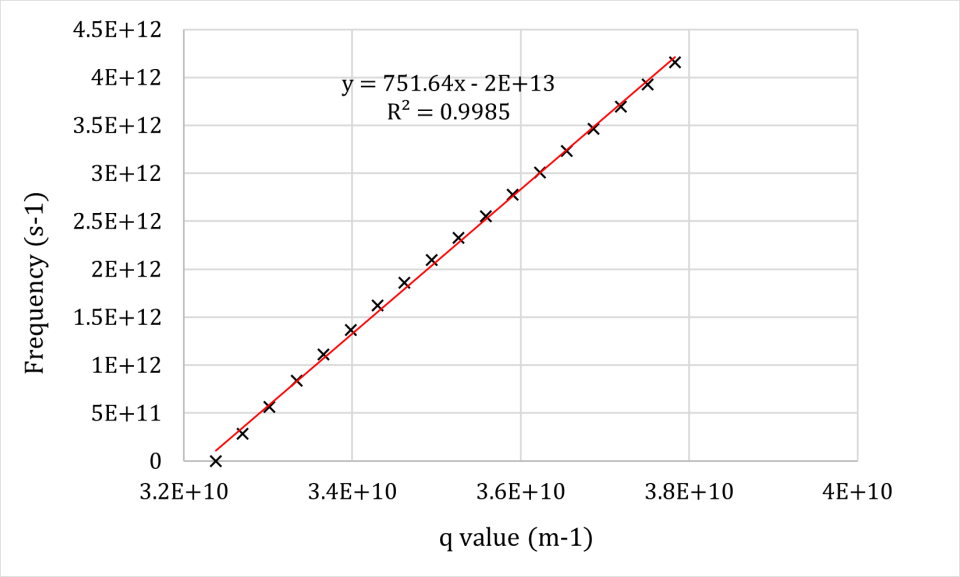

Figure 11: Close-up of the line representing the longitudinal acoustic (LA) phonon from the Gallium Arsenide phonon dispersion relation. We can read off the phonon group velocity from the gradient, $c_{LA} = 751.64\text{m} \cdot \text{s}^{-1}$.

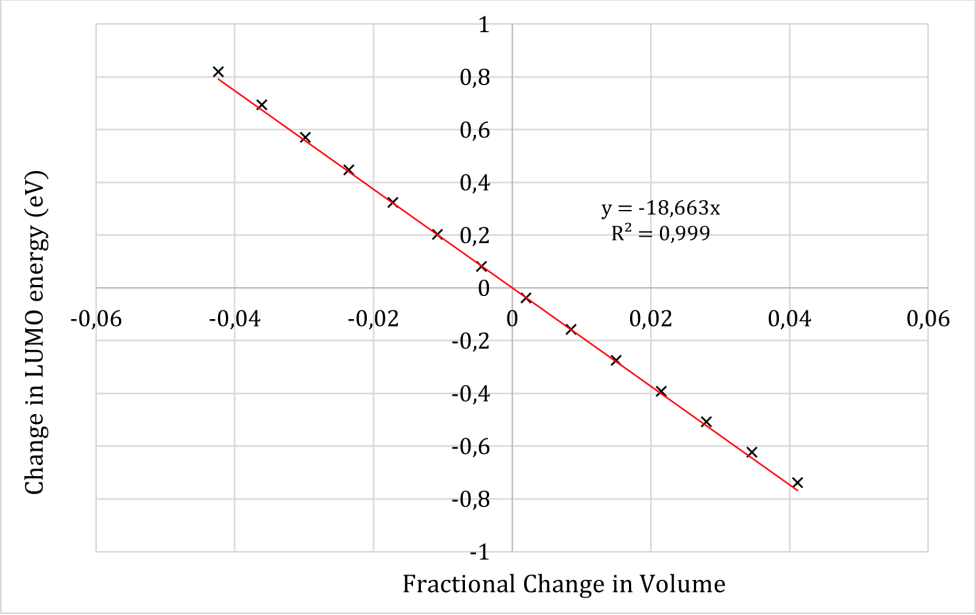

Figure 12: Graph showing the change in LUMO (Lowest Unoccupied Molecular Orbital) energy vs fractional change in volume for the GaAs. From the gradient we find the deformation potential D is -18.663eV.

Table 2: Calculated deformation potential, LA phonon group velocity, and other values used for Gallium Arsenide

Label	Value	Reference
Ω_0	1.8676×10^{-28} m^3	Fig. 9
D	-18.663 eV	Fig. 12
c_{LA}	751.64 m/s	Fig. 11
T	300 K	-
M	9.931×10^{-25} kg	Fig. 9 and [66]

or CBM, and GaAs is a direct band gap semiconductor making its CBM s-like, it is justifiable to compare our result to the one for the s-like band.

However, the current general consensus appears to be that the deformation potential of GaAs should be between -7eV and -13.5eV [66, 68]. In [69] the authors determined experimentally an (absolute value) deformation potential of 16.0eV±0.5eV using electrical transport measurements, which is in good agreement with the result calculated in this thesis. In [70] using the empirical pseudopotential method the authors calculated a value of -15.7eV for GaAs using the CBM, which is also in good agreement with our value.

Furthermore, the article [70] argues that since the deformation potential determined using shift in band gap $D_{conduction} - D_{valence}$ has been found experimentally to be between -8.2eV and -9.9eV [70] (in the datasheets of [66] values between -8.3eV and -8.75eV can be found), low values for $D_{conduction}$ such as -7eV are unreliable, as it would lead to a positive value for $D_{valence}$, which would be unphysical (see also calculated deformation potential values for the valence band in [66]).

Once again, using Equation 150 and the values in Table 2 we can get a simplified relation for $\tau(k)$ for GaAs:

$$\tau(k) = 3.281 \times 10^{-7} \text{s.m}^{-1} \cdot \frac{1}{k} \tag{154}$$

Following the same process as for Silicon, we plot $\tau(k)$ for GaAs in Figure 13.

From Figure 13 we find τ is of the order of 4.0×10^{-16} s, a fifth of the corresponding value for Silicon. Using our estimation of the electron-phonon self energy as for Silicon, we get a self energy of the order $\sim$ 800meV. This is much larger than the value found in this thesis and in [63] for Si.

GaAs having a much shorter electron-phonon interaction lifetime than Si would mean that for optimal efficiency, a GaAs SC would need to be much thinner than an Si SC, if there were not other relevant factors such as electron mobility. In practice, GaAs SCs are manufactured to be thinner than Si SCs, however this is more due to the manufacturing process being both more expensive than for Si, and that GaAs has much higher electron mobility [71], which

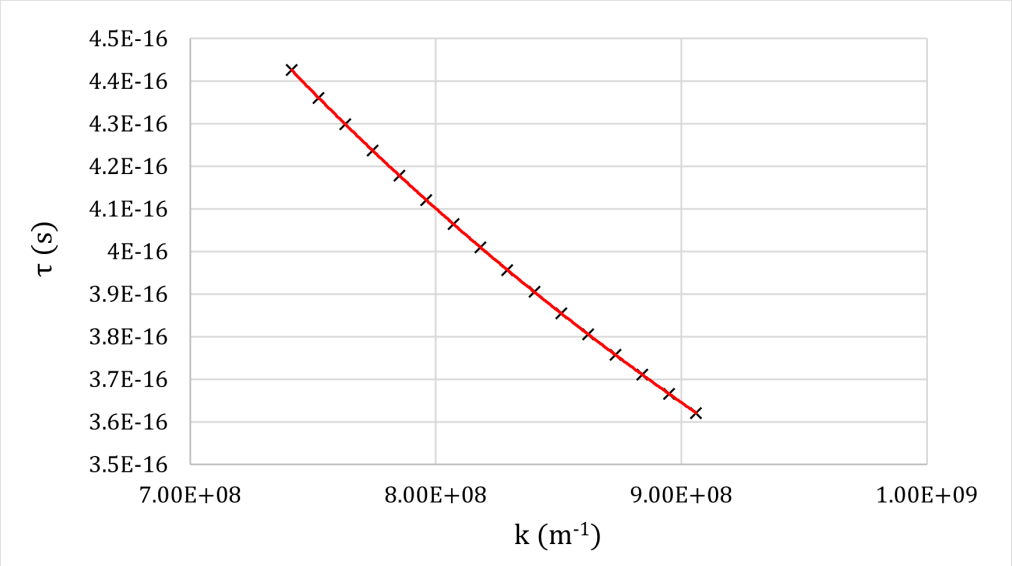

Figure 13: Graph showing the electron-phonon interaction lifetime τ vs the wavenumber k, for Gallium Arsenide. We can see that τ is of the order of 4.0×10^{-16} s. A fifth of the corresponding value for Silicon.

increases its efficiency to a satisfactory level even for a thinner solar cell.

5.4. Note on Band Gap

Materials are expected to become more conductive when compressed (i.e. the band gap decreases). However, certain simulations carried out during the course of this thesis *seemingly* yielded opposite results.

Initially an attempt was made to find the deformation potential by plotting the fractional change in unit cell volume vs change in material band gap, as opposed to single band energy. When doing this, using small changes in lattice constant as in the above sections, it was found that the band gap would increase with decreasing cell volume. That is, under compression, the material would be less conductive, and under expansion, the material would become more conductive. This seemed counter-intuitive, as it has been widely observed that conductivity increases under compression for various materials (for example in [72]). This leads one to wonder whether there is some kind of emergent property that leads to a decrease in band gap under compression, or whether the amount by which the lattice constant is varied determines whether the band gap increases or decreases. Alternatively, the phenomenon could be related to the Mott Transition [73], a metal-insulator transition that takes place when electron density of free electrons in a material reaches a certain concentration relative to the Bohr Radius.

This seemed to be explained by simulating changes in band gap using larger compressions. Previously, this thesis only required very small changes in lattice constant to accurately

determine the deformation potential, and these values were used when calculating band gap as well. Hence there was a possibility that using larger changes in lattice constant might cause the band gap to change behaviour. In Figure 14 are ab-initio simulated electronic band structures for Gallium Arsenide with lattice constants of 5.684Å, and 5.5Å, and then 5.25Å, 5Å, and 4Å.

In Figure 14 we can see that decreasing the lattice constant by a small amount from equilibrium does indeed appear to increase the band gap. However, as we continue to compress the material, the lowest point of the conduction band shifts from the point Γ to X. At this point, the nature of the band gap changes - it becomes indirect, and actually starts decreasing with decreasing lattice constant, until eventually the bands overlap and the material becomes metallic. Hence, the simulation does indeed confirm the known phenomenon that conductivity of a material increases with compression, and the decrease in conductivity only occurs for very small compression from equilibrium (and vice versa for expansion).

The band gap is also affected by the electron-phonon interaction. The retarded electron-phonon self-energy is given by the retarded Green's function in Equation 116. Only the imaginary part of the self-energy is needed to find the electron-phonon interaction lifetime (Equation 117), however, the real part of the self-energy corresponds to a shift in band energy. This in turn would change the band gap. Hence, lattice deformation will have an effect on the band gap, however calculating the real part of the self-energy was not related to the main aims of this thesis.

It would be interesting to further study the process which causes the band gap to behave this way (increasing for small compression from equilibrium, shifting position and decreasing for larger compression), how accurately this reflects reality, and at what point exactly the band gap starts decreasing instead of increasing. However that is beyond the scope of this thesis.

5.5. Discussion

Many authors caution against placing too much trust in ab initio simulation results. This thesis relied on numerous approximations and assumptions to arrive at a result for electron-phonon interaction lifetime, all of which could lead to errors:

1. In Section 3.1.1 we write the many-electron wavefunction as a Slater determinant, allowing for the electron density to be expressed in terms of single-particle spin-orbitals. This fictitious system on non-interacting single particle spin-orbitals lays the foundation for the Kohn-Sham equations.

2. We assumed the Born-Oppenheimer approximation for a many particle system in Section 3.1.3. Electrons are assumed to respond to an external potential much faster that nuclei, such that the nuclei are treated as fixed. Then the electrons are treated as a PES for the nuclear system.

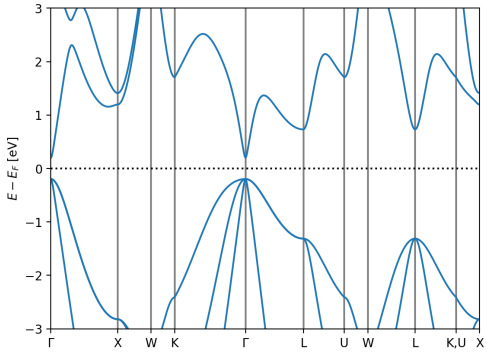

(a) GaAs electronic band structure at $a = 5.684$Å.

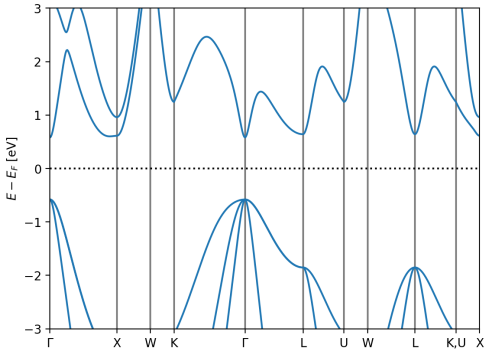

(b) GaAs electronic band structure with $a = 5.5$Å.

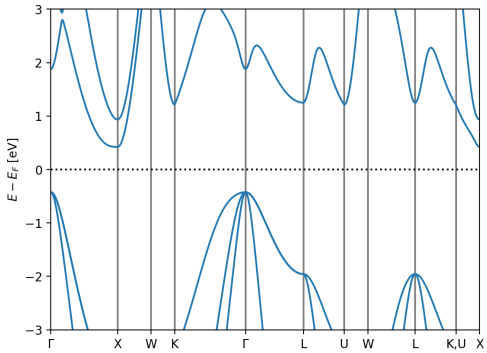

(c) GaAs electronic band structure at $a = 5.25$Å.

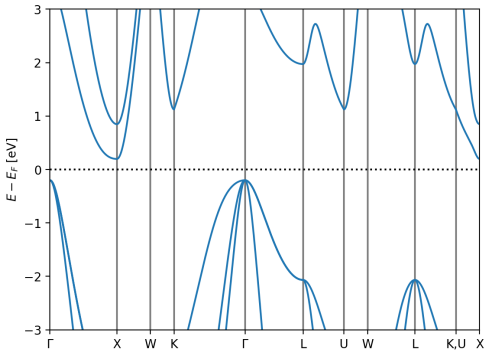

(d) GaAs electronic band structure at $a = 5$Å.

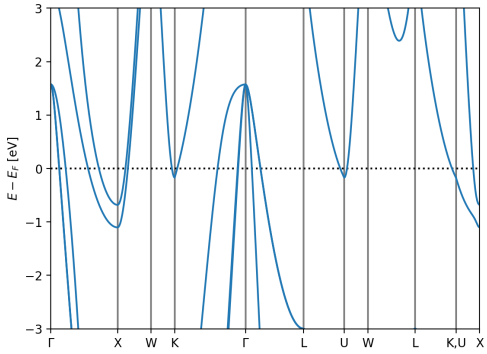

(e) GaAs electronic band structure at $a = 4$Å.

Figure 14: The evolution of GaAs electronic band structure under compression as the lattice constant is decreased from 5.684Å, to 4Å, calculated using ab initio simulation with GPAW. In fig. 14b we can see that the distance between the conduction band minimum and the valence band maximum has increased - band gap has increased, and so conductivity has decreased even though a is smaller. Decreasing a even more, in fig. 14c the structure of the conduction band has changed and the lowest point is no longer at Γ, but at X. The compressed GaAs now has an indirect band gap. In fig 14d the indirect band gap established in the previous image now begins to decrease as a decreases, i.e the GaAs is now becoming more conductive under compression, as previously expected. Finally, in fig. 14e, a is at an extreme 4Å, the conduction and valence bands overlap and the structure is metallic.

3. To find the matrix of IFCs, we employ the Hellmann-Feynman theorem. The Hellmann-Feynman theorem requires that the eigenfunctions Ψ_λ form a complete basis set for orthogonality to hold (see Equation 41). However the many-electron wavefunction $\Psi_{\mathbf{R}}(\mathfrak{r})$ does not necessarily yield a complete basis set. This leads to an error known as Pulay stress. The exclusion of these forces in calculations may not greatly affect the value obtained for Kohn-Sham ground state energies, but it will increase the time it takes for them to converge in numerical simulations [74].

4. The electron-electron interaction written in terms of the electron density (the Hartree term in the expression for the ground state energy functional, Equation 46) contains a self-interaction.

5. The exchange-correlation functional, which represents the electron exchange and correlation effects, is approximated. The numerical results in this thesis use the HSE06 [40] functional.

6. DFPT assumed quantum mechanical perturbation theory approximated to the first order (Equations 70 and 71).

7. In Section 3.3 we assume that atomic vibrations can be modelled as quantum harmonic oscillators.

8. When deriving the electron-phonon interaction Hamiltonian, we write out the Kohn-Sham potential V_{SCF} as a Taylor series about the equilibrium nuclear configuration (Equation 84). We approximate the interaction Hamiltonian to only the first order term of the series.

9. In Section 5.1.3 we approximate the electron occupation number as zero, and we also make some approximations to simplify the form of the phonon occupation number.

10. By determining the electron-phonon matrix element using the deformation potential method in Section 5, we assume that the electron-phonon interaction is only dependant on LA phonons.

Most of these approximations would individually have minimal impact on the result. The largest error in ab initio results likely comes from the approximate exchange-correlation functional. Finding improved and more accurate exchange-correlation functionals is an important topic in the field of DFT. Aside from that, the core assumption affecting the results in this thesis is that only LA phonons were used in determining the electron-phonon interaction lifetime.

To see what using only the LA phonon self-energy would mean for the value of the lifetime τ, we can write the electron-phonon self energy as a sum of the self-energies for the different

phonon modes.

$$\begin{aligned} -\frac{\hbar}{2\tau} &= \mathrm{Im}\Sigma^{ret} \\ \implies \tau &= -\frac{\hbar}{2}\frac{1}{\mathrm{Im}\Sigma^{ret}} \\ \tau &= -\frac{\hbar}{2}\frac{1}{\mathrm{Im}\left[\Sigma^{ret}_{LA}+\Sigma^{ret}_{TA}+\Sigma^{ret}_{L0}+\Sigma^{ret}_{TO}\right]} \end{aligned} \tag{155}$$

Since τ is positive, it implies the imaginary parts of the retarded self energies are all negative, or that they add up to a negative number. Assuming they are all negative, we would expect that taking only the LA contribution would yield a larger value for the lifetime than the true value. This seems to be the case for the value found for Si in Section 5.2. From the interaction lifetime for Si found in this thesis using the LA term only, we found an approximate self-energy of ∼160meV, which is larger than the approximate electron-phonon self energy of 20-50meV found in [63]. The approximate electron-phonon self energy found for GaAs was even larger at ∼ 800meV.

The values for the deformation potential found for GaAs and Si are in good agreement with literature. However, due to the many approximations made it is difficult to draw detailed conclusions on the importance of the electron-LA phonon interaction relative to the interaction with other phonon modes. If one assumes the approximate self-energies in this thesis are fairly accurate, then the LA phonon interaction would account for between one third and one eighth of the total electron-phonon self-energy. Within the scope of this thesis, the electron-phonon interaction lifetime found using only the LA phonon contribution is a good approximation for the true lifetime.

Future works could focus on determining the contributions to the electron-phonon self energy of other phonon modes (LO, TO and TA), and lead to determining a more accurate electron-phonon interaction lifetime. Comparing the results for other phonon modes to the results of this thesis could clarify whether the inaccuracies stemmed from the ab initio calculations or if they stemmed from the assumption that one can use the electron-LA phonon interaction only. It would also be interesting to compare the electron-phonon interaction lifetime of different SC materials to their optimal thickness, and determine if there is an experimentally observable correlation between the two values as expected.

6. Conclusion

Density Functional Theory based ab initio calculations are a promising application of Quantum Mechanics. Yet DFT often fails to accurately predict some material properties, such as band gaps, possibly on account of the fact that unoccupied conduction states do not contribute to the electron density. The process to carry out an ab initio calculation involves many approximations, and one would be right to question the validity of the result. However, constant advancements are being made with additions to DFT software and improved exchange-correlation functionals and pseudopotentials.

The process of thermalisation, the main result of efficiency loss in an SC, was studied. Phonon frequencies can be determined by deriving a dynamical matrix using DFT and DFPT, and the electron-phonon interaction self-energy is determined using the theory of Green's functions. The electron-phonon matrix element is approximated using a deformation potential, which is only valid for the electronic interaction with LA phonons. Once the matrix element is calculated, we determine the electron-phonon interaction lifetime, approximated by the electron-LA phonon interaction only.

To determine the phonon dispersion relations for Si and GaAs in Quantum Espresso, the ONCV pseudopotentials and HSE06 exchange-correlation functional were used. These resulted in a phonon group velocity of $1389.7\text{m}\cdot\text{s}^{-1}$ for Si and $751.64\text{m}\cdot\text{s}^{-1}$ for GaAs. Using the change in LUMO (or CBM) band energy in GPAW (using the plane-wave basis set), the hydrostatic deformation potentials were found to be -10.125eV for Si and -18.663eV for GaAs, in good agreement with literature [60, 69, 70]. This led to an electron-phonon interaction lifetime of $\tau \sim 2.0 \times 10^{-15}$s for Si and $\tau \sim 4.0 \times 10^{-16}$s for GaAs. This lifetime for Si corresponded roughly to an electron-phonon self-energy of ∼160meV, which is 3 to 8 times larger than the value of 20-30meV indicated in [63]. This indicates that using the LA phonon matrix element only when calculating the electron-phonon interaction lifetime is a relatively good approximation for the true lifetime. Future works could determine the self-energy contribution of other phonon modes for comparison.

Thermalisation is an important process that needs to be understood if the efficiency of SCs is to be improved. Ab initio numerical simulations are an excellent tool for doing this. With continuing research, the accuracy of ab initio simulations improves and they continue to provide insight into the nature of many bulk materials used in photovoltaics.

References

[1] Alexander Quandt and Robert Warmbier. Solar cell simulations based on ab initio methods. *Opt. Mater. Express*, 11(6):1763–1779, Jun 2021.

[2] University of Michigan Center for Sustainable Systems. Photovoltaic energy factsheet. *Pub. No. CSS07-08*, 2021.

[3] IRENA. Majority of new renewables undercut cheapest fossil fuel on cost. Online, 22 June 2021. http://www.irena.org/newsroom/pressreleases/2021/Jun/Majority-of-New-Renewables-Undercut-Cheapest-Fossil-Fuel-on-Cost Accessed 23 Feb. 2022.

[4] Lazard. Lazard's levelized cost of energy analysis (April 2023). Online. Found at https://www.lazard.com/research-insights/2023-levelized-cost-of-energyplus/ Accessed 26 Oct. 2023.

[5] Department of Mineral Resources and Government of South Africa Energy. Solar power. Online, 2022. http://www.energy.gov.za/files/esources/renewables/r/_solar.html Accessed 7 Feb. 2022.

[6] Valentin Milichko, Alexander Shalin, Ivan Mukhin, Aleksandr Kovrov, Andrei Krasilin, A. Vinogradov, Pavel Belov, and Constantin Simovskii. Solar photovoltaics: current state and trends. *Physics-Uspekhi*, 59, 08 2016.

[7] N. Shah, A. A. Shah, P. K. Leung, S. Khan, K. Sun, X. Zhu, and Q. Liao. A review of third generation solar cells. *Processes*, 11(6), 2023.

[8] Ao Wang and Yimin Xuan. A detailed study on loss processes in solar cells. *Energy*, 144:490–500, 2018.

[9] Harry Atwater, Albert Polman, Emily Kosten, Dennis Callahan, Pierpaolo Spinelli, Carissa Eisler, Matthew Escarra, Emily Warmann, and Cristofer Flowers. Nanophotonic design principles for ultrahigh efficiency photovoltaics. *AIP Conference Proceedings*, 1519(1):17–21, 2013.

[10] Mirkazem Omrani, Reza Keshavarzi, Mojtaba Abdi-Jalebi, and Peng Gao. Impacts of plasmonic nanoparticles incorporation and interface energy alignment for highly efficient carbon-based perovskite solar cells. *Scientific Reports*, 12:5367, 03 2022.

[11] Adnan Ali, Fedwa El Mellouhi, Anirban Mitra, and Brahim Aïssa. Research progress of plasmonic nanostructure-enhanced photovoltaic solar cells. *Nanomaterials*, 12:788, 02 2022.

[12] R.S. Ohl. Light-sensitive electric device. *U.S. Patent*, 2:402, 602, May 1941.

[13] Martin A Green. The path to 25% silicon solar cell efficiency: History of silicon cell evolution. *Progress in Photovoltaics: Research and Applications*, 17:183–189, 2009.

[14] William Shockley and Hans J. Queisser. Detailed Balance Limit of Efficiency of p-n Junction Solar Cells. *Journal of Applied Physics*, 32(3):510–519, March 1961.

[15] Feliciano Giustino. Electron-phonon interactions from first principles. *Reviews of Modern Physics*, 89(1), feb 2017.

[16] Paolo Giannozzi, Stefano Baroni, Nicola Bonini, Matteo Calandra, Roberto Car, Carlo Cavazzoni, Davide Ceresoli, Guido L Chiarotti, Matteo Cococcioni, Ismaila Dabo, Andrea Dal Corso, Stefano de Gironcoli, Stefano Fabris, Guido Fratesi, Ralph Gebauer, Uwe Gerstmann, Christos Gougoussis, Anton Kokalj, Michele Lazzeri, Layla Martin-Samos, Nicola Marzari, Francesco Mauri, Riccardo Mazzarello, Stefano Paolini, Alfredo Pasquarello, Lorenzo Paulatto, Carlo Sbraccia, Sandro Scandolo, Gabriele Sclauzero, Ari P Seitsonen, Alexander Smogunov, Paolo Umari, and Renata M Wentzcovitch. QUANTUM ESPRESSO: a modular and open-source software project for quantum simulations of materials. *Journal of Physics: Condensed Matter*, 21(39):395502, sep 2009.

[17] J Enkovaara, C Rostgaard, J J Mortensen, J Chen, M Dułak, L Ferrighi, J Gavnholt, C Glinsvad, V Haikola, H A Hansen, H H Kristoffersen, M Kuisma, A H Larsen, L Lehtovaara, M Ljungberg, O Lopez-Acevedo, P G Moses, J Ojanen, T Olsen, V Petzold, N A Romero, J Stausholm-Møller, M Strange, G A Tritsaris, M Vanin, M Walter, B Hammer, H Häkkinen, G K H Madsen, R M Nieminen, J K Nørskov, M Puska, T T Rantala, J Schiøtz, K S Thygesen, and K W Jacobsen. Electronic structure calculations with GPAW: a real-space implementation of the projector augmented-wave method. *Journal of Physics: Condensed Matter*, 22(25):253202, jun 2010.

[18] Andrea Marini, Conor Hogan, Myrta Grüning, and Daniele Varsano. yambo: An ab initio tool for excited state calculations. *Computer Physics Communications*, 180(8):1392–1403, aug 2009.

[19] D. Neamen. *Semiconductor Physics And Devices*. McGraw-Hill Higher Education, 2011.

[20] P. Hohenberg and W. Kohn. Inhomogeneous electron gas. *Phys. Rev.*, 136:B864–B871, Nov 1964.

[21] J. C. Slater. The theory of complex spectra. *Phys. Rev.*, 34:1293–1322, Nov 1929.

[22] R.M. Martin. *Electronic Structure: Basic Theory and Practical Methods*. Cambridge University Press, 2020.

[23] Stefano Baroni, Stefano de Gironcoli, Andrea Dal Corso, and Paolo Giannozzi. Phonons and related crystal properties from density-functional perturbation theory. *Rev. Mod. Phys.*, 73:515–, 07 2001.

[24] M. Born and R. Oppenheimer. Zur Quantentheorie der Molekeln. *Annalen der Physik*, 389(20):457–484, January 1927.

[25] G.F. Bassani, G.L. Liedl, and P. Wyder. *Encyclopedia of Condensed Matter Physics*. Number v. 1 in Encyclopedia of Condensed Matter Physics. Academic, 2005.

[26] David Wallace. *An Introduction To Hellmann-Feynman Theory*. Masters thesis, University of Central Florida, 2005. Available at https://stars.library.ucf.edu/etd/413.

[27] Wolfgang Pauli. Über das modell des wasserstoffmolekülions. *Annalen Der Physik*, 68, 1922.

[28] H. Hellmann. *Einführung in die Quantenchemie*. Deuticke, 1937.

[29] R. P. Feynman. Forces in molecules. *Phys. Rev.*, 56:340–343, Aug 1939.

[30] W. Kohn and L. J. Sham. Self-consistent equations including exchange and correlation effects. *Phys. Rev.*, 140:A1133–A1138, Nov 1965.

[31] D. R. Hartree. The wave mechanics of an atom with a non-Coulomb central field. *Mathematical Proceedings of the Cambridge Philosophical Society*, 24(1):111–132, 1928.

[32] Douglas Rayner Hartree and W. Hartree. Self-consistent field, with exchange, for beryllium. *Proceedings of the Royal Society of London. Series A - Mathematical and Physical Sciences*, 150(869):9–33, 1935.

[33] Quantum Espresso. Introduction. Online. https://www.quantum-espresso.org/Doc/user_guide/node2.html Accessed 15 Sept. 2023.

[34] Felix Bloch. Über die Quantenmechanik der Elektronen in Kristallgittern. *Zeitschrift fur Physik*, 52(7-8):555–600, July 1929. Translation can be found at https://courses.physics.ucsd.edu/2018/Fall/physics211a/topic/bloch.pdf.

[35] A. D. Becke. Density-functional exchange-energy approximation with correct asymptotic behavior. *Phys. Rev. A*, 38:3098–3100, Sep 1988.

[36] John P. Perdew, J. A. Chevary, S. H. Vosko, Koblar A. Jackson, Mark R. Pederson, D. J. Singh, and Carlos Fiolhais. Atoms, molecules, solids, and surfaces: Applications of the generalized gradient approximation for exchange and correlation. *Phys. Rev. B*, 46:6671–6687, Sep 1992.

[37] David C. Langreth and M. J. Mehl. Beyond the local-density approximation in calculations of ground-state electronic properties. *Phys. Rev. B*, 28:1809–1834, Aug 1983.

[38] John P. Perdew, Kieron Burke, and Yue Wang. Generalized gradient approximation for the exchange-correlation hole of a many-electron system. *Phys. Rev. B*, 54:16533–16539, Dec 1996.

[39] Axel D. Becke. A new mixing of Hartree-Fock and local density-functional theories. *The Journal of Chemical Physics*, 98(2):1372–1377, January 1993.

[40] Jochen Heyd, Gustavo E. Scuseria, and Matthias Ernzerhof. Hybrid functionals based on a screened Coulomb potential. *The Journal of Chemical Physics*, 118(18):8207–8215, 04 2003.

[41] Aliaksandr V. Krukau, Oleg A. Vydrov, Artur F. Izmaylov, and Gustavo E. Scuseria. Influence of the exchange screening parameter on the performance of screened hybrid functionals. *The Journal of Chemical Physics*, 125(22):224106, 12 2006.

[42] Jochen Heyd, Gustavo E. Scuseria, and Matthias Ernzerhof. Erratum: "Hybrid functionals based on a screened Coulomb potential" [J. Chem. Phys. 118, 8207 (2003)]. *The Journal of Chemical Physics*, 124(21):219906–219906, June 2006.

[43] R. M. Sternheimer. Electronic polarizabilities of ions from the Hartree-Fock wave functions. *Phys. Rev.*, 96:951–968, Nov 1954.

[44] D.J. Griffiths. *Introduction to Quantum Mechanics*. Cambridge University Press, 2017.

[45] Swapnil Dubey, Jatin Narotam Sarvaiya, and Bharath Seshadri. Temperature dependent photovoltaic (pv) efficiency and its effect on pv production in the world – a review. *Energy Procedia*, 33:311–321, 2013. PV Asia Pacific Conference 2012.

[46] G.D. Mahan. *Many-Particle Physics*. Physics of Solids and Liquids. Springer US, 2013.

[47] G.D. Mahan. *Condensed Matter in a Nutshell*. In a Nutshell. Princeton University Press, 2011.

[48] Tomokazu Kato, Tetsuro Kobayashi, and Mikio Namiki. Formal Theory of Green Functions. *Progress of Theoretical Physics Supplement*, 15:3–60, 03 1960.

[49] Takeo Matsubara. A New Approach to Quantum-Statistical Mechanics. *Progress of Theoretical Physics*, 14(4):351–378, 10 1955.

[50] W. Heisenberg. Über quantentheoretische Umdeutung kinematischer und mechanischer Beziehungen. *Zeitschrift fur Physik*, 33(1):879–893, December 1925.

[51] F. J. Dyson. The *s* matrix in quantum electrodynamics. *Phys. Rev.*, 75:1736–1755, Jun 1949.

[52] J. J. Mortensen, L. B. Hansen, and K. W. Jacobsen. Real-space grid implementation of the projector augmented wave method. *Phys. Rev. B*, 71:035109, Jan 2005.

[53] A. H. Larsen, M. Vanin, J. J. Mortensen, K. S. Thygesen, and K. W. Jacobsen. Localized atomic basis set in the projector augmented wave method. *Phys. Rev. B*, 80:195112, Nov 2009.

[54] Quantum Espresso. Using PHonon. Online. https://www.quantum-espresso.org/Doc/ph_user_guide/node7.html Accessed 15 Sept. 2023.

[55] D. R. Hamann. Optimized norm-conserving Vanderbilt pseudopotentials. *Phys. Rev. B*, 88:085117, Aug 2013.

[56] David Vanderbilt. Soft self-consistent pseudopotentials in a generalized eigenvalue formalism. *Phys. Rev. B*, 41:7892–7895, Apr 1990.

[57] John P. Perdew, Adrienn Ruzsinszky, Gábor I. Csonka, Oleg A. Vydrov, Gustavo E. Scuseria, Lucian A. Constantin, Xiaolan Zhou, and Kieron Burke. Restoring the density-gradient expansion for exchange in solids and surfaces. *Phys. Rev. Lett.*, 100:136406, Apr 2008.

[58] GPAW. GPAW: DFT and beyond within the projector-augmented wave method. Online. https://wiki.fysik.dtu.dk/gpaw/index.html Accessed 21 Sept. 2023.

[59] O. Madelung, U. Rössler, and M. Schulz. Silicon, lattice parameter, thermal expansion: Datasheet from Landolt-Börnstein - group iii condensed matter - volume 41a1b: Group iv elements, iv-iv and iii-v compounds. part b - electronic, transport, optical and other properties, 2002.

[60] A. Blacha, H. Presting, and M. Cardona. Deformation potentials of k = 0 states of tetrahedral semiconductors. *Physica Status Solidi (B)*, 126(1):11–36, 1984.

[61] O. Madelung, U. Rössler, and M. Schulz. Silicon (Si), Debye temperature, heat capacity, density, hardness, melting point: Datasheet from Landolt-Börnstein - Group III Condensed Matter - volume 41a1b: Group iv elements, iv-iv and iii-v compounds. part b - electronic, transport, optical and other properties, 2002.

[62] Quantum Espresso. Quantum ESPRESSO. Online. https://www.quantum-espresso.org/ Accessed 21 Sept. 2023.

[63] Andrea Marini. Competition between the electronic and phonon–mediated scattering channels in the out–of–equilibrium carrier dynamics of semiconductors: an ab-initio approach. *Journal of Physics: Conference Series*, 427(1):012003, mar 2013.

[64] Yambo. Yambo. Online. https://www.yambo-code.eu/ Accessed 14 Dec. 2023.

[65] P B Allen and V Heine. Theory of the temperature dependence of electronic band structures. 9(12):2305, jun 1976.

[66] O. Madelung, U. Rössler, and M. Schulz. Gallium Arsenide (GaAs), Debye temperature, heat capacity, density, hardness, melting point: Datasheet from landolt-börnstein - group iii condensed matter - volume 41a1b: Group iv elements, iv-iv and iii-v compounds. part b - electronic, transport, optical and other properties, 2002.

[67] O. Madelung, U. Rössler, and M. Schulz. Gallium Arsenide, lattice parameter, thermal expansion: Datasheet from Landolt-Börnstein - group iii condensed matter - volume 41a1b: Group iv elements, iv-iv and iii-v compounds. part b - electronic, transport, optical and other properties, 2002.

[68] Manuel Cardona and Niels E. Christensen. Acoustic deformation potentials and heterostructure band offsets in semiconductors. *Phys. Rev. B*, 35:6182–6194, Apr 1987.

[69] H. J. Lee, J. Basinski, L. Y. Juravel, and J. C. Woolley. Electrical transport and band structure of GaAs. *Canadian Journal of Physics*, 57(2):233–242, 1979.

[70] P. Pfeffer, I. Gorczyca, and W. Zawadzki. Theory of free-electron optical absorption in n-GaAs. *Solid State Communications*, 51(3):179–183, 1984.

[71] Nikola Papež, Rashid Dallaev, Ştefan Ţălu, and Jaroslav Kaštyl. Overview of the current state of Gallium Arsenide-based solar cells. *Materials (Basel)*, 14(11):3075, 06 2021.

[72] Adila Rani, Seung-Woong Nam, Kyoung-Ah Oh, and Min Park. Electrical conductivity of chemically reduced graphene powders under compression. *Carbon letters*, 11:90–95, 06 2010.

[73] N. F. Mott. Metal-insulator transition. *Rev. Mod. Phys.*, 40:677–683, Oct 1968.

[74] Álvaro Ruiz-Serrano, Nicholas D. M. Hine, and Chris-Kriton Skylaris. Pulay forces from localized orbitals optimized in situ using a psinc basis set. *The Journal of Chemical Physics*, 136(23):234101, 06 2012.

A. Reducing the Slater Determinant

We wish to show how orthornomality will reduce the determinant in Equation 17 to a simple product of the three states as functions of their corresponding variables. For simplicity, we will show this for the case where Ψ is written as a Slater determinant of two states. Then, the operator $\hat{H} = \hat{h}_1 + \hat{h}_2$

$$\begin{aligned}
\langle\Psi|\hat{H}|\Psi\rangle =& \frac{1}{2!}\int\int \det(\alpha,\beta)^*\hat{H}\det(\alpha,\beta)\mathrm{d}\mathbf{r}_1\mathrm{d}\mathbf{r}_2 \\
=& \frac{1}{2}\int\int (\alpha(\mathbf{r}_1)\beta(\mathbf{r}_2) - \alpha(\mathbf{r}_2)\beta(\mathbf{r}_1))^*\hat{H}(\alpha(\mathbf{r}_1)\beta(\mathbf{r}_2) \\
& - \alpha(\mathbf{r}_2)\beta(\mathbf{r}_1))\mathrm{d}\mathbf{r}_1\mathrm{d}\mathbf{r}_2 \\
=& \frac{1}{2}\int\int \big[\alpha(\mathbf{r}_1)^*\beta(\mathbf{r}_2)^*\hat{H}\alpha(\mathbf{r}_1)\beta(\mathbf{r}_2) - \alpha(\mathbf{r}_1)^*\beta(\mathbf{r}_2)^*\hat{H}\alpha(\mathbf{r}_2)\beta(\mathbf{r}_1) \\
& - \alpha(\mathbf{r}_2)^*\beta(\mathbf{r}_1)^*\hat{H}(\alpha(\mathbf{r}_1)\beta(\mathbf{r}_2) + \alpha(\mathbf{r}_2)^*\beta(\mathbf{r}_1)^*\hat{H}\alpha(\mathbf{r}_2)\beta(\mathbf{r}_1)\big]\mathrm{d}\mathbf{r}_1\mathrm{d}\mathbf{r}_2 \\
=& \frac{1}{2}\int\int \big[\alpha(\mathbf{r}_1)^*\beta(\mathbf{r}_2)^*\hat{h}_1\alpha(\mathbf{r}_1)\beta(\mathbf{r}_2) + \alpha(\mathbf{r}_1)^*\beta(\mathbf{r}_2)^*\hat{h}_2\alpha(\mathbf{r}_1)\beta(\mathbf{r}_2) \\
& - \alpha(\mathbf{r}_1)^*\beta(\mathbf{r}_2)^*\hat{h}_1\alpha(\mathbf{r}_2)\beta(\mathbf{r}_1) - \alpha(\mathbf{r}_1)^*\beta(\mathbf{r}_2)^*\hat{h}_2\alpha(\mathbf{r}_2)\beta(\mathbf{r}_1) \\
& - \alpha(\mathbf{r}_2)^*\beta(\mathbf{r}_1)^*\hat{h}_1\alpha(\mathbf{r}_1)\beta(\mathbf{r}_2) - \alpha(\mathbf{r}_2)^*\beta(\mathbf{r}_1)^*\hat{h}_2\alpha(\mathbf{r}_1)\beta(\mathbf{r}_2) \\
& + \alpha(\mathbf{r}_2)^*\beta(\mathbf{r}_1)^*\hat{h}_1\alpha(\mathbf{r}_2)\beta(\mathbf{r}_1) + \alpha(\mathbf{r}_2)^*\beta(\mathbf{r}_1)^*\hat{h}_2\alpha(\mathbf{r}_2)\beta(\mathbf{r}_1)\big]\mathrm{d}\mathbf{r}_1\mathrm{d}\mathbf{r}_2
\end{aligned} \tag{156}$$

The operator $\hat{h}_1$ only acts on functions of $\mathbf{r}_1$, and similarly for $\hat{h}_2$. This means that for each term where the operator is $\hat{h}_1$, functions of $\mathbf{r}_2$ can be treated like constants and moved to either side of the operator, and vice versa for terms with $\hat{h}_2$.

$$\begin{aligned}
\langle\Psi|\hat{H}|\Psi\rangle =& \frac{1}{2}\int\int \big[\beta(\mathbf{r}_2)^*\beta(\mathbf{r}_2)\alpha(\mathbf{r}_1)^*\hat{h}_1\alpha(\mathbf{r}_1) + \alpha(\mathbf{r}_1)^*\alpha(\mathbf{r}_1)\beta(\mathbf{r}_2)^*\hat{h}_2\beta(\mathbf{r}_2) \\
& - \beta(\mathbf{r}_2)^*\alpha(\mathbf{r}_2)\alpha(\mathbf{r}_1)^*\hat{h}_1\beta(\mathbf{r}_1) - \alpha(\mathbf{r}_1)^*\beta(\mathbf{r}_1)\beta(\mathbf{r}_2)^*\hat{h}_2\alpha(\mathbf{r}_2) \\
& - \alpha(\mathbf{r}_2)^*\beta(\mathbf{r}_2)\beta(\mathbf{r}_1)^*\hat{h}_1\alpha(\mathbf{r}_1) - \beta(\mathbf{r}_1)^*\alpha(\mathbf{r}_1)\alpha(\mathbf{r}_2)^*\hat{h}_2\beta(\mathbf{r}_2) \\
& + \alpha(\mathbf{r}_2)^*\alpha(\mathbf{r}_2)\beta(\mathbf{r}_1)^*\hat{h}_1\beta(\mathbf{r}_1) + \beta(\mathbf{r}_1)^*\beta(\mathbf{r}_1)\alpha(\mathbf{r}_2)^*\hat{h}_2\alpha(\mathbf{r}_2)\big]\mathrm{d}\mathbf{r}_1\mathrm{d}\mathbf{r}_2 \\
=& \frac{1}{2}\Big[\int \alpha(\mathbf{r}_1)^*\hat{h}_1\alpha(\mathbf{r}_1)\mathrm{d}\mathbf{r}_1 + \int \beta(\mathbf{r}_2)^*\hat{h}_2\beta(\mathbf{r}_2)\mathrm{d}\mathbf{r}_2 \\
& - \int \beta(\mathbf{r}_2)^*\alpha(\mathbf{r}_2)\mathrm{d}\mathbf{r}_2\int \alpha(\mathbf{r}_1)^*\hat{h}_1\beta(\mathbf{r}_1)\mathrm{d}\mathbf{r}_1 - \int \alpha(\mathbf{r}_1)^*\beta(\mathbf{r}_1)\mathrm{d}\mathbf{r}_1\int \beta(\mathbf{r}_2)^*\hat{h}_2\alpha(\mathbf{r}_2)\mathrm{d}\mathbf{r}_2 \\
& - \int \alpha(\mathbf{r}_2)^*\beta(\mathbf{r}_2)\mathrm{d}\mathbf{r}_2\int \beta(\mathbf{r}_1)^*\hat{h}_1\alpha(\mathbf{r}_1)\mathrm{d}\mathbf{r}_1 - \int \beta(\mathbf{r}_1)^*\alpha(\mathbf{r}_1)\mathrm{d}\mathbf{r}_1\int \alpha(\mathbf{r}_2)^*\hat{h}_2\beta(\mathbf{r}_2)\mathrm{d}\mathbf{r}_2 \\
& + \int \beta(\mathbf{r}_1)^*\hat{h}_1\beta(\mathbf{r}_1)\mathrm{d}\mathbf{r}_1 + \int \alpha(\mathbf{r}_2)^*\hat{h}_2\alpha(\mathbf{r}_2)\mathrm{d}\mathbf{r}_2\Big]
\end{aligned} \tag{157}$$

Due to α and β being normalised states, the integrals of their products with their complex conjugates yield 1, leading to the first two and last two terms in the equation above being shortened. Due to orthogonality, any integrals of $\alpha^*\beta$ or $\beta^*\alpha$ vanish. Hence we are left with:

$$\begin{aligned}\langle\Psi|\hat{H}|\Psi\rangle =&\frac{1}{2}\Big[\int \alpha(\mathbf{r}_1)^*\hat{h}_1\alpha(\mathbf{r}_1)\mathrm{d}\mathbf{r}_1 + \int \beta(\mathbf{r}_2)^*\hat{h}_2\beta(\mathbf{r}_2)\mathrm{d}\mathbf{r}_2 \\ &+ \int \beta(\mathbf{r}_1)^*\hat{h}_1\beta(\mathbf{r}_1)\mathrm{d}\mathbf{r}_1 + \int \alpha(\mathbf{r}_2)^*\hat{h}_2\alpha(\mathbf{r}_2)\mathrm{d}\mathbf{r}_2\Big]\end{aligned} \tag{158}$$

But, now that all the integrals have been separated, the labels $\mathbf{r}_1$ and $\mathbf{r}_2$ become arbitrary since fermions are identical. Hence:

$$\begin{aligned}\langle\Psi|\hat{H}|\Psi\rangle =&\frac{1}{2}\Big[\int \alpha(\mathbf{r}_1)^*\hat{h}_1\alpha(\mathbf{r}_1)\mathrm{d}\mathbf{r}_1 + \int \beta(\mathbf{r}_2)^*\hat{h}_2\beta(\mathbf{r}_2)\mathrm{d}\mathbf{r}_2 \\ &+ \int \beta(\mathbf{r}_2)^*\hat{h}_2\beta(\mathbf{r}_2)\mathrm{d}\mathbf{r}_2 + \int \alpha(\mathbf{r}_1)^*\hat{h}_1\alpha(\mathbf{r}_1)\mathrm{d}\mathbf{r}_1\Big] \\ =&\int \alpha(\mathbf{r}_1)^*\hat{h}_1\alpha(\mathbf{r}_1)\mathrm{d}\mathbf{r}_1 + \int \beta(\mathbf{r}_2)^*\hat{h}_2\beta(\mathbf{r}_2)\mathrm{d}\mathbf{r}_2 \\ =&\int\int (\alpha(\mathbf{r}_1)\beta(\mathbf{r}_2))^*\hat{H}(\alpha(\mathbf{r}_1)\beta(\mathbf{r}_2))\mathrm{d}\mathbf{r}_1\mathrm{d}\mathbf{r}_2\end{aligned} \tag{159}$$

Here we made use of the property that an operator which is a sum of single particle operators can be expressed as a trace over single-particle operators, $\langle\Psi|\hat{H}|\Psi\rangle = \sum_i^N \langle\psi_i|\hat{h}|\psi_i\rangle$, where Ψ is a product of single particle states ψ_i.